A Ph.D. Research Thesis

# An Intelligent System for Fault Diagnosis in Gearboxes

by

Jital Dwarkesh Shah
Dept. of Mechanical Engineering

Advisor:
Dr. Wilson Wang

2022

# Abstract

Gearboxes are commonly used in rotating machinery for power transmission. A gearbox consists of shafts, gears, and bearings, each component having specific mechanical dynamics and fault properties. Reliable gearbox fault detection and health monitoring techniques are critically needed in industries for more efficient predictive maintenance applications. The objective of this work is to develop a new technology for health monitoring of gearboxes. Firstly, a new wavelet analysis method is technique for analysis of gear faults in a gearbox with demodulation from other rotating components such as shaft and bearings. Secondly, a mode decomposition technique is proposed to highlight bearing fault features in a gearbox. Thirdly, a new evolving neuro-fuzzy (eNF) classifier is developed to integrate the merits of different fault detection techniques for real-time health condition monitoring of gear systems. The effectiveness of the proposed techniques is verified by simulation and experimental tests.

# Acknowledgements

First and foremost, thanks to the God, the Almighty, for his blessings during my research work to complete the research successfully.

I would like to express my deep and sincere gratitude to my research supervisor, Dr. Wilson Wang, Ph.D., P.Eng., Professor, Dept. of Mechanical Engineering, Lakehead University, Thunder Bay, for granting me the opportunity to do research and providing priceless guidance throughout this research. It was a great privilege and honor to work and study under his guidance. I am extremely grateful for what he has offered me. I am extending my heartfelt thanks to his research team for their acceptance and patience during the discussion.

I would like to express my gratefulness and thanks to my PhD committee members, the external examiner Dr. Zhigang (Will) Tian (Department of Mechanical Engineering), Dr. Jian Deng (Department of Civil Engineering) and Dr. Kefu Liu (Department of Mechanical Engineering) for their presence, encouragement and endow with their precious time to review my thesis and insightful feedback. Appreciation is also given to Dr. Ali Tarokh and Dr. Murari Roy for being the coordinator.

I am extremely grateful to my parents and my family for their love, prayers, caring and sacrifices for educating and preparing me for my future. Also I express my thanks to my sisters, brother and brother in laws for their support and valuable prayers. My Special thanks goes to my friend and brother in law Prof. A. Patel for the keen interest shown to complete this thesis successfully.

I would like to say thanks to my friends and research colleagues, A. Shukla, H. Gohel, Dr. S. Osman, Dr. P. Liu, Dr. M. Mahumud and Dr. M Ahwiadi for their constant encouragement as well as genuine support throughout this research work.

Finally, my thanks go to all the people who have supported me to complete the research work directly or indirectly.

# Table of Content

# Table of Figures

# List of Tables

# List of Abbreviations

| | |
|---|---|
| eNF | Evolving neuro-fuzzy |
| NF | Neuro-fuzzy |
| TSA | Time synchronous averaging |
| GMF ($f_m$) | Gear mesh frequency |
| WT | Wavelet transform |
| FT | Fourier transform |
| HHT | Hilbert Haung Transform |
| EMD | Empirical mode decomposition |
| IMFs | Intrinsic mode functions |
| eTS | Evolving Takagi Sugeno |
| LSE | Least square estimator |
| TWNFI | Transductive neuro-fuzzy inference |
| LMD | Local mode decomposition |
| iFFT | Inverse Fourier transform |
| LD | Local mean decomposition |
| HT | Hilbert transform |
| PFs | Product functions |
| IF | Instantaneous frequency |
| MFs | Gaussian membership functions |
| GD | Gradient descent |
| NaD | Normalized Adadelta method |
| SEF | Self evolving fuzzy classifier |
| SDPC | Sensing, Diagnostic, Prognostics, and Control |

# Chapter 1

# Introduction

## 1.1 Introduction to Gear Systems

Gearboxes (i.e., gear systems) are among the most ubiquitous mechanical systems, which are commonly used in rotating machinery in a wide variety of industries such as the automotive, manufacturing, and chemical engineering. A gearbox can be used to transmit power and rotation from the drive motor to the driven machinery [1, 2]. Correspondingly, the gearbox health condition is critical to ensuring that machines operate at desired operation accuracy and efficiency [3-5]. A gearbox consists of many components such as gears, bearings and shafts; all of these rotating components will contribute to the state of gearbox health conditions [6]. Each rotating component has its own dynamics, and specific types of faults [7, 8]. A shaft is used to support gears, and transmit the forces to the gearbox case through bearings. Bearings allow shaft to have a relative motion with respect to fixed structure of gearbox. The gear has the function of transmitting torque from one shaft to another shaft by tooth meshing operations. Fig. 1.1 shows two examples of gearboxes [9, 10] with helical gears and spur gears.

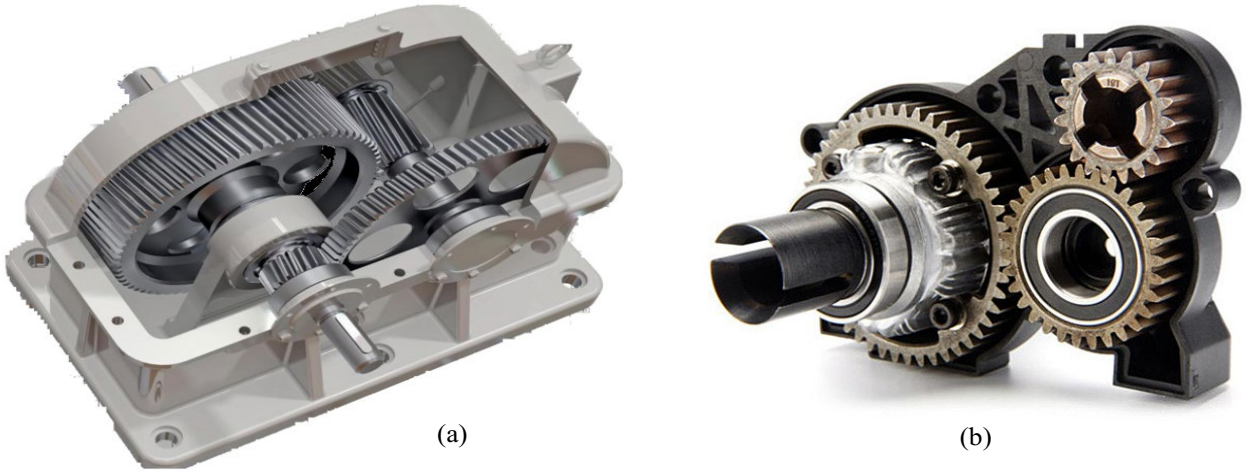

(a) (b)

Fig. 1.1 Examples of gearboxes [9, 10]: (a) helical gears, (b) spur gears.

The efficiency of a gearbox depends on the proper functioning of each rotating constituent component [11]. Any defect in the gearbox will not only have adverse impacts on the transmission accuracy, but also increase vibration and noise levels [12]. Damage to the gear system may also result in serious accidents and even catastrophic failures in some safety-critical applications such as aircraft and chemical engineering facilities [13]. Thus, reliable gearbox health monitoring techniques and systems are critically needed in industries for production quality control and the maintenance service planning. The next section will provide discussions on types of faults in gearboxes.

## 1.2 Faults in a Gearbox System

Fault in each rotating component in a gearbox can result in degradation of transmission accuracy of the gear train. Some of the common faults in gearboxes are summarized below.

### 1.2.1 Shaft Faults

The main shaft defects include misalignment and imbalance. Misalignment in a shaft is caused by shaft elastic deformation, manufacturing inaccuracy and assembly errors [14]. If the shaft misalignment error, as illustrated in Fig 1.2, is beyond some threshold, the gear train transmission accuracy degrades.

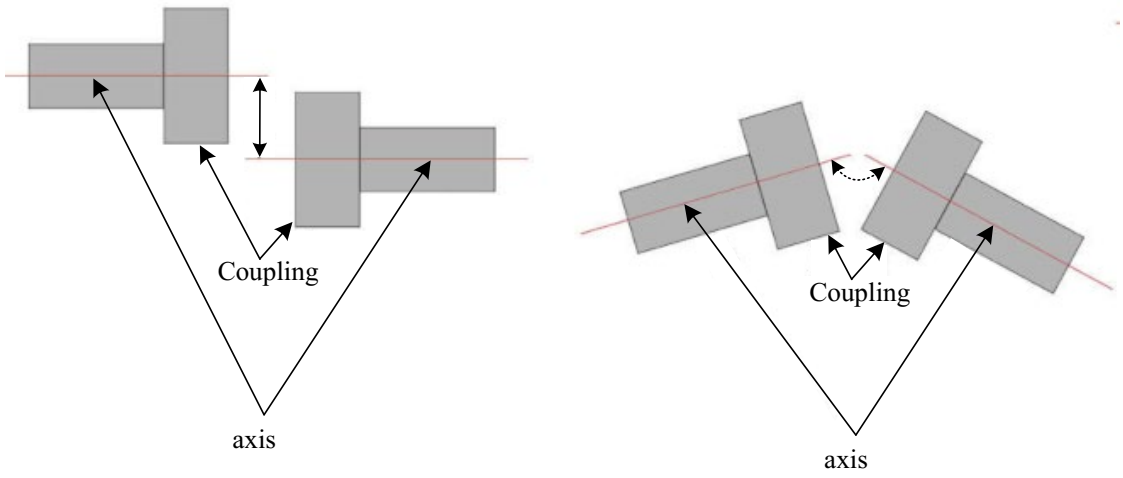


Fig. 1.2 Examples of misalignment fault in shaft: (a) Parallel shaft, (b) Angular shaft [15].

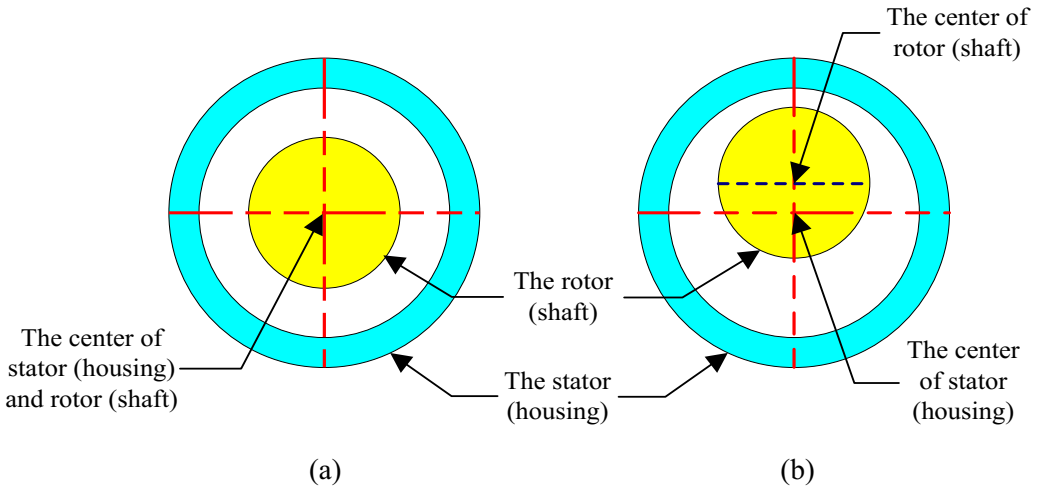


Fig. 1.3 Examples of eccentricity in shaft (a) without eccentricity, (b) with eccentricity [16].

Shaft imbalance fault is related to excessive eccentricity, which occurs when the rotor mass center does not coincide with its rotation center. The imbalance is observed due to errors in mass distribution of the rotor, as illustrated in Fig. 1.3. The imbalance can be caused by reasons such as manufacturing errors and elastic deformation in operation [17]. Gear vibrations in the shafts can also cause eccentricity. In addition, when a shaft skews too much to one side, it may cause lubrication problems. A gearbox without proper lubrication can result in problems related to pressure loss, friction, and excessive wear [18].

### 1.2.2 Gear Faults

Gearbox design is based on power transmission requirements. In parallel shaft gearboxes, gears can have spur or helical forms [19]. In spur gears as shown in Fig. 1.1(b), tooth flanks are parallel to the axis of the shaft, and no extra axial forces are generated in transmission operation in theory. Gear vibrations are generated due to the engagement of the teeth in operation. Helical gears have slanted tooth flanks, as shown in Fig. 1.1(a). In comparison to the spur gears, the helical gears have larger contact ratio, which can transmit larger forces with higher transmission accuracy and less vibration [20].

Gear tooth failures can be classified in two categories: distributed faults and localized defect. In general the initial gear faults are the localized faults such as pitting, and broken tooth [19, 21]. Pitting (i.e., small spalls) can be generated by the removal of surface material due to excess contact fatigue stress as shown in Fig. 1.4. Broken tooth as shown in Fig. 1.5 can be caused due to fatigue, or high impact load on tooth.

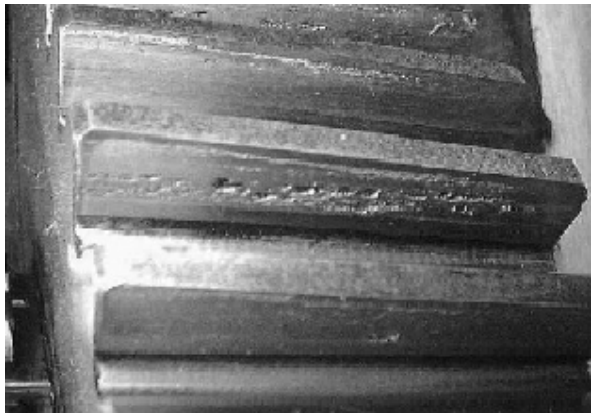

Fig. 1.4 An example of pitting defect in gears [22].

Fig. 1.5 An example of a broken gear tooth defect [23].

Distributed defects include excessive wear and scoring [19, 21]. Wear is a result of continuous, abrasive process of material removal from gear surface. It is typically observed in lack of sufficient lubricant between tooth surfaces, which will result in damage to tooth profile and variable contact ratio. Scoring (i.e., scratches) on the gear surface can be caused by insufficient lubrication in meshing as shown in Fig. 1.6. The

gear has to be replaced when it is damaged to prevent transmission degradation. This work will focus on fault detection of localized gear defects.

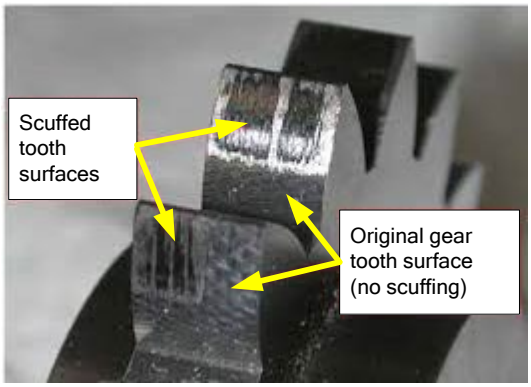


Fig. 1.6 An example of tooth surface severe scoring defect [24].

### 1.2.3 Bearing Faults

Bearings can be classified as journal bearings and rolling element bearings [25, 26]. Journal bearings, also known as sliding bearings, comprise of a rotating shaft (journal) and a fixed bearing. A rolling element bearing has a series of rolling elements between the inner race and outer race to reduce the friction. Rolling element bearings are commonly used in rotating machinery; this work will focus on fault detection in rolling element bearings.

Different from a shaft or a gear, a rolling element bearing is a system consisting of an inner race, an outer race, rolling elements and a cage [25]. Rolling element bearings are classified, on basis of rolling element structures, into balls, cylindrical rollers, tapered rollers, etc. Defects in rolling element bearings are classified as distributed fault (e.g., surface roughness, wear, and misaligned races) and localized defects (e.g., cracks, pits, and spalls). The localized faults are caused by dynamic fatigue loading on bearing components. This work will focus on detecting localized bearing faults.

The bearing fault can occur in the outer race, inner race, or roller elements. Even a healthy bearing generates vibration and noise due to contact stiffness variations. A faulty bearing will generate excessive vibration and noise, which will influence transmission

accuracy [26]. Most machinery defects are related to bearing imperfections. Thus, condition monitoring of rolling element bearings is of higher priority not only in academic research and development but also in industrial applications.

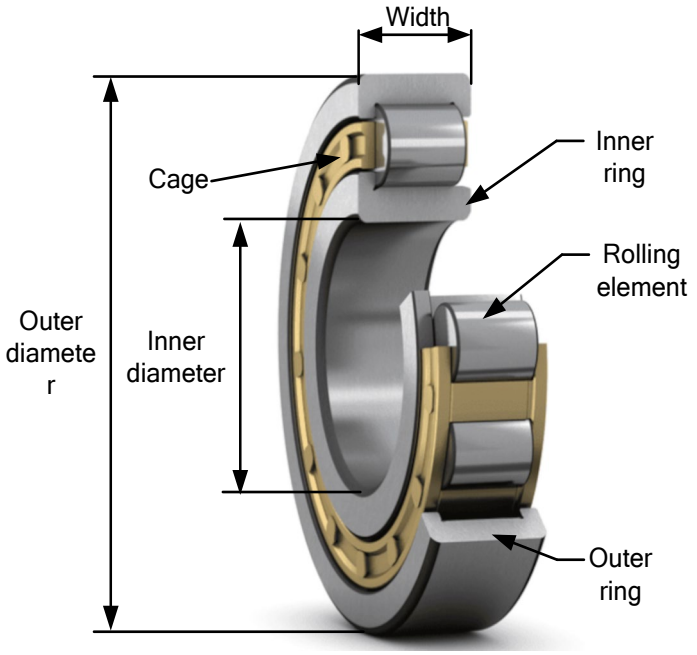


Fig. 1.7 Structure of a rolling element (cylindrical roller) bearing [27].

## 1.3 Literature Review

Fault detection in gearboxes can be undertaken using different type of information carrier such as lubrication, temperature, or vibration [21, 28-29]. Out of all, vibration analysis could be the most commonly used method over thermal analysis and lubrication analysis as it is relatively easy to measure and could provide higher signal-to-noise ratio [30, 31]. Vibration analysis is non-destructive and does not need shut-down of machines; it is easier to be implemented in machines for defect detection than many other types (e.g., lubricant-based) of condition monitoring [32]. The vibration signal from a gearbox is complex in nature and requires advanced techniques to extract representative features to diagnose the presence of machinery faults [6, 8]. Vibration-based analysis will be used in this project.

Every rotating mechanical part generates a specific vibration signature [34]. Even a brand-new healthy gearbox will generate vibration signals, which can be used as the baseline for gear system health condition monitoring [29, 31].

### 1.3.1 Gear Fault Analysis

Gear fault detection can be undertaken in the time, frequency, or time-frequency domains [35-38]. The related signal processing-based fault detection techniques are discussed below.

The vibration signal generated from a gear system in the time domain can be characterized by properties such as the amplitude, statistical measures and phase. On basis of statistical analyses, the signal properties can be processed using indicators like signal demodulation, probability density function and signal average [36, 39]. These indicators are sometimes sensitive to the gear health conditions. The time synchronous averaging (TSA) filtering is a useful method of averaging signals over some cycles/rotations from the measured signals to recognize features to a specific gear [40, 41]. The signal average generated by TSA is a representation of tooth meshing vibration, which could contain the features of gear health conditions [42]. Time domain signal of gear vibration can be used for determining some gear faults and severity of those faults [39, 41-43].

Frequency domain analysis represents the repetitive occurrence of periodic events in a time signal. In a gear system, the energy is mainly distributed around the gear mesh frequency (GMF) and its harmonics [31]. The sidebands of GMF could contain information related to bearing defect and shaft faults (e.g., misalignment, imbalance, etc.). Generally, the frequency domain analysis may provide features to detect stationary gear faults, but it is very difficult to separate gear fault from other events occurring within a gearbox system, especially those time-varying signatures. To resolve this problem, the time-frequency domain analysis of gear systems has been adopted by the researchers.

Time-frequency analysis of a signal can highlight time dependent components in the frequency domain [44]. For example, the EMD method can decompose the signal into

different energy bands in the time-frequency domain for machinery fault detection [45]. The wavelet transform (WT) can predict gear fault from examining abrupt and non-stationary features in signals [44, 46], where the continuous WT can even achieve better time resolution at high frequencies than the discrete WT [47, 48]. Even though there are several approaches proposed in the literature to improve signal processing accuracy, reliable gear fault diagnosis still remains a challenging task because the gear data varies with operating conditions in terms of load and speed. More robust techniques are needed to provide better insight into gear system dynamics so as to improve gear fault diagnosis.

The first goal of this research is to investigate features of different components (e.g., gears and bearings) of a gearbox so as to have a better understanding of the gear vibration signals. An averaged WT technique will be proposed for gear fault detection.

### 1.3.2 Bearing System Faults Analysis

As mentioned in subsection 1.3.3, rolling element bearings generate vibrations even though they are healthy. If a bearing is damaged, extra impacts will be generated, which will excite resonances in the bearing system and the bearing supporting structures [50]. Vibration-based bearing fault detection can also be processed in the time, frequency, and time-frequency domains. Some of bearing fault detection techniques in literature are discussed as below.

If defect occurs on the fixed ring race (usually the outer ring), the fault location is fixed and the impacts between the damaged location and rolling elements are periodic at ball-pass frequency, which is easier to detection [26, 51]. If defect occurs in the rotating ring (i.e., the inner race) or a rolling element, the related vibration signatures could be non-stationary and more difficult to analyze. In a gearbox system, the gear vibrations are dominant signals, which can bury and modulate bearing fault-related signatures [26]. Therefore, for gearbox condition monitoring, bearing fault detection in the time domain still remains a very challenging task in this research and development field, which will be discussed in the following subsection.

In frequency domain analysis, the Fourier transform (FT) can separate periodic features in the original vibration signal [52, 53]. Frequency spectrum can be useful in

analyzing the characteristic frequencies of a bearing especially for outer race defect [53]. However, the energy spectrum of bearing vibration is distributed over a wide range frequency bandwidth and it is difficult to explore fault features with time-varying properties.

Many techniques have been proposed in the time-frequency domain for bearing fault detection, such as the short time FT [54, 56], the Hilbert Haung Transform (HHT) [58, 59] and the WT [60-62]. The short-time FT generates a frequency spectrum related to a selected time window [57], for bearing fault frequency analysis [56]. However, the short-time FT has low resolutions, which makes it difficult to recognize bearing fault information with time-varying properties [26, 56]. The WT uses variable size windows for bearing fault detection, or using large windows to extract low frequency components and short windows to extract high frequency components. In the WT, however, some high frequency components are affected by aliasing and distortion [62]. The HHT decomposes a signal into intrinsic mode functions (IMFs) by using a shifting process [58]. The Hilbert transform can be used to add an imaginary part to each IMF. Although the HHT can generate better resolution over the selected frequency bandwidth, however, the correlation of the IMF with faults is not straight forward and needs advanced investigations to improve bearing fault detection reliability, especially for bearings in gearboxes.

### 1.3.3 Bearing Faults Analysis in a Gearbox

In a multi-component system, such as a gearbox, the signal is a result of integrated effects from all the rotating components [32]. The collected signal is a mixture of bearing data modulated by gear meshing vibrations, which can be observed over any frequency spectrum of a gearbox. This modulated signal is a result of coupling of the gear and bearings through the shaft [62]. Thus, it is very challenging to predict the bearing fault under the modulation of gear mesh vibrations [63, 64]. The researchers face a crucial challenge in designing advanced simulation models for a gearbox that can represent the interaction between the fixed structure and the rotating components of the gear train [32, 66]. The dynamic response of a gearbox is highly influenced by the characteristics of the

support structure used to support rolling element bearings and shafts [56]. Along with modulated side-bands from other components, manufacturing errors in gears can also result in extra dynamic gear mesh forces in the form of amplitude modulation, frequency modulation, and phase modulation [32, 56]. However, the number of sidebands around gear MF and its harmonics may also vary due to change in deformations of the gear train. The components involved in gear load sharing have an impact on the amplitude modulation and the dynamic gear mesh forces [62]. Thus, a strategy to improve diagnostic accuracy is to account impedance of signal transmission path from the vibrating source (fault) to the measurement sensors. To fulfill this requirement, the sensors/transducers should be placed at a location as close as possible to the bearing of interest. The current study aims to separate gear and bearing signatures from gearbox signal for bearing fault detection.

Up to date, machine condition monitoring has gained a drag towards detecting bearing fault in gearboxes under the effect of strong interfering gear signatures [65]. In gearboxes, as gear signatures and bearing signals may inter-modulate each other in a complex way, more emphasis is placed on the process of separating them [66]. The decoupling strategies to achieve this type of distinction are essentially based on recognizing gear signatures as being periodic in nature, whereas bearing signals are random and can be approximated as a second-order cyclostationary function [67]. Such distinction can provide more accurate detection for bearing faults in gearboxes, by separating stochastic (bearing) signals from deterministic (gear) contents [65, 67]. Fault detection of a rolling element bearing in gearboxes can be achieved by different vibration-based monitoring techniques, which can be classified into time domain, frequency domain, and time-frequency domain analysis. A brief discussion of techniques from each domain is provided below.

In time domain analysis, statistical parameters could be the most commonly used fault detection technique. In this method, a comparison is made between the information obtained from current state of the gearbox to the characteristics determined at its healthy state [68]. Some of the fault detection techniques are based on the TSA signals [69]. However, this analysis needs prior knowledge of the operating frequency, to extract the

periodic signal. These techniques, however, have limitations that they are sensitive to different load and speed conditions. Some time domain techniques are also implemented into linear prediction, such as autoregressive models using the Yule-Walker method [70], by which the future samples are predicted based on previously determined samples. However, an autoregressive model has a major limitation that the modeling process cannot properly use all of the available information. As a result, it becomes difficult to detect the consequential mesh harmonics and corresponding sidebands in gearbox spectra, because the each spectral component has a complex interaction with other components.

In frequency domain analysis, the envelope spectrum of the measured signal is one of the common techniques for bearing fault diagnosis [71]. However, the envelope spectrum cannot differentiate between the bearing fault and the high energy deterministic spectral components of gear MF and its harmonics. As a result, the bearing characteristic frequencies are usually coated by these high-energy spectral components of gear MF in the amplitude spectrum [72]. The inverse FT of the estimated spectrum, referred to as Cepstrum analysis, can detect echoes in acoustic signals, which can use an equivalent liftering approach to remove harmonics but preserving the resonances [73-75]. Even though it could be used to separate the bearing signatures from the gear vibration signal, it may not be suitable to detect a bearing defect in the machine where prior baseline information is not available.

The time-frequency analysis can study multi-resolution information in the vibration signals, for the examination of transient feature properties, using techniques such as the short-time FT [76-78], HHT [79, 81], and WT [82-84]. These techniques can analyze non-stationary signals with time-varying spectral contents and statistical properties. The short-time FT performs the FT over a time-shifted window, which is capable of extracting spectral information from the gearbox and bearing vibration signals [76, 77]. However, as discussed in section 1.3.2, the short-time FT cannot differentiate some frequencies in a signal due to the use of fix windows in analysis [78].

As commented in subsection 1.3.3, the HHT utilizes EMD to extract IMFs from the non-stationary signal and then applies the Hilbert transform for signal property analysis [79- 80]. Although EMD can decompose the signal into various frequency components, the presence of noise interference may impact results [81]. In recent years, the Variational Mode Decomposition (VMD) technique has been used to reduce errors occurring during the EMD decomposition [85]. VMD implements a concurrent variational model to minimize errors between the extracted IMFs. In contrast to the classical EMD method, the VMD has rigorous mathematical foundations for decoupling different features [86]. However, the VMD requires some complex post-processing procedures due to interaction between different spectral components. In processing the vibration signals from a gearbox, which are non-stationary and nonlinear, the complex computation in VMD would limit its application in real-time machine health monitoring.

### 1.3.4 Neuro-Fuzzy Classifiers

From the aforementioned analysis, each fault detection technique has its own merits and limitations to predict defects in bearings and gears. For automatic condition monitoring, some intelligent tools can be used to integrate the merits of several fault detection techniques for real-time machinery health fault diagnosis.

Decision-making is a process to classify representative features into different health categories of a machinery system. Soft-computing tools have been widely used in automatic fault diagnosis, by the use of tools such as fuzzy logic, neural networks, and synergetic paradigms such as neuro-fuzzy (NF) schemes for machinery fault diagnostics and prognosis [87-89]. In most of these diagnostic classifiers, fixed reasoning structures were used in reasoning operations, while system parameters were updated online. But these classifiers with fixed reasoning structures may not be suitable for monitoring applications of gearbox systems with time varying operating conditions. An alternative solution to this problem is implementing some clustering algorithm to diagnostic classification.

An evolving system uses some clustering algorithm to generate classifier structures, while system parameters are properly trained. Continuous and gradual adaptation will

make the classification operation smooth and regular over different input information [90]. As a fuzzy system is a universal approximator and can extract knowledge with mimic of human reasoning to understand and predict the outcome of a decision-making process [91], it is generally used as the platform in designing evolving systems. For example, Angelov et al. proposed an evolving Takagi-Sugeno (eTS) scheme for system control [92]. Formation of the clusters was determined by a potential measure in terms of the center and spread of clusters, while a least square estimator algorithm was used to update linear parameters. Pratama et al. suggested a parsimonious ensemble evolving classifier [93] to make adaptive selection of input features, where the selection of subset varied in each iteration; a problem of this clustering approach, however, is that the predefined cluster information (e.g., centers and spreads) is sensitive to noise in the data sets and processing errors. Kasabov suggested a transductive NF inference (TWNFI) system by taking weighted data normalization for transductive reasoning [94]. Comparing with the eTS in modeling of non-linear systems, the TWNFI usually generates more clusters/rules and thus may result in lower processing efficiency [90, 91].

One of the problems in the aforementioned evolving classifiers is related to their blind classification of the output space, which could degrade the diagnostic reliability. In order to tackle this problem, the third objective of this work is to develop a new evolving NF classifier for real-time gearbox health condition monitoring.

## 1.4 Proposed Research Objectives

Based on the aforementioned analysis, specific research objectives of this work are summarized as follows:

1) A new signal processing technique will be proposed to extract representative features for gear fault detection in a gearbox.

2) A novel envelope decomposition technique will be suggested for fault detection in rolling element bearings. This technique will tackle the problem of overlapping at nodes to preserve the fault information in mode functions.

3) A new adaptive evolving NF classifier will be developed to integrate the merits of several fault detection techniques for automatic fault diagnosis and condition monitoring in gear systems.

4) A new training algorithm based on normalized Adadelta (NaD) will be proposed to train system parameters in the evolving NF classifier.

5) The effectiveness of the proposed techniques will be verified by simulation and experimental tests.

## 1.5 Thesis Outline

The outline of this study is as follows:

Chapter 2 discusses the averaged WT technique for gear system analysis to detect faults.

Chapter 3 presents the proposed local mode decomposition technique for bearing fault detection.

Chapter 4 discusses the developed evolving NF system for diagnostic classification of gear systems. A normalized adadelta method is proposed to train system parameters of the evolving NF classifier.

Chapter 5 presents the experimental examination to examine the effectiveness of the proposed techniques.

Chapter 6 summarizes concluding remarks of this study and future research.

# Chapter 2

# Averaged Wavelet Analysis for Gear Faults

## 2.1 Introduction to Gear Fault Analysis

Gear systems are universal and irreplaceable for mechanical power transmission in many industries. The dynamic response of gear systems can be very complex due to excitation torque, multiple teeth contact, and backlash between teeth surfaces [95, 96]. As a result, under varying load, a distinctive gear system generates non-linear signals with complex behavior [97].

Gear fault consists of localized damage and distributed defects (e.g., wear and pitting). This study focuses on localized gear fault diagnosis because initial gear damage is a localized fault, while a distributed defect also initiates from a localized fault. Furthermore, a localized fault will not only generate transmission errors but it also may cause sudden failures. For example, a tiny fatigue crack may occur at a gear tooth due to dynamic loading and stress concentration, which may then grow continuously. Unfortunately, by the time the crack is visible, the gear may be more than 90% used up. When a tooth is broken out, the following teeth will be damaged quickly because of the extra impact. As discussed in Chapter 1, this research is using vibration signal analysis for gear system health monitoring.

In gear systems, vibration signals are inherent to gear mesh operation. During a contact between gear teeth, an impact is produced, resulting into a vibration signal. The frequency of impact is represented as a GMF $f_m$ [98, 99]. For a healthy gear system, the gear mesh vibration energy is concentric at the GMF and its harmonics. When the gear teeth have defects, such as crack, the stiffness at the contact point is modulated and the resultant vibration will have higher amplitude at second and third harmonic of the GMF [100].

The time domain vibration signal of a gear is periodic with respect to its rotation. In time domain analysis, the gear signal can be firstly processed by time-synchronous

average (TSA) by filtering out the vibration signals non-synchronous to the rotation of the gear of interest [101]. The signal average then can be used for advanced analysis to detect presence of fault and its severity.

A frequency spectrum of a normal gear train mainly presents peaks at rotation frequencies of the gears and to the GMF ($f_m$) of each pair of gear in contact [98]. On the other hand, gear vibrations are sensitive to the load conditions and peaks in frequency spectrum do not always correspond to faults. Some other factors to influence the vibration spectrum include surface finish of gear teeth, irregular concentricity of teeth profile, and gear misalignments [102]. Based on the frequency domain analysis, the faults with periodic features can be distinguished based on gear characteristic frequencies. But for gear defect with non-periodic features caused by impacts, researchers are moving towards time-frequency analysis.

A fault gear train generates non-stationary signals with distinct frequency characteristics [103]. In such cases, it is recommended to use techniques that offer combined time-frequency analysis, to provide comparative indications of changes in frequency with time. It can prevent loss of information of dynamic functions localized in the time domain and/or the frequency domain in gear signal processing.

Many techniques have been proposed in the literature for gear signal analysis and fault detection in the time-frequency domain [104, 105], such as using the WT [106, 107]. This study will extract time-domain features using the WT to detect presence of fault in gear system, in order to provide a more accurate gear fault detection technique to minimize machinery maintenance costs.

## 2.2 Analysis of Gearbox Signals

### 2.1.1 Gear Mesh Frequency

Gearbox consists of multiple pairs of gear trains, the corresponding GMF $f_m$ is determined by:

$$f_m = Z f_r; \tag{2.1}$$

where $Z$ is the number of teeth of the gear of interest, and $f_r$ is running speed of the gear.

For a healthy gear system, the corresponding vibration signal spectrum has dominating components of GMF and its harmonics. Depending on the contact location of gear, there exists a varying force in gear mating operations due to variable contact stiffness [131, 132], which depends on GMF $f_m$ and its harmonics [69, 133].

### 2.1.2 Time Synchronous Average Filtering

Time synchronous average (TSA) is a signal averaging process over a certain number of rotations of the gear of interest (or the shaft) in the gearbox [134]. It can extract signature to a specific gear by filtering out the signals non-synchronous to the rotation of the gear. The output is the signal average $X[n]$ represented over one revolution of the gear:

$$X[n] = \frac{1}{Z}\{\sum(x[n+(z-1)N])\}; \tag{2.2}$$

where $x[n]$ is the collected vibration signal over $Z$ revolutions, and each revolution is consisting of $N$ data samples, $n$ = 0,1, …, $N$-1.

Nevertheless, a major drawback of this TSA method is the loss of scattered information that could contain representative fault features of a gear system [11, 135]. There are many techniques proposed in literature for gear fault detection. For example, the amplitude modulation analyzes the signal envelope, which could be used for gear fault analysis [108]. The phase demodulation analysis can be applied to examine gear fault-related phase distortion [108].

## 2.3 Wavelet Transform Analysis

The WT is a recently developed signal processing technique with a strong potential in time and frequency domain analysis. The WT is independent of time and can provide detailed information regarding local events of the signal. The WT uses wavelets and a set of elementary functions to decompose and reconstruct the signal for advanced processing of signal properties.

In recent decade, many WT analysis techniques have been proposed for fault detection and diagnosis of rotating machines. A time-frequency spectrum reveals the magnitude of signal's frequencies along with the time duration of each individual frequency [26, 108]. In particular, during condition monitoring of a gearbox, the WT can be used for identification of the transients in vibration signals, which are generated by faults [109]. The WT acquires numerous resolutions for localization of the short time components from different types of gear faults, highlighted with time-scaled distribution analysis [110, 111]. The WT represents the amplitude $W(a,b)$ in terms of the mother wavelet function around region of $(b,\omega_0/a)$ such that:

$$W(a,b) = \frac{1}{\sqrt{|a|}} \int_{-\infty}^{\infty} x(t) \Psi^* \left( \frac{t-b}{a} \right) dt; \tag{2.3}$$

where $\Psi^*$ is the mother wavelet function, $a$ is the scale factor (index) and $b$ represents the time shifting parameter.

Based on the type of mother wavelet function ($\Psi^*$), the WTs are categorized into three classes: the continuous, discrete and multi-resolution WTs. The continuous WT compares the signal with shifted and scaled copies of mother wavelet. The continuous WT is very resistant to the noise in the signal, which helps to extract more information regarding the system [112]. In the continuous WT, the signal of finite energy is processed in the time-frequency domain by the shifts of mother wavelet function ($\Psi^*$) in $L^2(R)$ universe. The subspace of scale $a$ is defined by:

$$\psi_{a,b}(t) = \frac{1}{\sqrt{|a|}} \Psi^*_{a,b} \left( \frac{t-b}{a} \right); \tag{2.4}$$

where $\Psi^*$ is the mother wavelet function, $a$ represents the scale factor (index) and $b$ represents the time shifting parameter.

The projected signal in the subspace of scale $a$ can be expressed as:

$$w_a(t) = \int_R W_\psi \{x\}(a,b) \bullet \psi_{a,b}(t) db; \tag{2.5}$$

where the wavelet coefficients are $W_{\psi}\{x\}(a,b) = \int_R x_a(t)\psi_{a,b}(t)dt.$

In general, the continuous WT uses wavelet decomposition or reconstruction of the signal [113]. The classic mother wavelets include poisson wavelet, shannon wavelet, or morlet wavelet. The poisson wavelet has a single peak; but the signal from a gear system has multiple impulses. The shannon wavelet is either a real or a complex type. The morlet wavelet is composed of a complex exponential function (carrier signal) multiplied by a Gaussian window (envelope), as shown in Fig. 2.1.

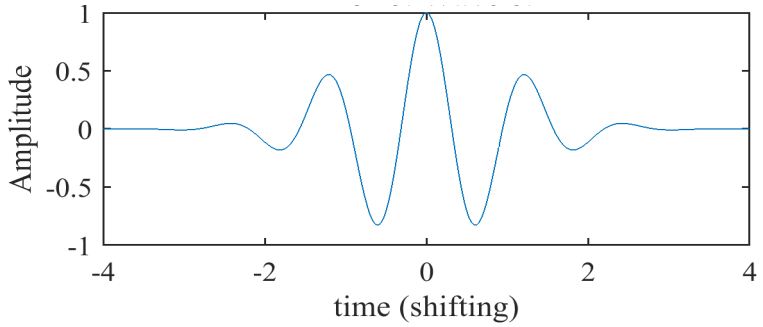


Fig. 2.1 Morlet wavelet function

The morlet wavelet function can be defined as:

$$\Psi_{\sigma}(t) = c_{\sigma}\pi^{-\frac{1}{4}}e^{-\frac{1}{2}t^2}\left(e^{i\sigma t} - e^{-\frac{1}{2}\sigma^2}\right); \tag{2.6}$$

where $\sigma$ is the spread which can define the time and frequency resolutions (usually $\sigma > 5$), and $c_{\sigma}$ is normalization constant defined as:

$$c_{\sigma} = \left(1 + e^{-\sigma^2} - 2e^{-\frac{3}{4}\sigma^2}\right)^{-\frac{1}{2}}. \tag{2.7}$$

As the Morlet mother wavelet function can match gear fault feature properties better, it will be used in this work for gear fault detection.

## 2.4 Averaged Wavelet Power Spectrum Analysis

As discussed in section 2.2, the WT is time-frequency domain analysis, implemented to analyze signal properties with complex structures. The morlet mother wavelet will be used for analysis. The proposed averaged wavelet power spectrum analysis technique follows the following procedures for gear fault detection:

Step 1: Input gearbox vibration signal $x(t)$ and the one-pulse-per-revolution (reference) signal $p(t)$.

Step 2: Perform the TSA filtering to get the signal average $y(t)$ from the vibration signal $x(t)$.

Step 3: Calculate the continuous wavelet coefficients $w_a(t)$ from Eq. (2.5).

Step 4: Calculate the averaged wavelet function $T_a(t)$:

$$T_a(t) = \frac{1}{\overline{w_a(t)}} \sum_{t=0}^{T} w_a(t); \tag{2.8}$$

Step 5: Generate the power spectrum of averaged wavelet function $T_a(t)$ to highlight the fault features for fault detection.

## 2.5 Gear Health Monitoring Indices

In this study, the fault diagnosis of a gear system is conducted gear by gear. As stated before, because the measured vibration is an overall signal generated from various rotary sources, the primary step is to differentiate the signal specific to each gear by using the TSA filter [107]. In this filtering process, all of the signals that are non-synchronous to the rotation of the gear of interest (e.g., those from bearings, shafts, and other gears) are removed. As a result, each gear signal is computed and represented in one full revolution, which is called the signal average that will be used for advanced analysis.

Several techniques have been proposed in the literature for gear fault detection. Because of the complexity of the machinery structure and operating conditions, however, each signal processing technique has its own advantages and limitations and could be useful for specific applications only [107]. The more features are applied in fault

diagnosis, however, the more possible it is to achieve conflicting diagnostic results. In this work, three features are employed for this diagnostic classification. The selected features should be robust, or sensitive to component defects but insensitive to noise (i.e., the signal not carrying information of interest). The selected features are from three information domains—energy, amplitude, and phase:

1) wavelet energy function, using the overall residual signal that is obtained by a bandstop filtering out the GMF $f_m = f_r Z$ and its harmonics, where $f_r$ is the rotation frequency (in hertz) of the gear of interest, and $Z$ is the number of teeth of the gear;

2) beta kurtosis, using the overall residual signal; and

3) phase demodulation [108], using the signal average. The reference functions are proposed as follows.

1) Wavelet Energy Reference Function $W(z)$:

If $R(t)$ is the overall residual of the signal average $y(t)$ , the wavelet energy function is proposed as

$$W(z) = \int_{f_1}^{f_2} \left| \int_0^{\infty} R(t) \sqrt{a} \Psi(t-\tau) d\tau \right| ds; \tag{2.9}$$

where $a$ and $t$ are the scale (frequency) variables and time variables, respectively, and $f_1$ and $f_2$ are the frequency limits of interest. For the gear system in this paper, $f_1 = 0.5Zf_r$, and $f_2 = 4.5Zf_r$; $\Psi(t)$ is the mother wavelet, which is a modified Morlet function

$$\Psi(t) = \exp\left( -\frac{9 \ln 2}{\pi^2} f_r^2 t^2 \right) \exp(2\pi k f_r t); \tag{2.10}$$

where $k = 1, 2,..., 5Z$.

2) Beta Kurtosis Reference Function $B(z)$:

The beta kurtosis is the normalized fourth moment of a signal in terms of the beta function instead of a generally used Gaussian function. If $\mu_z$ and $\sigma_z^2$ represent the mean

and variance of a one-tooth data block $T_z$, centered at $z$, then the Beta Kurtosis reference function $B(z)$ is defined as the reciprocal of the kurtosis

$$B(z) = \frac{\alpha\beta(\alpha+\beta+2)(\alpha+\beta+3)}{3(\alpha+\beta+1)(2\alpha^2 - 2\alpha\beta + \alpha^2\beta + \alpha\beta^2 + 2\beta^2)}; \tag{2.11}$$

where $\alpha = (\mu_z / \sigma_z^2)(\mu_z - \mu_z^2 - \sigma_z^2)$; and $\beta = ((1-\mu_z)/\sigma_z^2)(\mu_z - \mu_z^2 - \sigma_z^2)$. The details about derivation of Eq. (2.11) can be found in [89].

3) Phase Modulation Reference Function $P(z)$:

For a pair of healthy gears with sound installation and ideal operating conditions, the meshing vibration $y(t)$ can be approximately expressed as

$$y(t) = \sum_{m=o}^{M} A_m \cos(2m\pi f_r Z t + \theta_m); \tag{2.12}$$

where $M$ is the total number of mesh-frequency harmonics considered.

If a fault occurs in one tooth, because of a change in tooth stiffness, the amplitude and phase functions of the gear mesh vibration will be modulated such that

$$y(t) = \sum_{m=o}^{M} (A_m + a_m) \cos(2m\pi f_r Z t + \theta_m + \varphi(t)); \tag{2.13}$$

The phase modulation $\varphi(t)$ can be obtained from the analytical signal of Eq. (2.13), which is computed by taking the Hilbert transformation of $y(t)$. The phase reference function $P(z)$ is suggested as the maximum phase difference over a tooth period $T_z$ centered at $z$, or

$$P(z) = \varphi_{\max}(\tau) - \varphi_{\min}(\tau); \quad \tau \in [z - 0.5T_z, z + 0.5T_z]. \tag{2.14}$$

4) Gear Monitoring Indices:

Based on the derived reference functions, the monitoring indices are determined to quantify the feature characteristics, which are further used as input for gear health classification in Chapter 5. The monitoring indices are proposed as the normalized maximum amplitude values of the reference functions:

$$\begin{aligned} x_1 &= \frac{\max(W(z)) - \overline{W(z)}}{\sigma_w}; \\ x_2 &= \frac{\max(B(z)) - \overline{B(z)}}{\sigma_b}; \\ x_3 &= \frac{\max(P(z)) - \overline{P(z)}}{\sigma_p}; \end{aligned} \tag{2.15}$$

where $\sigma_w$, $\sigma_b$, and $\sigma_p$ are the spreads of the wavelet energy, beta kurtosis, and phase modulation reference functions, respectively; $\overline{W(z)}$, $\overline{B(z)}$, and $\overline{P(z)}$ are the respective mean values of the three functions outside the maximum locations (with one tooth period, $T_z$).

Usually, these three maximum index values occur within a few tooth periods if the signature irregularity is caused by a real fault [114]. Thus, four tooth periods are selected to be an influence window in this work. If the indices in Eq. (2.15) are not within one influence window (e.g., no fault or more than one fault), more than one set of inputs should be provided to the diagnostic system. For example, if $x_3$ does not fall within the influence window determined by $x_1$ and $x_2$, two sets of inputs will be given to the diagnostic system. The first input is $\{x_1, x_2, x_3\}$, where $x_3 = \max\{P(\tau)\}$, and $\tau$ lies in the influence window determined by $x_1$ and $x_2$. The second input is $\{x_1, x_2, x_3\}$, where $x_1 = \max\{W(\tau)\}$, $x_2 = \max\{B(\tau)\}$, and $\tau$ lies within the influence window determined by $x_3$.

## 2.6 Gear Fault Analysis

A 2-stage gearbox system will be analyzed in this study, as illustrated in Fig. 2.2. There are 2 gear pairs, where first gear pair has 32 and 80 teeth on pinion and gear,

respectively, and second gear pair has 96 and 48 teeth on pinion and gear, respectively. The vibration signal is collected from the system using vibration accelerometers.

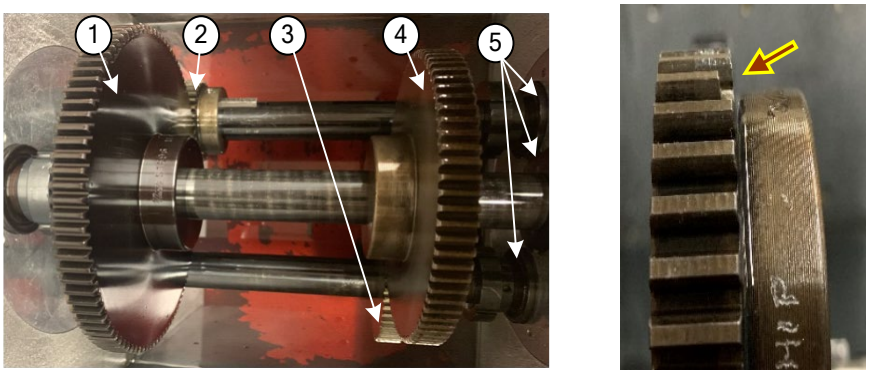


(a) (b)

Fig. 2.2 (a) A two-stage gear system: (1) input gear; (2) input pinion; (3) output pinion; (4) output gear (5) the roller bearings. (b) A simulated damaged gear with one partially broken tooth (chipped gear).

In this work, the pinion of first gear pair is used for analysis. Three different gear health conditions are for analysis: (a) healthy gear, (b) cracked gear, and (c) broken tooth gear. Further details are discussed in following section.

## 2.7 Result Analysis

Fig. 2.3 shows part of the corrected vibration signal of gearbox. The TSA filtering is used to differentiate the gear signal from the rest of the components, as shown in Fig 2.4. The TSA signal is further analyzed using the WT to obtain time-frequency components of the gear of interest, as illustrated in Fig. 2.5-2.7. In the WT maps, the *x*-axis represents number of samples (time domain), *y*-axis denotes the scale factor (frequency domain) and the color (*z*-axis) represents the wavelet energy amplitude.

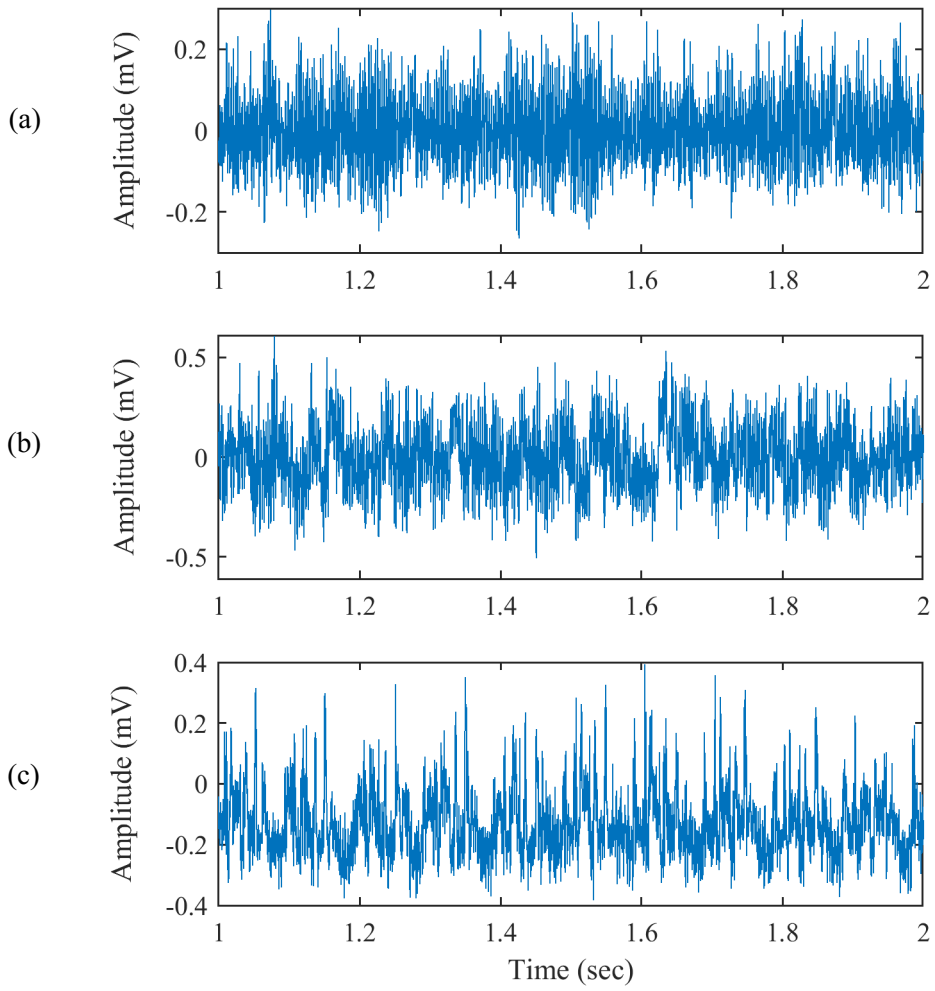


Fig. 2.3 Part of the collected gear signals from different gear conditions: (a) Healthy gear, (b) gear with crack fault, (c) a gear with broken tooth fault.

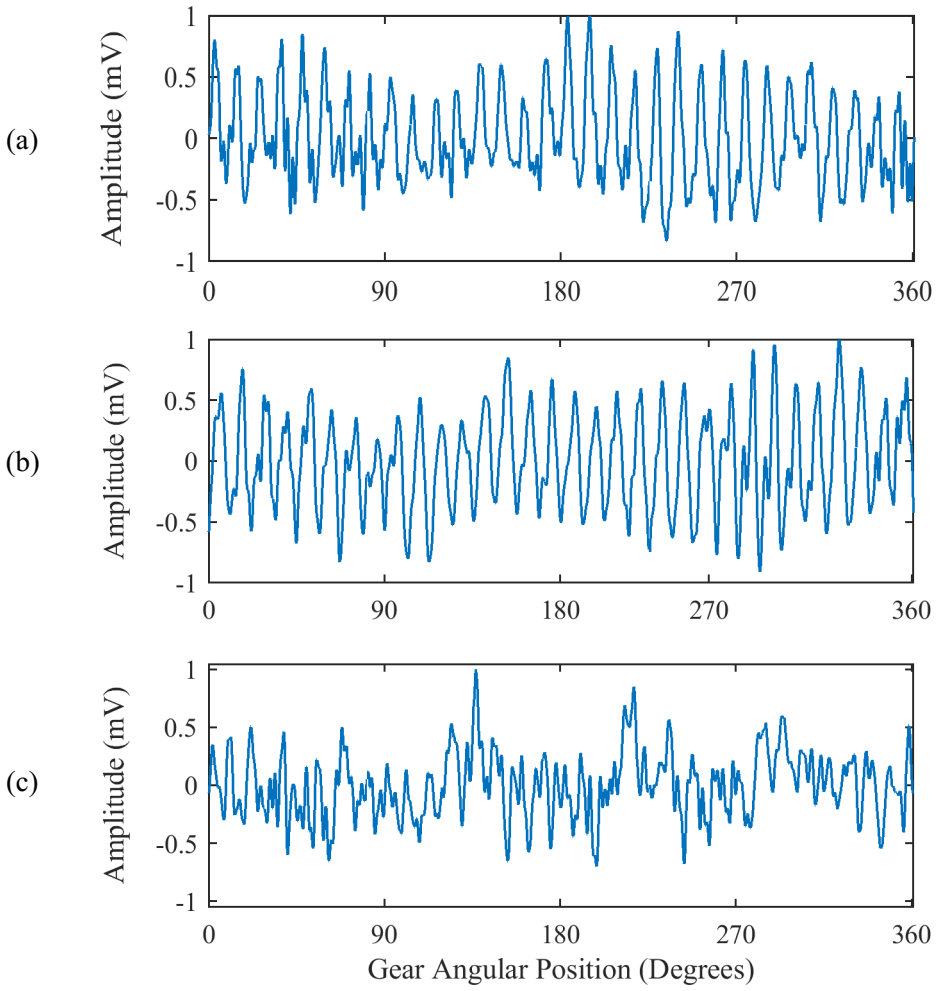


Fig. 2.4 TSA of gear signal from different gear conditions: (a) Healthy gear, (b) a gear with crack fault, (c) a gear with broken tooth fault.

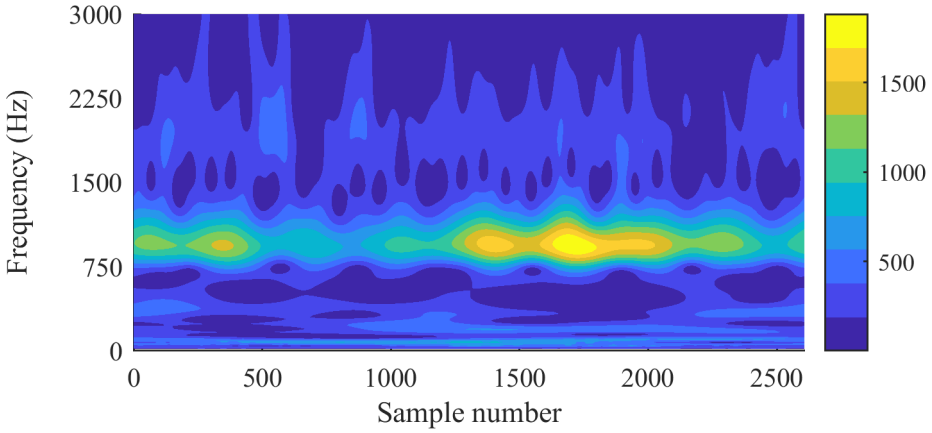


Fig. 2.5 Wavelet transform of the healthy gear signal.

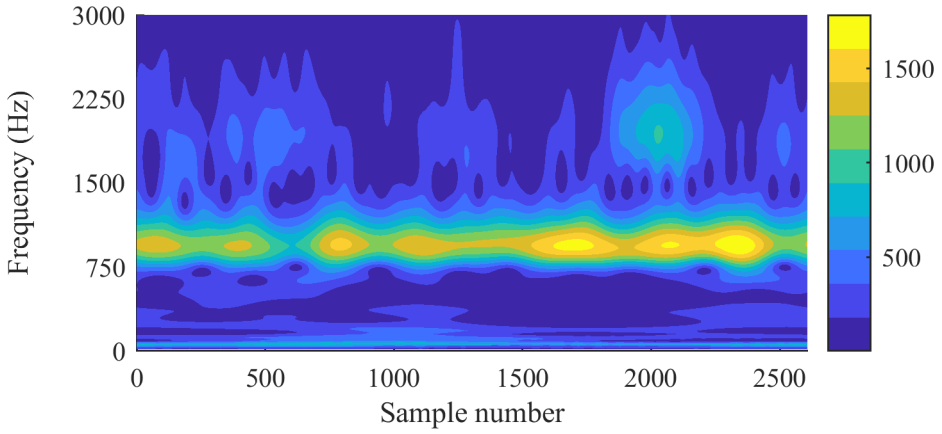


Fig. 2.6 Wavelet transform of the cracked gear signal.

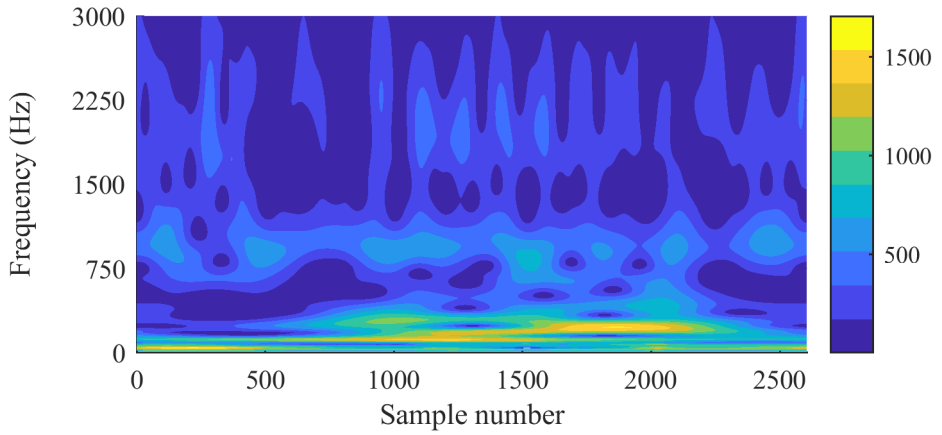


Fig. 2.7 Wavelet transform of the broken tooth gear signal.

The averaged wavelet technique will convert 3D wavelet energy representation into a 2D spectral map, which can highlight the peaks of the output as shown in Fig. 2.6. It is observed that the processing results from healthy gear (Fig. 2.8(a)) and cracked gear (Fig.2.8(b)) show peaks at GMF (i.e., 960 Hz), but the signature of the crack gear (Fig. 2.8(b)) is almost doubled the amplitude in comparison of healthy gear (Fig. 2.8(a)). The broken tooth data (Fig. 2.8(c)) shows peaks at the shaft speed (i.e., 30 Hz), due to one strike per rotation of the gear shaft.

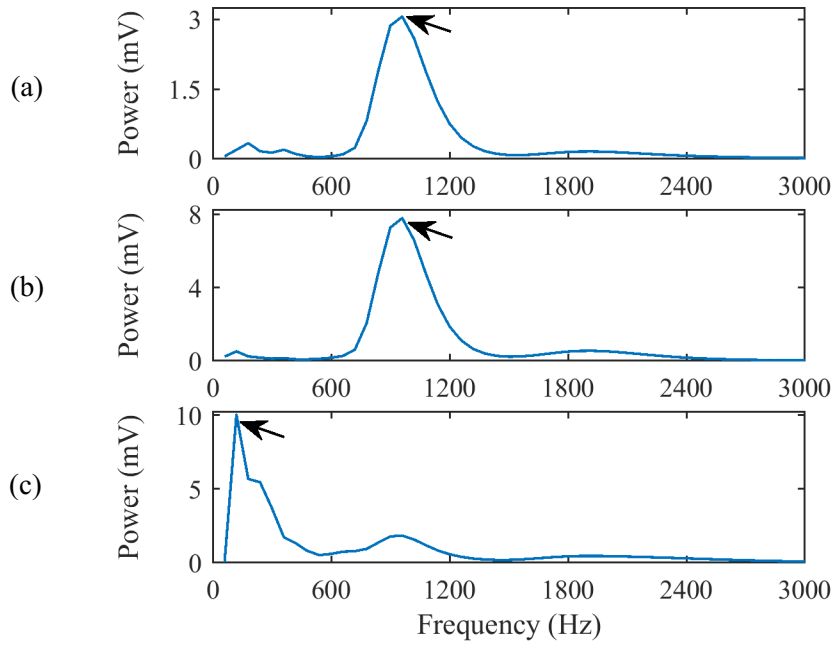


Fig. 2.8 Averaged power wavelet spectrum for gear system (a) Healthy gear, (b) cracked gear, (c) broken tooth gear.

These monitoring indices will be used in the developed evolving NF classifier in Chapter 4 for real-time gear system monitoring.

## 2.8 Discussion

Gear fault analysis plays a significant role for condition monitoring of gearbox systems. The output of the wavelet analysis can provide promising results for time-frequency analysis. Though the output has complex coefficients, it can provide the fault features/information. The averaged wavelet features obtained from wavelet coefficients can extract the frequency features and can transform the complex coefficients into 2D graphs. The averaged wavelet spectrum can highlight the spectral peaks and fault characteristic frequencies to improve the accuracy of fault diagnosis of gear systems.

# Chapter 3

# Local Mode Decomposition (LMD) Technique for Bearing Fault Detection

## 3.1 Bearing Faults in a Gearbox

The gearbox has a complex system consisting of many components, each having its own specific faults and corresponding dynamics. It is necessary to study the health conditions of each of these components in the gearbox. As discussed in Introduction, gears and bearings are main reasons of faults in a gearbox. As discussed in Chapter 2, gear signals are periodic and strong in magnitude, which are relatively easier to analyze [26]. But bearing signals are usually weak in magnitude and modulated by strong gear meshing vibrations, and thus bearing signatures are difficult to extract from the collected vibration. This chapter focuses on bearing fault detection using the proposed local mode decomposition (LMD) technique.

Many studies have been undertaken for bearing fault detection in gearboxes [26, 115]. In general, vibration-based analysis is more reliable for fault detection of bearings in a gearbox, due to its higher signal-to-noise ratio. The contact of defect and rolling elements generates repetitive impulses with specific resonance properties. The signal from a bearing could be in high frequency or low frequency, depending on the location and type of the bearing defect [116]. The signals measured from a gearbox could contain vibration components not only from rolling element bearings, but also from the drive motor, gears, shafts, couplings, etc., which are very complex for direct analysis. In this study, the sensors are installed on the gearbox housing near the bearing of interest to minimize the vibratory effect from other components in the gearbox.

Fig. 3.1 shows a rolling element bearing, where $d$ is the rolling element (ball) diameter, $N_b$ is number of rolling elements (balls), $\theta$ is the contact angle, and $D$ is the pitch diameter. If the shaft rotating frequency is $f_r$ in Hz, the fault characteristic frequencies (in Hz) for defect on the outer race $f_{OR}$, inner race $f_{IR}$, and roller ball $f_{RB}$ will be [117]:

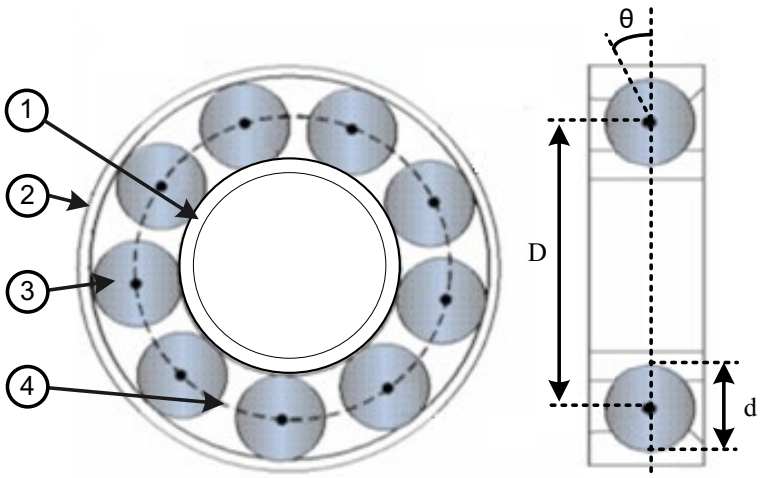


Fig. 3.1 Structure of a rolling element bearing 1) inner race, 2) outer race, 3) rolling element (ball), 4) cage [118].

$$f_{OR} = f_r\left[\frac{N_b}{2}\left(1-\frac{d\cos\theta}{D}\right)\right]; \tag{3.1}$$

$$f_{IR} = f_r\left[\frac{N_b}{2}\left(1+\frac{d\cos\theta}{D}\right)\right]; \tag{3.2}$$

$$f_{RB} = f_r\left[\frac{D}{d}\left(1-\frac{d^2\cos^2\theta}{D^2}\right)\right]; \tag{3.3}$$

## 3.2 Proposed Local Mode Decomposition (LMD) Technique

As discussed in Introduction in Chapter 1, bearing fault analysis can be performed in different processing domains. In the time domain, for example, bearing fault can be detected by statistical moment indicator analysis [47-49, 51] and envelope analysis by examining the high frequency components [52, 53]. In frequency domain analysis, for example, depending on the running speed and bearing geometry, the bearing fault characteristic frequencies are calculated first, bearing health condition can then be analyzed by examining spectrum properties with the comparison of these theoretical fault characteristic frequencies. In general, if defect occurs on the outer race, the fault features are periodic in nature and relatively easy to detect. However, if defect occurs on the rotating ring (e.g., the inner race) or a rolling element, fault features may be non-periodic

in nature especially considering slip and elastic deformation, which is difficult to detect. A new LMD technique will be proposed in this work to tackle this challenge.

### 3.2.1 Basic Mode Decomposition Techniques

As summarized in Chapter 1, a lot of research efforts have been undertaken to propose signal processing techniques in the time-frequency domain for bearing fault detection in recent decends [116]. Some of well-accepted methods include the empirical mode decomposition (EMD), Hilbert-Haung transform (HHT), ensembled EMD, and local-mean decomposition (LD), etc. [118-121].

The EMD is a process of decomposing the signal in the time domain to generate intrinsic mode functions (IMFs). An IMF should meet two mode function requirements [119]:

1) An IMF has a mean value of zero;

2) The difference between the numbers of extrema points and zero crossing points is no more than one.

Each IMF has information of frequency behavior of the original signal. The selected number of IMFs for analysis depends on the complexity of the signal and analysis requirements.

The HHT can highlight the frequency components by applying the Hilbert transform and spectral analysis. The Hilbert transform is a process of extracting instantaneous frequency from IMFs by adding the corresponding imaginary part for each IMF. The HHT results can be represented in a time-frequency distribution to highlight the localized features that could be associated with signature transients or bearing faults [119]. The ensembled EMD is a time-domain analysis method, with white noise added to the signal [120]. The ensemble of a signal is calculated by a shifting function and the output is computed by averaging to remove the white noise from the signal. In general, the ensembled EMD can provide better solution than EMD, but it needs a proper selection of white noise amplitude [121].

The LD method is proposed in [122] for time-variant signal analysis, which focuses on local trends like fault features in a signal. The LD decomposes a signal into a series of mono-component signatures, referred to as product functions that are products of envelopes and frequency modulated signatures. The LD uses the moving average to gradually smooth a signal. Similar to EMD, the LD also calculates the instantaneous frequency of each product functions, which has been used in fault detection in rotating machinery [121]. However, the LD has some drawbacks in applications:

(a) The orthogonality between product functions and their corresponding instantaneous frequencies is difficult to achieve in many applications.

(b) In product function computation, some outliers are observed, which can affect the decomposition results.

(c) It has mode mixing effect, which will cause distortion to some of the product function signatures.

(d) It is not robust in application for bearing fault detection applications.

To tackle these related problems in the LD, a new LMD technique will be proposed in this work to extract and highlight fault features for bearing fault detection in gearboxes.

### 3.2.2 The Proposed LMD Technique

The processing procedures of the proposed LMD technique are illustrated in Fig. 3.2, which are summarized below:

Step 1: Extract all the local envelope from the signal. Calculate local mean values $M(t)$ based on the upper envelope $E_U$, and lower envelope $E_L$.

$$M_i(t) = \frac{E_U + (-E_L)}{2}; \tag{3.4}$$

Step 2: Calculate the average envelope $E_i(t)$ :

$$E_i(t) = \frac{E_U + E_L}{2}; \tag{3.5}$$

Step 3: Calculate the local signal $L_i(t)$:

$$T_i(t) = x(t) - E_i(t); \tag{3.6}$$

$$L_i(t) = \frac{T_i(t)}{M_i(t)}; \tag{3.7}$$

Step 4: Use $L_i(t)$ as a new signal if it does not meet the mode functions requirements as mentioned in subsection 3.2.1. Repeat Steps 1-3. For the $i^{th}$ iteration, Eq. (3.6) and Eq. (3.7) become:

$$T_i(t) = L_i(t) - E_i(t); \tag{3.8}$$

$$L_i(t) = \frac{T_i(t)}{M_i(t)}; \tag{3.9}$$

Step 5: If $L_i(t)$ is a mode function, calculate the local mode functions ($\Psi_j$):

$$A(t) = \prod_{i=1}^{j} M_i(t); \tag{3.10}$$

$$\Psi_j(t) = A(t) \bullet L_i(t); \tag{3.11}$$

where $A(t)$ is amplitude and the corresponding instantaneous frequency can be calculated as:

$$f_j(t) = \frac{1}{2\pi}\frac{d}{dt}\left[\arccos\left(L_i(t)\right)\right]; \tag{3.12}$$

Step 6: Calculate transition residual $T_1(t)$, which will be the input signal for the next mode function. Repeat this procedure until $T_k(t)$ becomes a monotonous function:

$$\begin{aligned} T_1(t) &= x_i(t) - \Psi_i(t); \\ &\vdots \\ T_k(t) &= T_{k\text{-}1}(t) - \Psi_{k\text{-}1}(t); \end{aligned} \tag{3.13}$$

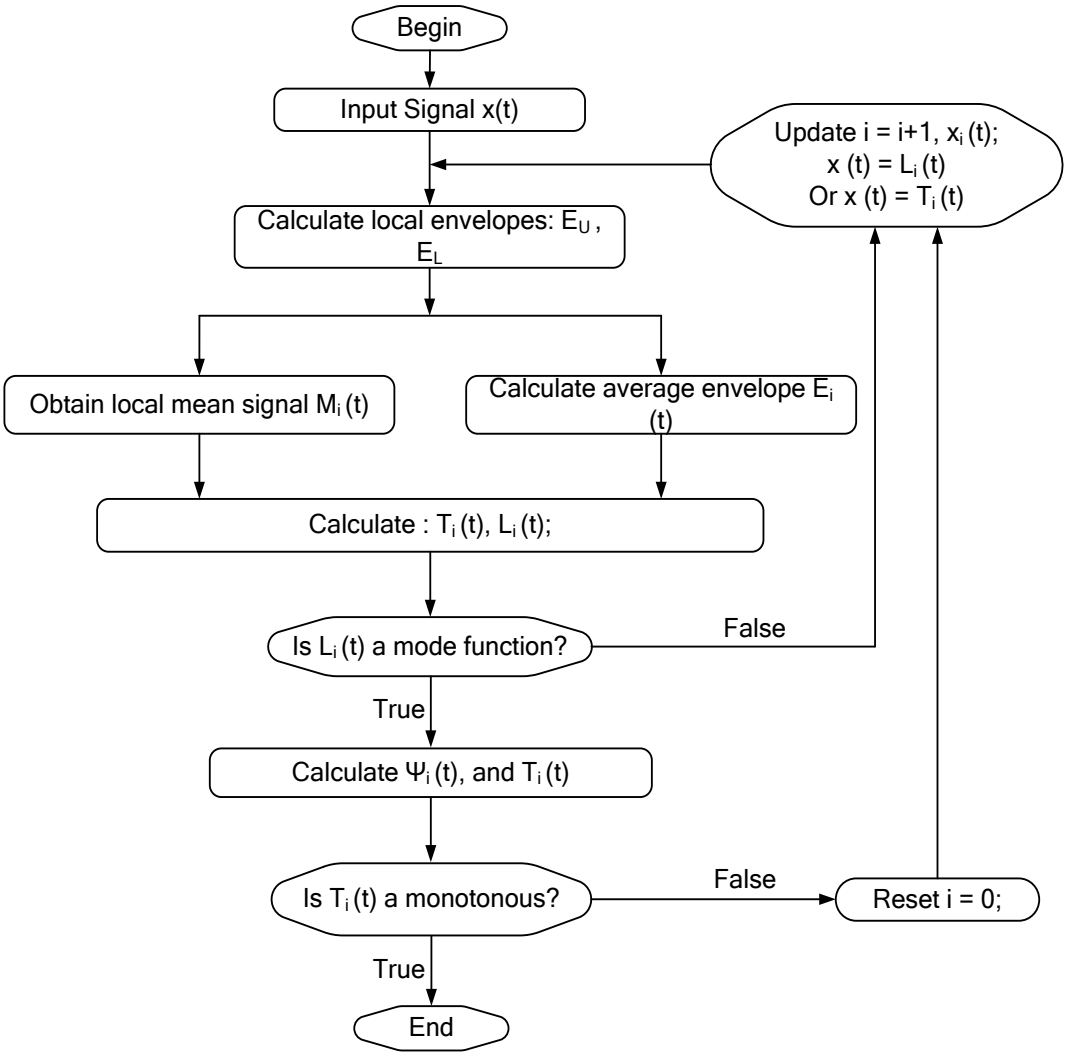


Fig. 3.2 The processing procedures of the LMD technique.

When $T_k(t)$ becomes a monotonous function after $(k\text{-}1)^{\text{th}}$ iterations, the original signal can be represented as:

$$x(t) = \sum_{k=1}^{K} \Psi_k(t) + T_k(t);$$

where K is the total number of local mode functions ($\Psi$) generated from a signal $x(t)$.

After all the local mode functions ($\Psi$) are calculated, spectrum analysis will be undertaken for observing the presence of fault features. This LMD technique could overcome the mode mixing effect in the LD and provide better resolution in fault detection in bearings in a gearbox.

## 3.3 Performance Evaluation

The effectiveness of the proposed LMD technique is verified in this section using data sets from Case Western Reserve University Dataset [123]. The test apparatus is shown in Fig. 3.3, which consists of a motor, a torque transducer and a dynamometer (load motor). A 2-HP electric motor is used to drive the system, and the motor bearings are tested for analysis. Accelerometers are placed at both drive-end and fan-end of the motor housing using magnetic bases and are used to collect vibration signals. The signal from the motor drive-end side is used for bearing health analysis in this study. Vibration signals are collected using a 16-channel digital audio tape recorder at a sampling frequency of 48,000 Hz. The torque transducer/encoder is used to manually record other related data like shaft speed and torque.

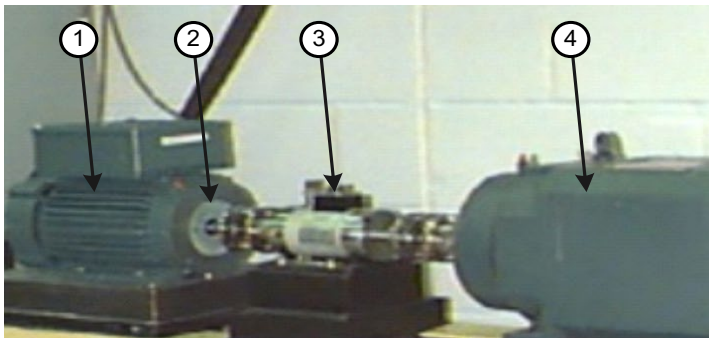


Fig. 3.3 Experimental (simulation) setup. 1) electrical driving motor (2 HP), 2) drive end bearing (used for analysis), 3) torque transducer, 4) load motor [123].

A detailed description about the bearing materials and properties, defect specifications, experimental setup, and test conditions can be found in [123]. The tested bearings have different health conditions (e.g., healthy, outer race faults, inner race faults, and rolling element faults). As an example, the processing results using some data sets corresponding to shaft speed of 1772 RPM (or $f_r$ = 29.53 Hz) are used for demonstration in this thesis work. The corresponding characteristic frequencies are summarized in Table 3.1. Parts of the corrected vibration signals from the experimental setup are shown in Fig. 3.4 and the corresponding frequency spectrums are shown in Fig. 3.5.

**Table 3.1. Bearing fault characteristic frequencies at shaft speed $f_r$.**

| Bearing condition | Shaft speed wrt $f_r$ |
|---|---|
| Normal/Healthy bearing | $f_H = f_r$ |
| Outer race fault | $f_{OD} = 3.58 \times f_r$ |
| Inner race fault | $f_{ID} = 5.42 \times f_r$ |
| Rolling element fault | $f_{BD} = 4.71 \times f_r$ |

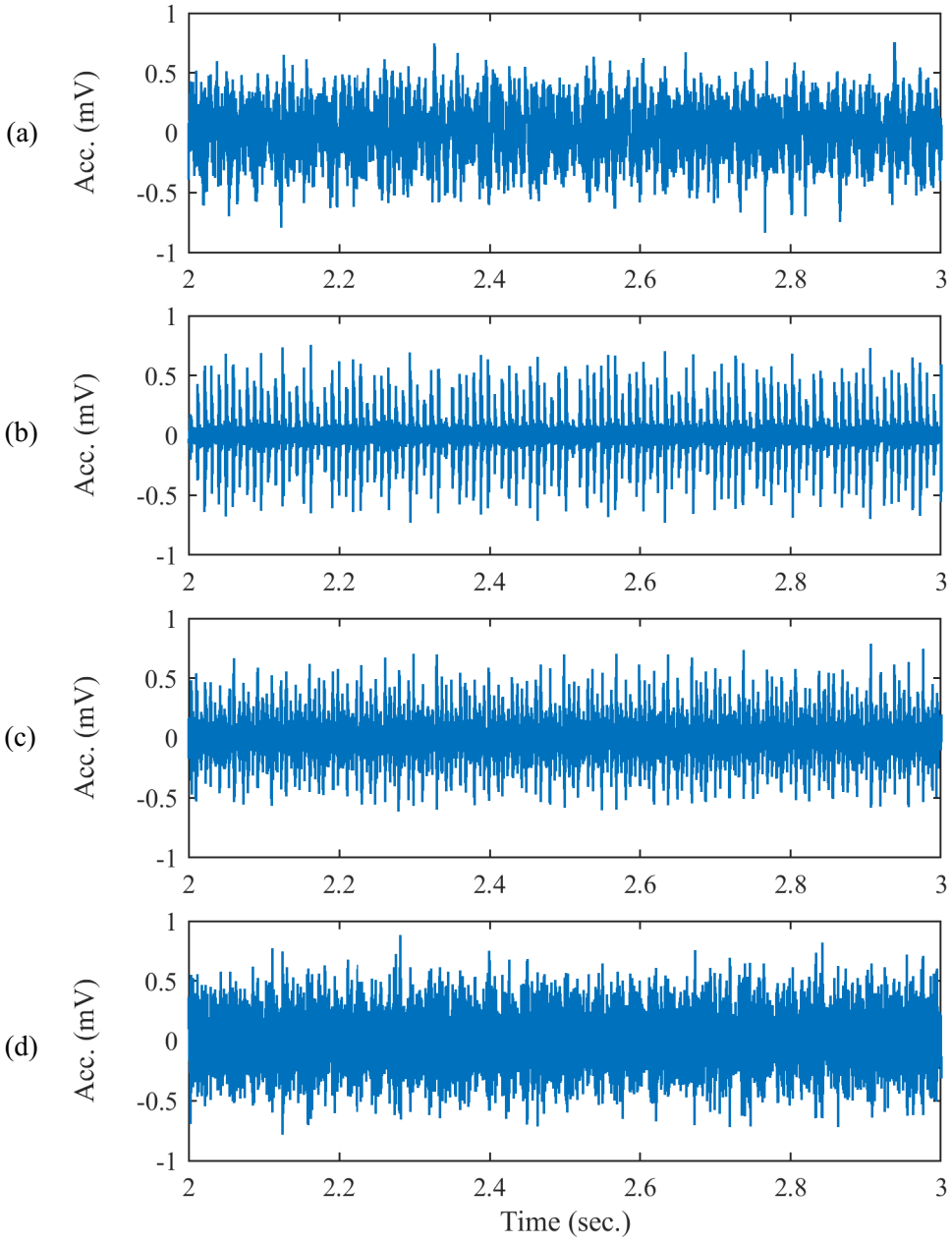


Fig. 3.4 Part of the collected bearing signals from different bearing conditions: (a) Healthy, (b) Outer race fault, (c) Inner race fault, (d) Roller element fault.

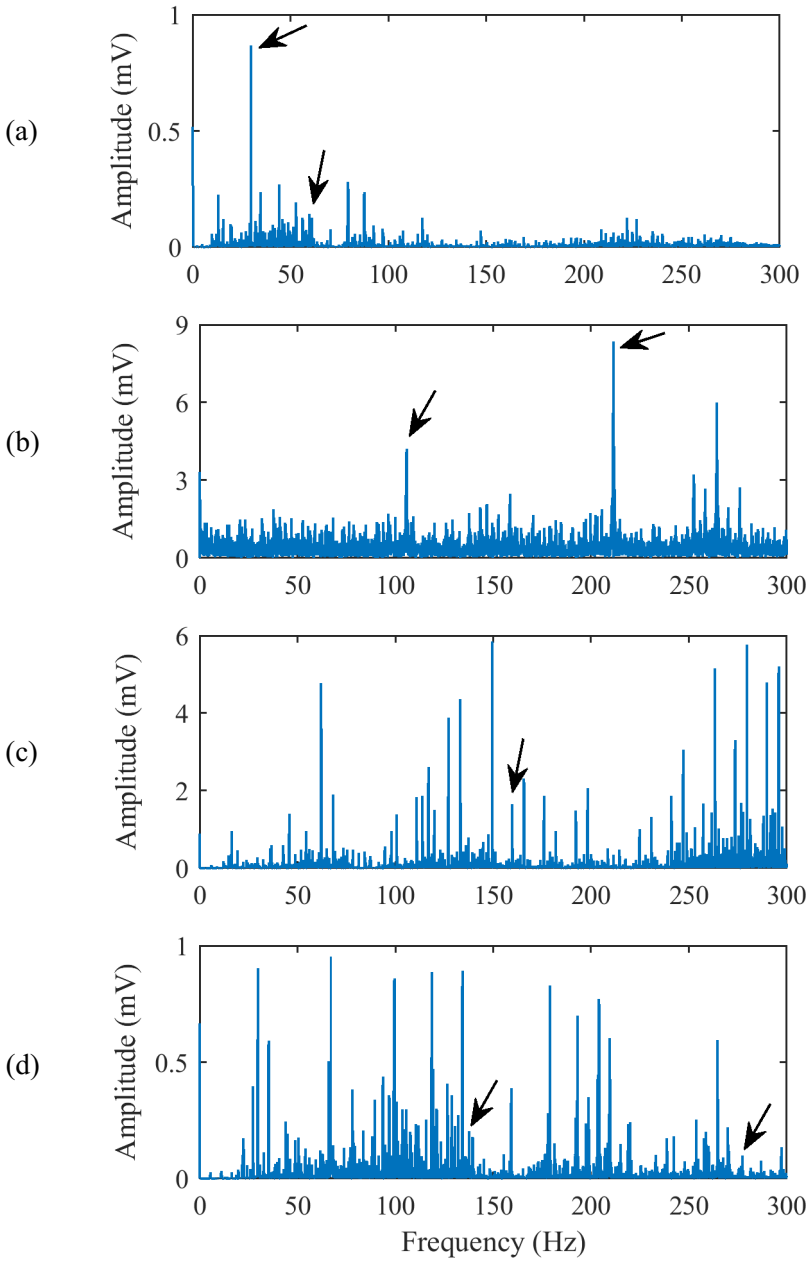


Fig. 3.5 Frequency spectrum of bearing data: (a) Healthy, (b) Outer race fault, (c) Inner race fault, (d) Roller element fault. (Arrows indicate the bearing characteristic frequency and its harmonics).

The corresponding mode functions $\Psi_j$ from the proposed LMD technique are extracted, and the processing results corresponding to different bearing health conditions are discussed below.

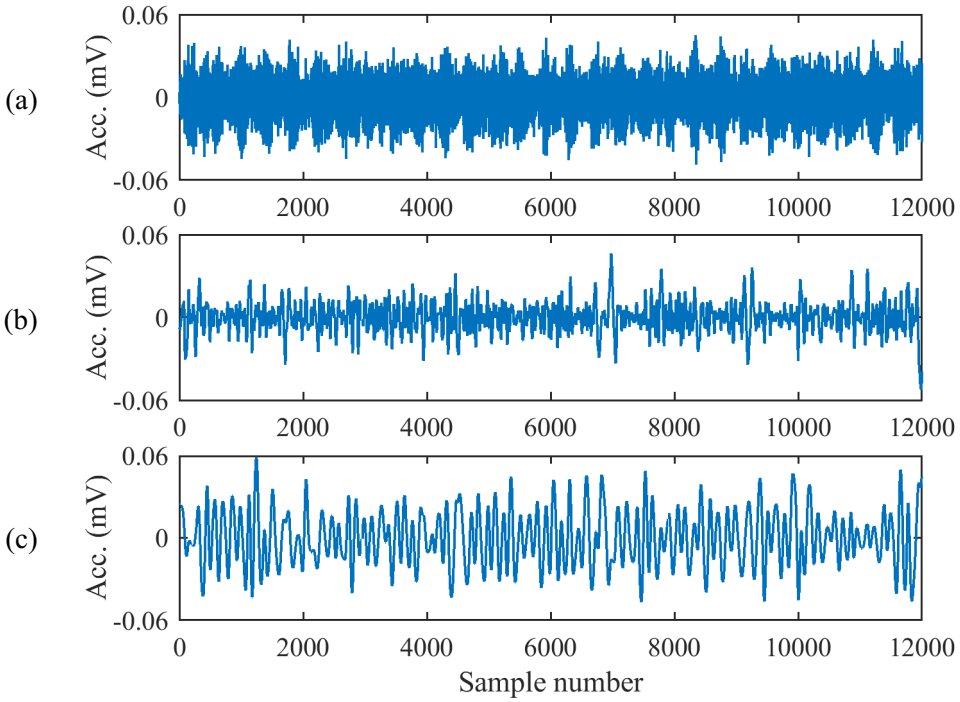


Fig. 3.6 The first three mode functions (Ψ) from a healthy bearing.

The first three mode functions are shown for a bearing with healthy condition (Fig. 3.6), outer race fault (Fig. 3.7), inner race fault (Fig. 3.8), and rolling element (ball) fault (Fig. 3.9). The first mode function includes most of the high peaks from the signal, which also has information related to health condition of bearing. The second and third mode functions have low amplitude data, mostly from surrounding components.

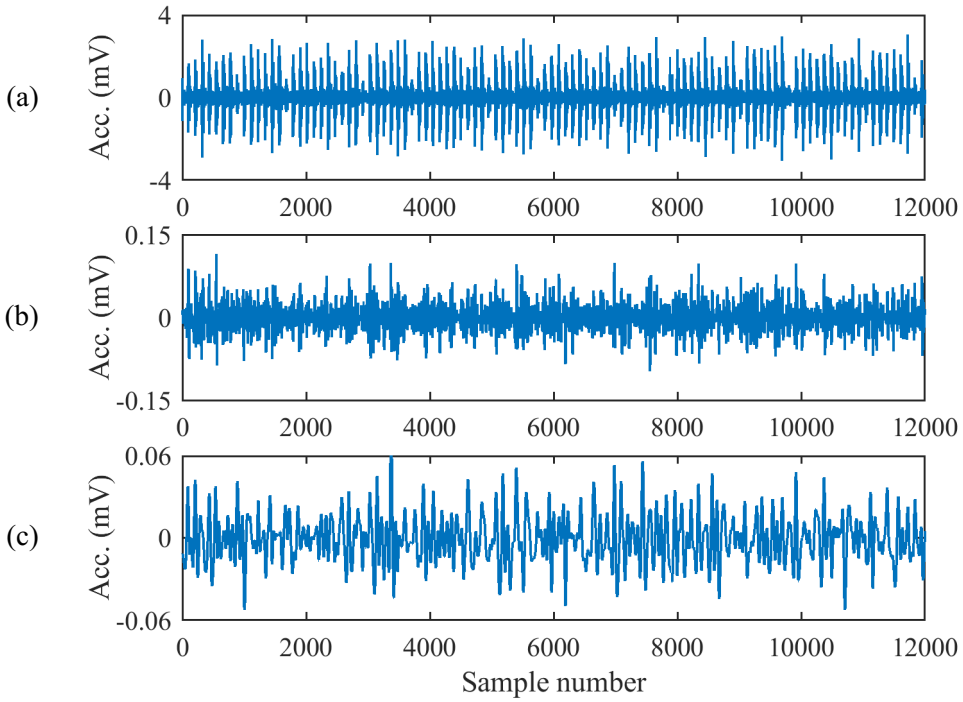


Fig. 3.7 The first three local mode functions (Ψ) from a bearing with outer race fault.

The first mode function is used for comparison of health condition of the bearing system. It is observed that the amplitude of healthy bearing (Fig. 3.6(a)) is much lower than bearing with fault. The bearing with an outer race fault shows the highest amplitude in the first mode function (Fig. 3.7(a)) as a result of periodic strikes between the rolling element and fault location. It shows clearly that visible peaks are periodic in nature and can provide initial indication towards the presence of outer race fault in the bearing system.

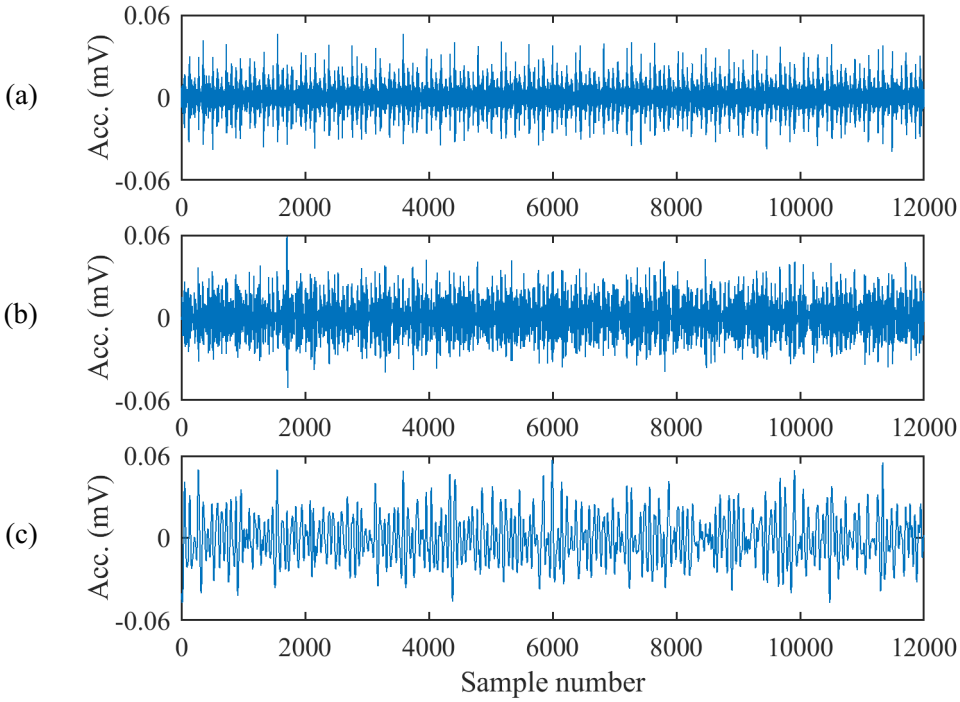


Fig. 3.8 The first three local mode functions (Ψ) from a bearing with inner race fault

The Fig. 3.8(a), the first mode function of the bearing with inner race fault, shows that the amplitude is not as high as in mode function of the bearing with outer race fault (Fig. 3.7(a)); but it is still much higher than that of the healthy bearing (Fig. 3.6(a)). The peaks are still visible, but are not of same amplitude, indicating that the strikes between the rolling element and fault location are not periodic or of same intensity. This can indicate the presence of inner race faults, which are aperiodic in nature.

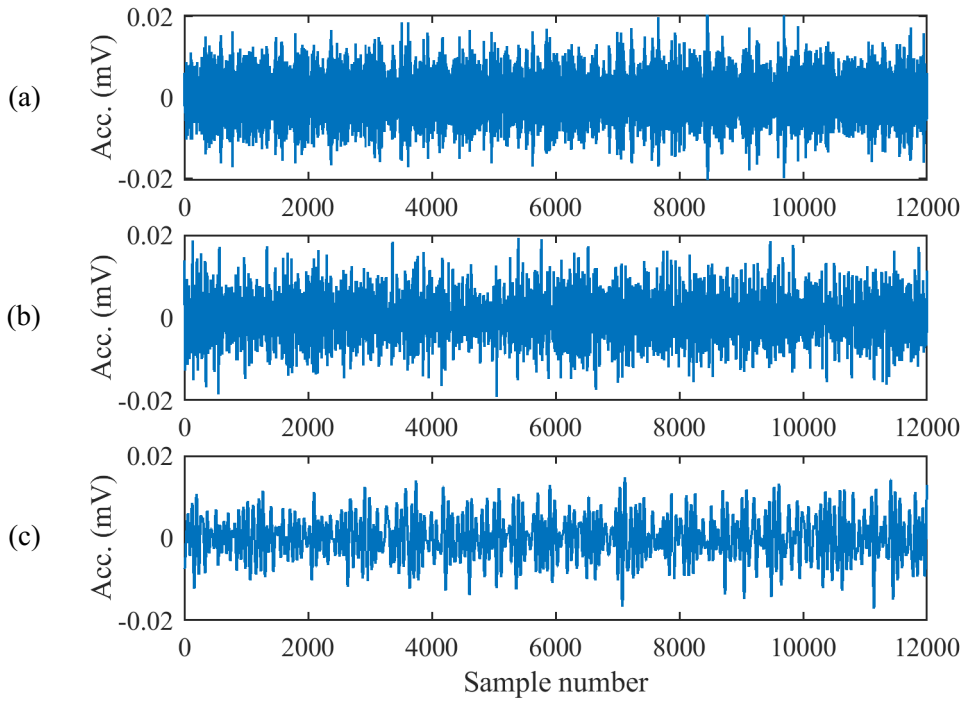


Fig. 3.9 The first three local mode functions (Ψ) from a bearing with rolling element (ball) fault.

The first mode function for the bearing with rolling element fault, shown in Fig. 3.9(a), has lower amplitude than the amplitude of the bearing with other fault conditions; but is still higher than the amplitude of healthy bearing. It can be observed that the peaks are aligned with the signal, which makes it difficult to even detect the presence of the fault. The frequency spectrum of the respective mode functions can be conducted for a detailed analysis for bearing health conditions.

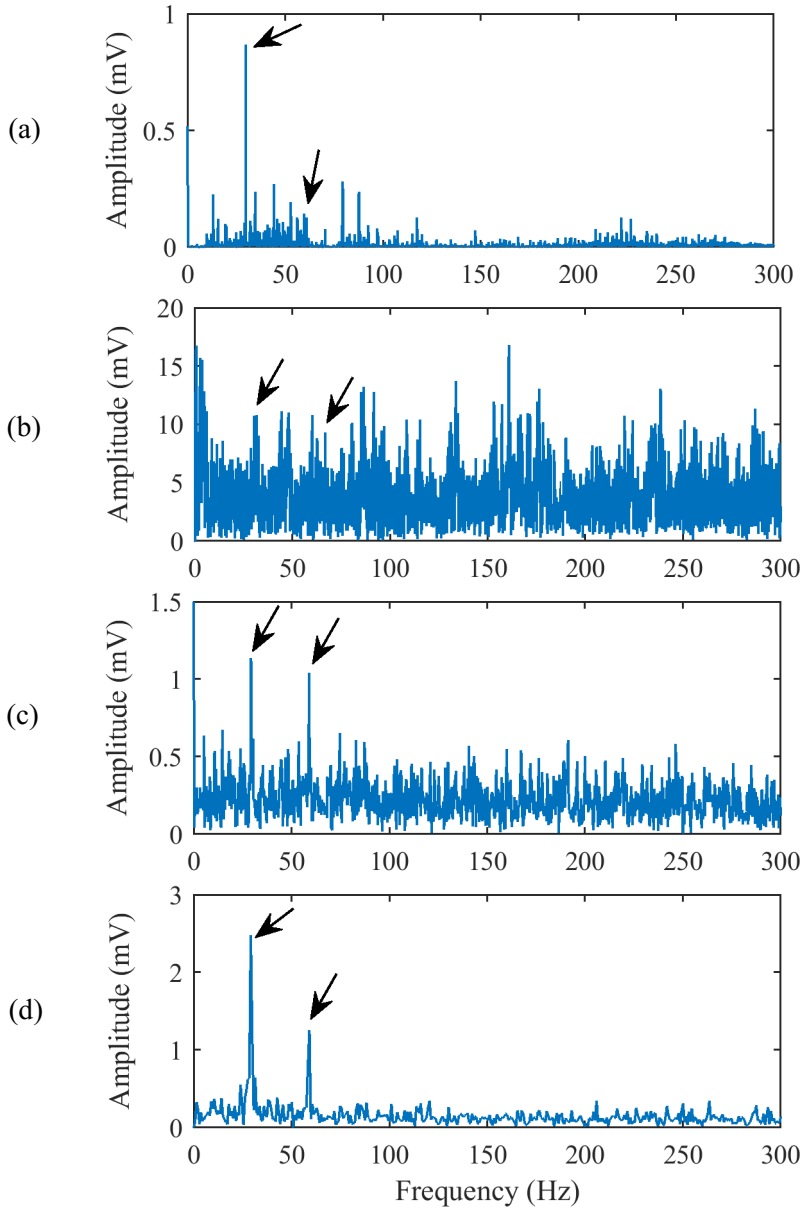


Fig. 3.10 Results from a healthy bearing (a) Frequency spectrum of the original data, (b) Frequency spectrum of the first IMF from EMD, (c) Frequency spectrum of the first Ψ function from LMD, (d) Power spectrum of the first Ψ function from LMD. (Arrows indicate the bearing characteristic frequency and its harmonics).

Fig. 3.10 shows the processing results from a healthy bearing. In this case, the bearing characteristic frequency is 29.82 Hz or the shaft frequency in this case. Fig. 3.10(a) shows the frequency spectrum of the health bearing signal where the black arrows indicate the characteristic frequency and its second harmonic. The Fig. 3.10(b) shows the frequency spectrum of the first IMF obtained from EMD processing. Fig. 3.10(c)

illustrates the spectral map of the first $\Psi$ function obtained from the proposed LMD technique, while Fig. 3.10(d) depicts the power spectrum of the first $\Psi$ function. It is seen that the proposed LMD technique performs better than EMD technique in healthy bearing condition monitoring due to its ability to suppress the noise signatures and highlight bearing characteristic frequency and its harmonics.

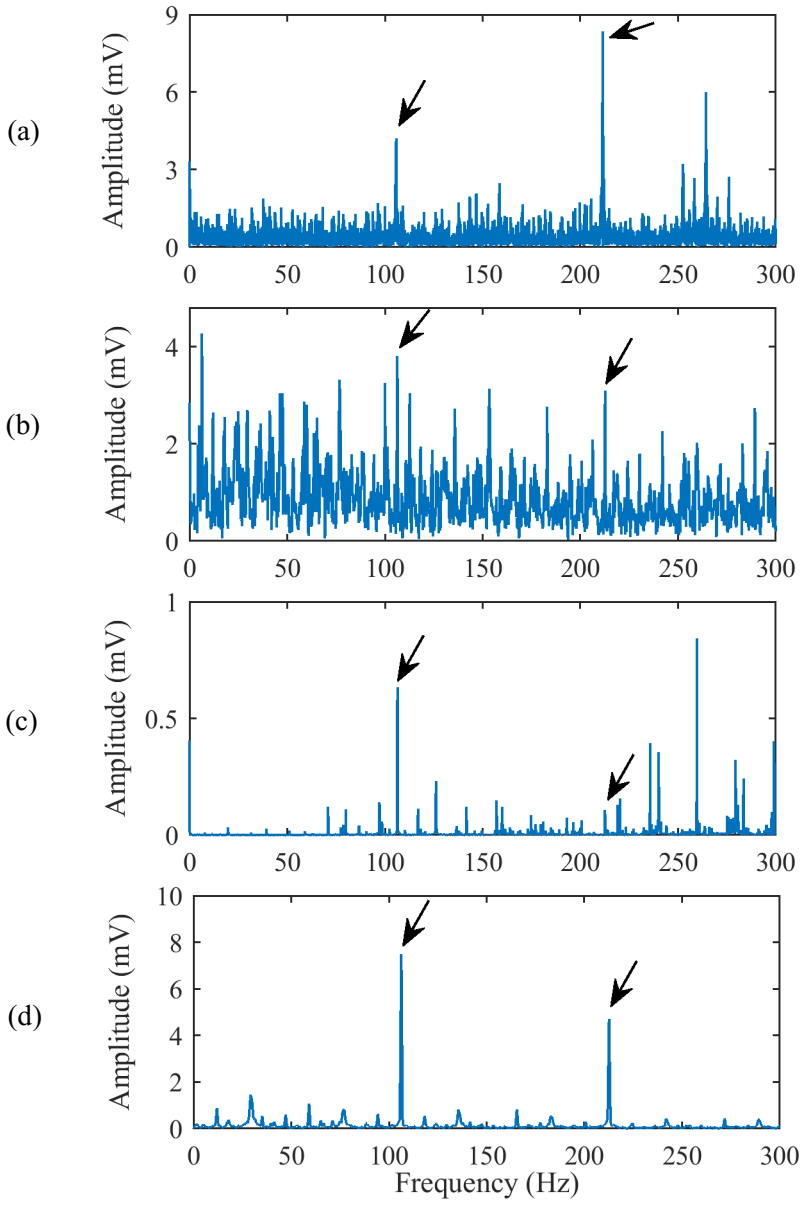


Fig. 3.11 Results from a bearing with outer race fault (a) Frequency spectrum of the original data, (b) Frequency spectrum of the first IMF from EMD, (c) Frequency spectrum of the first Ψ function from LMD, (d) Power spectrum of the first Ψ function from LMD. (Arrows indicate the bearing characteristic frequency and its harmonics).

Fig. 3.11 shows the results for a signal from a bearing with outer race fault, with fault characteristic frequency 106.3 Hz. It is seen that EMD technique can predict the outer race fault, but it cannot remove the surrounding noise frequencies. The frequency spectrum as well as power spectrum of the first $\Psi$ function shows clear and dominant peaks at outer race fault frequency as well as the corresponding first harmonics.

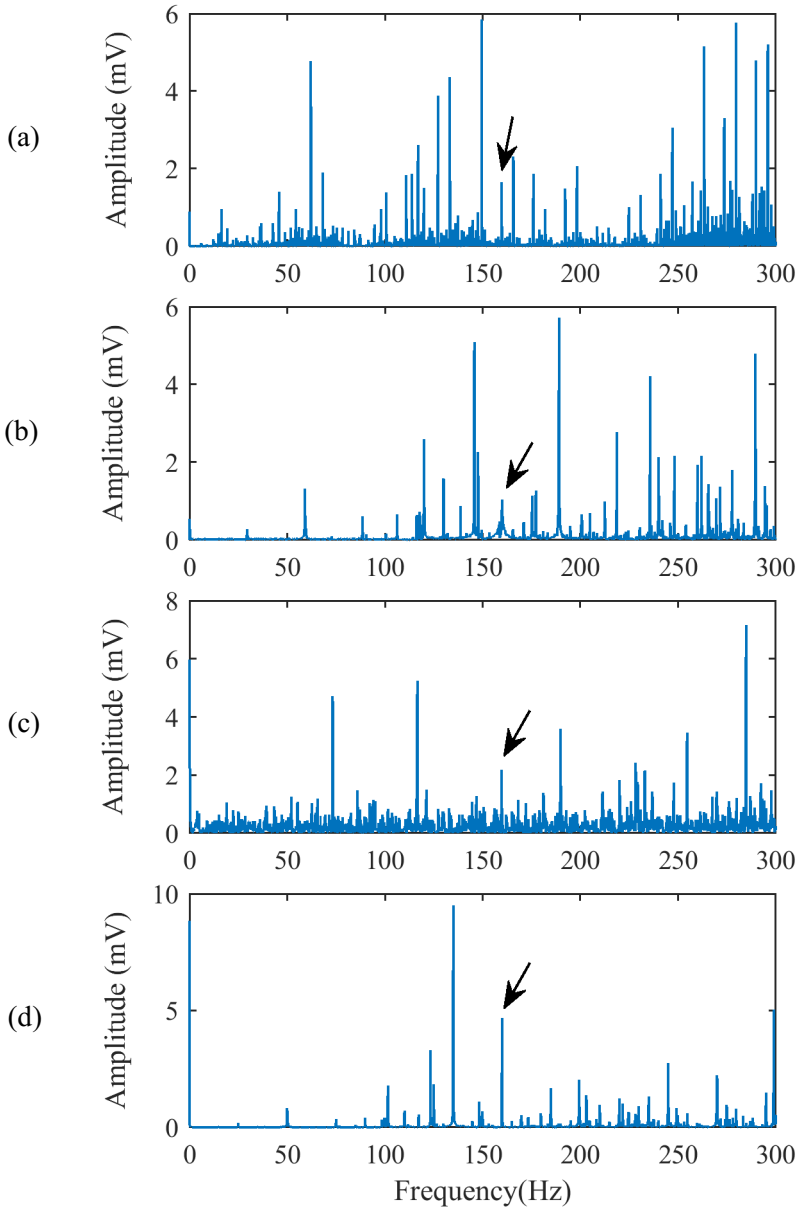


Fig. 3.12 Results from a bearing with inner race fault (a) Frequency spectrum of the original data, (b) Frequency spectrum of the first IMF from EMD, (c) Frequency spectrum of the first Ψ function from LMD, (d) Power spectrum of the first Ψ function from LMD. (Arrows indicate the bearing characteristic frequency and its harmonics).

Fig. 3.12 shows the results for a signal from a bearing with inner race fault, with fault characteristic frequency 159.7 Hz. It is seen that EMD technique can predict the inner race fault, but with a lower signal-to-noise ratio. The frequency spectrum as well as power spectrum of the first $\Psi$ function can recognize the existence of the inner race fault.

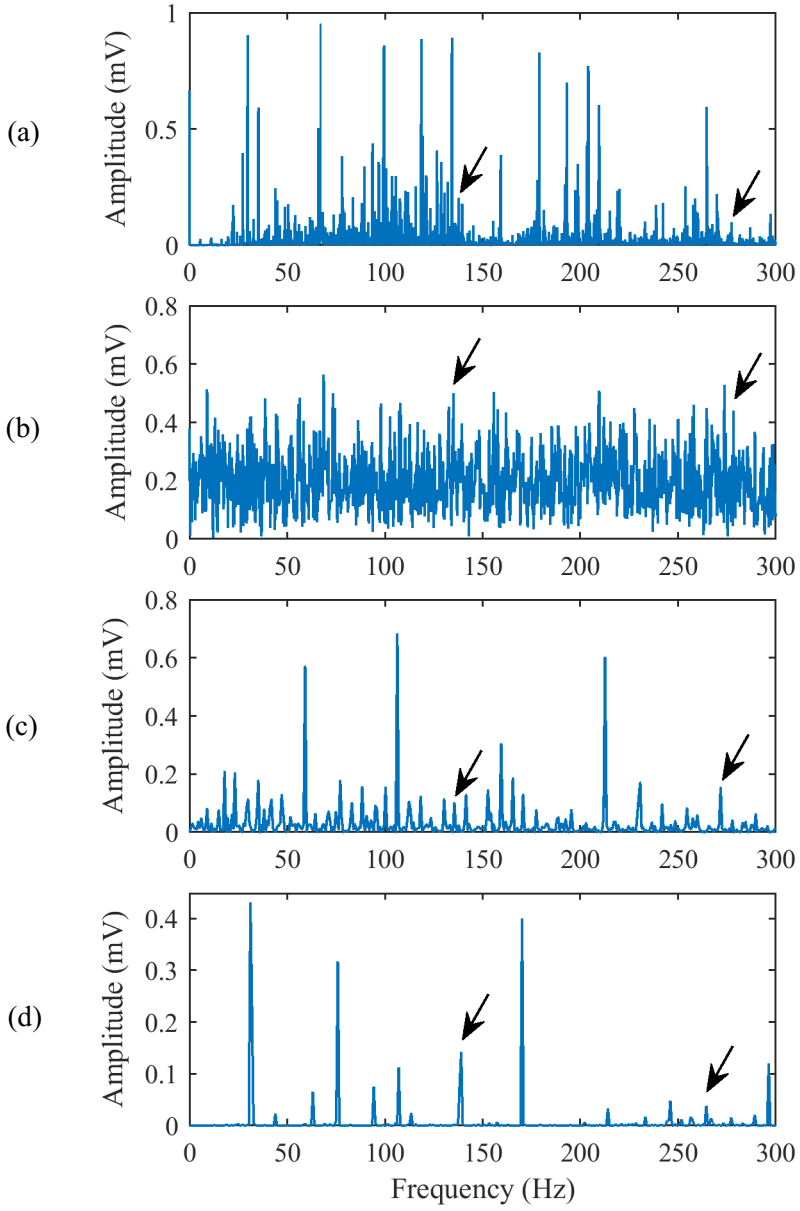


Fig. 3.13 Results from a bearing with rolling element fault (a) Frequency spectrum of the original data, (b) Frequency spectrum of the first IMF from EMD, (c) Frequency spectrum of the first Ψ function from LM D, (d) Power spectrum of the first Ψ function from LMD. (Arrows indicate the bearing characteristic frequency and its harmonics).

Fig. 3.13 shows the results for a signal from a bearing with rolling element fault, with fault characteristic frequency 139.5 Hz. The EMD technique cannot recognize the corresponding fault frequency, which is suppressed by frequencies of other components. The frequency spectrum of the first $\Psi$ function can recognize the bearing fault, but it is not a dominant spectral component. The power spectrum of the first $\Psi$ function can predict the existence of the rolling element fault even though their magnitudes are relatively low.

It is seen that LMD technique is effective, which can easily detect the presence of fault in the system. The LMD technique also is more efficient to separate the healthy bearing from the faulty bearings. For roller element (ball) fault, as its amplitude is suppressed under effect of other components, the LMD technique can detect the presence of the fault, but fails to provide dominant results.

## 3.4 Discussion

A novel LMD method has been developed in this work for bearing fault analysis in a gearbox system. The main purpose of this technique is to amplify the mode functions with respect to mean values to highlight the peak features. This helps to highlight the periodic events (e.g. outer race faults) and can also enhance the suppressed events (e.g. inner race fault, rolling elements faults) of a bearing system. The power spectrum of the local mode functions ($\Psi$) are analyzed to provide more clear peaks for fault frequencies. The simulation is conducted and evaluated using Case Western Reserve University dataset. The results have shown that proposed technique can detect bearing faults. The combination of the proposed LMD technique and power spectrum analysis has a potential for a fault diagnosis of bearing system in complex structures (e.g. gearbox).

# Chapter 4

# Evolving Neuro-Fuzzy Classifier Technique

## 4.1 Evolving Classifiers

Evolving classification is based on some clustering algorithms to generate classification reasoning architecture, while system parameters are properly trained. The classification operation should be undertaken continuously and smoothly over the interval of inputs. As a fuzzy system is a universal approximator and can extract knowledge with mimic of human reasoning to understand and predict the outcome of a process [89, 91], it is generally used as the platform in designing evolving systems. Several evolving systems have been proposed in literature for different processing purposes [90-94]. For example, Angelov et al. have proposed an evolving Takagi-Sugeno (eTS) scheme for system control [92]; formation of the clusters is based on a potential measure in terms of the center and spread of clusters, while the least square estimator (LSE) algorithm is used to update linear parameters. A problem of this clustering approach is that the predefined cluster information (e.g., centers and spreads) is sensitive to noise in the data sets and processing errors. Kasabov has suggested a transductive weighted neuro-fuzzy inference (TWNFI) system by introducing weighted data normalization for transductive reasoning [94]. Comparing with the eTS in modeling of non-linear systems, the TWNFI usually generates more clusters/rules and thus may result in lower processing efficiency [90, 91].

One of the problems in the classical evolving classifiers is related to their blind classification of the output space, which could degrade the accuracy of diagnostic results. In order to tackle this problem, the objective of this work is to propose a new evolving neuro-fuzzy (eNF) technique for gear system fault diagnostics. Compared with these available evolving systems, the proposed eNF classifier has the following novel contributions:

1) A new potential calculation method is proposed for better partition of the output space and elimination of contradictory clusters/rules generated due to noise-affected data sets.

2) A new training algorithm based on a normalized Adadelta (NaD) function is suggested to control the rate of weight change in training the eNF classifier. Its effectiveness is verified by simulation and experimental tests.

## 4.2 Proposed Evolving Neuro-Fuzzy (eNF) System

### 4.2.1 The eNF Fuzzy Model

The proposed eNF classifier applies fuzzy If-Then rules to map the input space to the output space; an improved training algorithm will be used for optimization of the system parameters. Consider an input vector $X = \{x_1, x_2, \ldots, x_n\}$. The eNF reasoning is performed by the following fuzzy representation:

$$\Re_j : \text{If } (x_1 \text{ is } A_1^j) \text{ and } (x_2 \text{ is } A_2^j) \text{ and } \ldots (x_n \text{ is } A_n^j) \text{ Then } (y_j \text{ is } O_j) \text{ with } w_j \qquad (4.1)$$

where $j \in [1, C]$, $C$ is the total number of fuzzy clusters/rules; $A_i^j$ is the $j$-th input fuzzy set for $x_i$, $i \in [1, n]$; $y_j$ is an output indicator, and $O_j$ is the output fuzzy set (e.g., healthy, possibly damaged, and damaged). $w_j$ is a weight factor representing the contribution of the related cluster/rule to the diagnostic classification.

Data geometry is a representation of data samples in the input/output spaces. The rules are linear representation of multiple clusters corresponding to different system conditions. In the proposed eNF classifier, Gaussian membership functions (MFs) are used to describe all the fuzzy such that:

$$M_{A_i}^j = \exp\left(-\frac{(x-\mu_{ij})^2}{2\sigma_{ij}^2}\right); \qquad (4.2)$$

where $\mu_{ij}$ and $\sigma_{ij}$ are the centers and spreads of the clusters, respectively.

In evolving fuzzy systems, a Gaussian MF is more commonly used as it is continuous and generalized, which can be decomposed into multiple one-dimensional Gaussian MFs corresponding to different input variables with proper input/output partitions [124].

If a max-product inference operator is used for the premise fuzzy reasoning, the firing strength can be expressed as:

$$w_j = \prod_{i=1}^{n} \left( M_{A_i}^{j} \right) = \prod_{i=1}^{n} \left[ \exp\left( - \frac{(x_j - \mu_{ij})^2}{2\sigma_{ij}^2} \right) \right];$$

$$= \exp\left[ - \sum_{i=1}^{n} \left( \frac{(x_j - \mu_{ij})^2}{2\sigma_{ij}^2} \right) \right];, \; i, j \in [1, C] \tag{4.3}$$

After normalization of firing strengths, the output is obtained as:

$$y_j = \sum_{j=1}^{C} \left( \frac{w_j O_j}{W_j} \right); \qquad j \in [1, C] \tag{4.4}$$

where $W_j = \sum_{j=1}^{C} w_j$ .

An example of a evolving NF model is shown in Fig. 4.1. Initially, each input variable (in layer 1) has 3 MFs (in layer 2): *S.*, *M.* and *L.* that are related to each cluster formulation based on Eq. (4.2). The evolving operation helps in formation of rules (in layer 3), $R_1 \sim R_5$. At the same time, the MFs of each input are related to $R_1 - R_5$. The firing strength of each rule is calculated in layer 3 by the related inference operation (Eq. 4.3). After normalization in layer 4, the output indicator ($y$) can be computed by defuzzification (e.g., centroid) in layer 5.

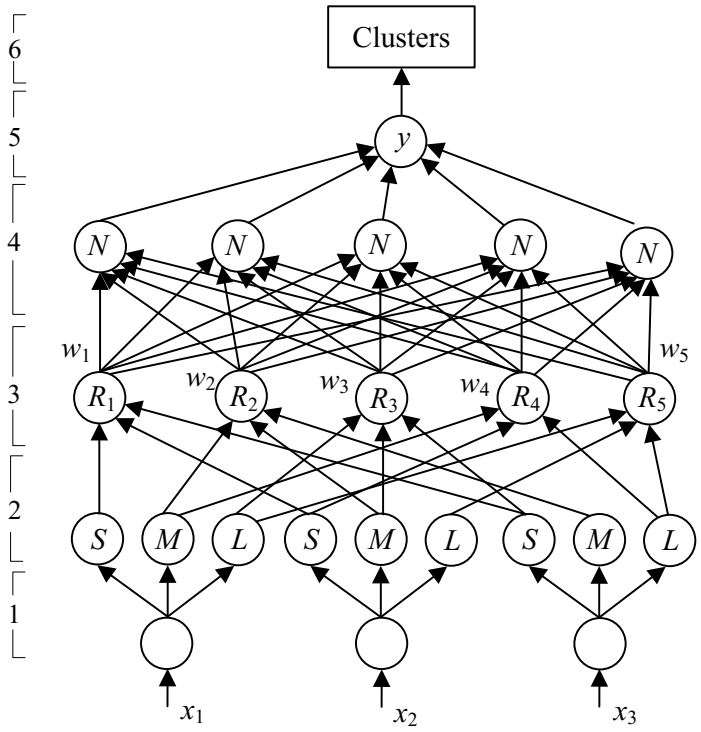


Fig. 4.1 An example of an evolving NF model.

### 4.2.2 The Proposed eNF Classifier

The proposed eNF system formulates clusters in a gradual and continuous way. In the evolving operation, input and output patterns are mapped with required consistency, as so to prevent unnecessary cluster overlapping due to noise/outliers and make the clusters well-distributed over the input and output spaces. Different from the eTS [125] and the TWNFI [126], the proposed eNF approach has constrained partition generated in the output space related to machinery health states. The steps of the eNF clustering are summarized as follows:

1) Initialization: The first input data is expressed as $D_a = [x_a, y_a]$, when $a := 1$, the first cluster center is $B_a := D_a$. Other parameters of the new cluster will be initialized as $C := 1$, $n := 1$, $\mu_C^I := x_a$, $\sigma_C^I := 0.2$, $\mu_C^O := y_a$, $\sigma_C^O := 0.2$, $P_a(D_a) := 1$, $P_a(B_a) := 1$, where $C$ is the number of clusters (rules) of the eNF; $n$ is number of rules in a cluster; $\mu_C^I, \sigma_C^I, \mu_C^O, \sigma_C^O$ are centers and spreads of the cluster in the input space and output space, respectively.

2) Calculating potential of new input data: For $a := a+1$, new input data to system is $D_a = [x_a, y_a]$. The potential can be calculated by:

$$P_a(D_a) = \frac{a}{a(\alpha_a + 1) + (\sigma_a + 1) - (2\varphi_a + 1)}; \tag{4.5}$$

where $\alpha_a = \sum_{i=0}^{l} (D_a^i)^2$; $\sigma_a = \sigma_{a-1} + \alpha_{a-1}$; $\varphi_a = \sum_{i=0}^{l} (D_a^i \beta_a^i)$; $\beta_a^i = \beta_{a-1}^i + D_{a-1}^i$. $\beta_a^i$ and $\sigma_a$ are initialized as vectors of zeros with appropriate lengths of inputs.

3) Updating the cluster parameters: If the potential of the new input data is less than potential of the cluster center, or $P_a(D_a) < P_a(B_a)$, then update the potential of existing clusters such as:

$$P_a(B_a) = \frac{aP_{a-1}(B_a)}{(a+1) + P_{a-1}(B_a) + P_{a-1}(B_a)\delta}; \tag{4.6}$$

where $\delta = \sum_{i=1}^{n} (D_a^i - D_{a\text{-}1}^i)^2$; is sum of distance between the new input and previous data.

4) Determining the winner cluster: By comparing the potential of new input data and existing cluster, if $P_a(D_a) < P_a(B_a)$;, then go to step 6). Otherwise, if $P_a(D_a) > P_a(B_a)$; then determine the winning clusters in the respective input and output spaces, by the following process:

$$WC^I = C_{winner}^I = \arg\left( \min_{a=1}^{L_a} \left\| \mu_a^I - x_a \right\| \right);$$

$$WC^O = C_{winner}^O = \arg\left( \min_{a=1}^{L_a} \left\| \mu_a^O - y_a \right\| \right);$$

where $a = [1, L]$, and $L$ is the total number of data pairs.

5) Recognizing the structure of cluster: If $WC^I = WC^O$;, and descriptive grade $d_{WC,a} = \left\| \mu_{WC} - \mu_a \right\| < d_{\min}$; ($d_{min}$ = 0.07 in this case), merge new data to the winning cluster. The cluster parameters are updated by:

$$(\sigma_{WC,a}^{I})^2 = (\sigma_{WC,a-1}^{I})^2 + \frac{1}{n}\left[(x_a - \mu_{WC,a-1}^{I})^2 - (\sigma_{WC,a-1}^{I})^2\right];$$

$$(\mu_{WC,a}^{I}) = (\mu_{WC,a-1}^{I}) + \frac{1}{n}\left[(x_a - \mu_{WC,a-1}^{I})\right];$$

$$(\sigma_{WC,a}^{O})^2 = (\sigma_{WC,a-1}^{O})^2 + \frac{1}{n}\left[(y_a - \mu_{WC,a-1}^{O})^2 - (\sigma_{WC,a-1}^{O})^2\right];$$

$$(\mu_{WC,a}^{O}) = (\mu_{WC,a-1}^{O}) + \frac{1}{n}\left[(y_a - \mu_{WC,a-1}^{O})\right];$$

Otherwise, if no winner cluster is recognized or the descriptive grade $d_{WC,a} > d_{\min}$, create a new cluster with following initial parameters:

$C := C + 1,\ n := n + 1,\ \mu_C^I := x_a,\ \sigma_C^I := 0.2,\ \mu_C^O := y_a,\ \sigma_C^O := 0.2.$

These parameters are properly chosen to prevent contradictory clusters/rules. Specifically, if two inputs are too close (e.g., $\sigma < 0.1$), they can be separated by these output space partition constraints.

6) Updating the weight factors: Based on the values of $w_j$ determined by Eq. (4.3), depending on centers and spreads of the clusters, the weight factors will be updated as per Eq. (4.11) as discussed in section 4.2.3.

7) Repeating the processes from step 2) to step 6) for all the data samples. Compute the classification output by Eq. (4.4).

### 4.2.3 The eNF Training using Normalized Adadelta (NaD) Method

A NF system usually contains both linear and non-linear parameters [127]. The linear parameters are usually optimized by using the LSE. Many methods are proposed in literature to update non-linear parameters, such as gradient descent (GD), Newton Gaussian, Levenberg-Marquardt, etc. The GD algorithm could be the fundamental method for nonlinear parameter optimization; however, it has some problems in applications such as sensitive to noise and high computing costs [128]. To tackle these challenges related classical GD algorithms, Adadelta method is introduced in [128],

which takes an adaptive learning rate to make the search process less sensitivity to noisy gradient information.

The GD algorithm for the optimization of the parameters $\theta$ at the $(t+1)^{th}$ iteration can be expressed as:

$$\theta_{t+1} = \theta_t - \eta g_t; \tag{4.7}$$

where $\eta$ is a rate of change in parameter updating, and $g_t$ is the gradient of parameters at the $t^{th}$ iteration.

The Adadelta method updates the parameter changes $\Delta\theta_t$ by the use of the root mean square measure on a selected data range, or

$$\Delta\theta_{t+1} = \Delta\theta_t + \eta\left(\frac{g_t}{R(g_t)}\right); \tag{4.8}$$

where $R(g_t) = \sqrt{E(g_t^2) + \varepsilon}$; is the root mean square; $E(\bullet)$ is the expectation; and $\varepsilon$ is a residual.

In Eq. (4.8), the size of the diagonal matrix equals to length of data. The large dimension in matrices will affect the implementation and calculation efficiency, and make it difficult for real-time monitoring applications. To solve this problem, a normalized Adadelta, or NaD, will be proposed in this work to improve the convergence and computational efficiency of the classical Adadelta method. The NaD algorithm takes the following processing steps:

1) Initialize the weight parameter matrix $\theta$ with all the initial values of 1, or $\theta_1 = 1$. Initialize the controller matrix $C_1 = 10^3 \times I$, where $I$ is an identity matrix.

2) Perform the feed-forward pass of eNF classifier to calculate $y_k$ using Eq. (4.2)- Eq. (4.4).

3) Calculate the new convergence rate:

$$\eta_k = \frac{\overline{n}_k}{N_d}; \tag{4.9}$$

where $\overline{n}_k$ is number of error output, and $N_d$ is total number of outputs calculated in each training epoch.

4) Update the controller matrix

$$C_k = C_{k-1} + \frac{C_{k-1}^T W_{k-1}^T W_k C_{k-1}}{1 + W_k^T C_{k-1} W_k}; \tag{4.10}$$

where $W_k$ is sum of normalized weights in eNF classifier.

5) Update the weight parameters of the eNF system:

$$\theta_k = \theta_{k-1} + C_k W_k \eta_k \left| y_k^d - y_k \right|. \tag{4.11}$$

## 4.3 Performance Evaluation of Proposed eNF Classifier

Firstly, the effectiveness of the proposed eNF classifier is examined by simulation tests. Later, in Chapter 5, it is implemented for gear system health condition monitoring. Some related classifiers are used for comparison: eTS and TWNFI trained by hybrid methods of LSE and GD. Another comparison is undertaken with a self-evolving fuzzy classifier (SEF), which has been proposed in our research team to minimize rules and improve processing convergence [90]. The developed eNF classifier, trained by the LSE and GD algorithms denoted by eNF-GD, will be executed to compare and examine the effectiveness of the proposed eNF evolving algorithm. The eNF classifier trained by the proposed NaD, represented by eNF-NaD, will be compared with eNF-GD to check the efficiency of the NaD training algorithm. All of these classifiers will use the same inputs, with same training conditions and initial values of the parameters to be updated.

### 4.3.1 Iris dataset

The first simulation test is undertaken using the Iris dataset [129]. Iris dataset has 4 inputs: sepal length ($x_1$), sepal width ($x_2$), petal length ($x_3$), and petal width ($x_4$). All these

4 variables are related to 3 output conditions: Iris Setosa, Iris Versicolour, and Iris Virginica. The output space is partitioned in 3 sections.

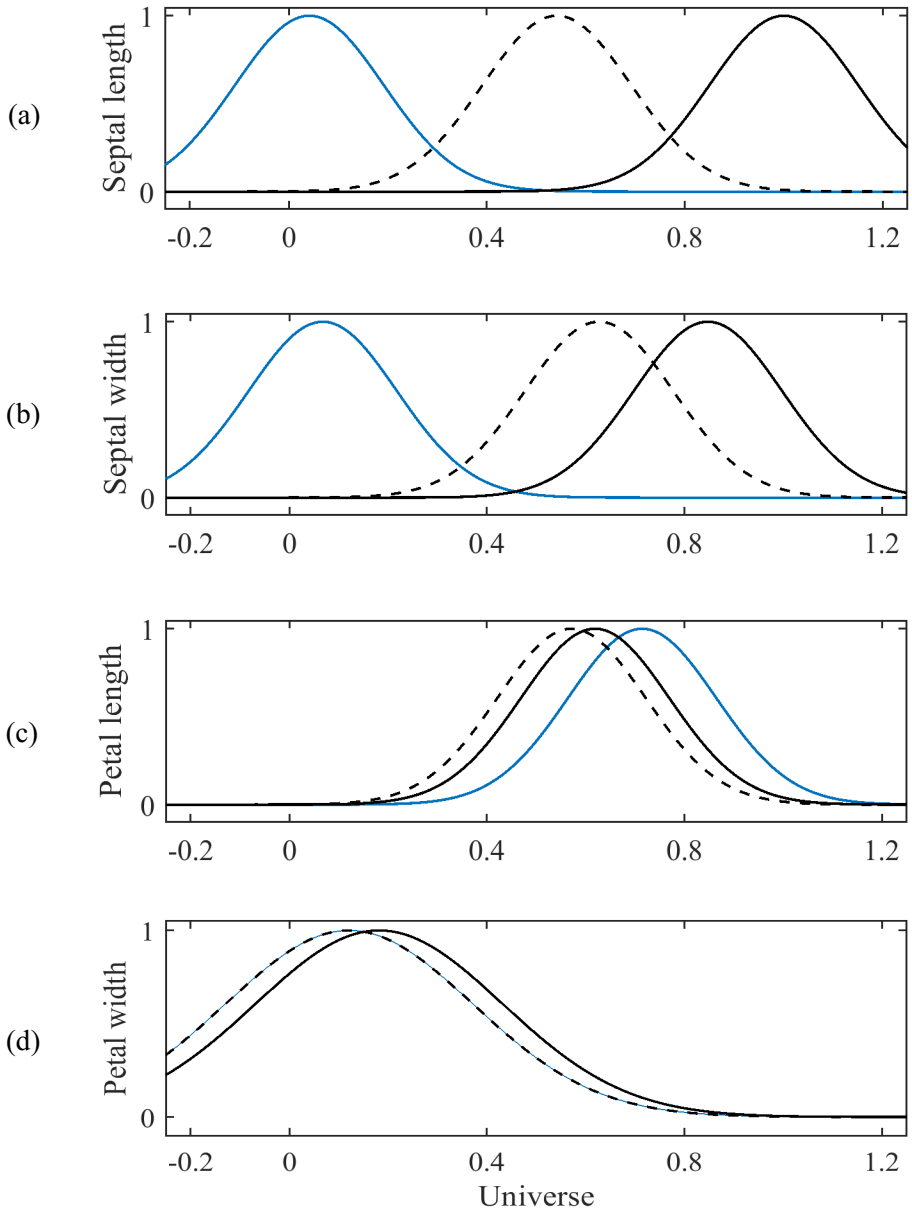


Fig. 4.2 Initial membership functions (MFs) for Iris dataset (a) Septal length, (b) Septal width, (c) Petal length, (d) Petal width.

There are 150 data pairs in this dataset: 75 of them will be used for training and remaining 75 pairs will be used for verification. In the evolving process, the initial MFs of these four inputs are shown in Fig. 4.2 which correspond to the first data pair.

The updated centers and spreads of the input variables are shown in Fig. 4.3, which are obtained after training by the use of the proposed eNF-NaD technique. It can be seen that $\{x_1, x_2, x_3, x_4\}$ have different relations with the output space. The output zone shows that $x_1$ has only 2 clusters/rules, $x_3$ has 3 clusters/rules, while $x_2$ and $x_4$ have 4 clusters/rules.

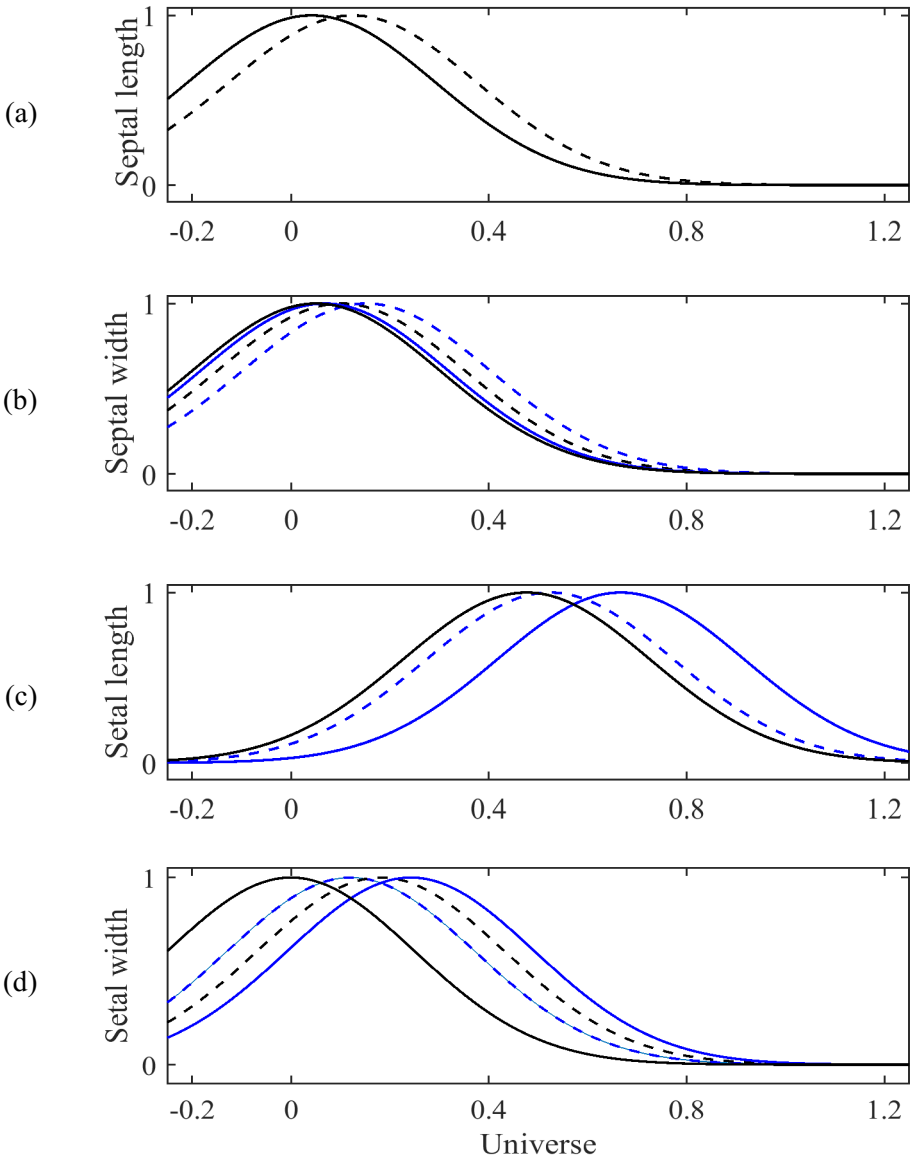


Fig. 4.3 Final MFs of the eNF-NaD classifier for Iris dataset (a) Septal length, (b) Septal width, (c) Petal length, (d) Petal width.

The simulation is undertaken using MATLAB 2016b. In classification process, once the clusters are evolved and MFs are formulated, the classifier undergoes a forward pass processing to calculate the system output. Based on the error in each training epoch, the related training algorithms are used to optimize classifier parameters. Table 4.1 summarizes the comparison results using the related classifiers. All of the selected classifiers are operated to achieve convergence based on the input conditions. The success rates of each classifier are the states before training and after training; it is clear that the related training can significantly improve classification accuracy.

**Table 4.1. Performance comparison of the related classifiers using the Iris data.**

| Classifier | Success Rate (%) | | No. of Clusters | No. of Rules | Average Operation Time (sec) |
|---|---|---|---|---|---|
| | Before Training | After Training | | | |
| TWNFI | 80.1 | 85.33 | 5 | 6 | 2.25 |
| eTS | 56.95 | 62.67 | 5 | 4 | 1.96 |
| SEF | 73.35 | 76.06 | 3 | 3 | 2.19 |
| eNF-GD | 78.15 | 85.33 | 3 | 4 | 1.52 |
| eNF-NaD | 92.67 | 94.67 | 3 | 4 | 1.31 |

From Table 4.1, it is seen that during verification, the TWNFI performs better than the eTS classifier (85.33% vs. 62.67%), even though both have generated 5 clusters. The SEF and eNF classifiers have generated 3 clusters only, which can speed up the diagnostic classification processing. However, the eNF-GD outperforms the SEF (76.06% vs. 85.33%) due to the more efficient evolving algorithm, which can be related to the use of fewer rules (3 vs. 4) of the SEF. Comparing eNF-GD and eNF-NaD, it is seen that the proposed NaD algorithm can effectively control weights of the eNF system to further improve diagnostic accuracy (94.67% vs. 85.33%) and processing time (1.31 sec vs. 1.52 sec).

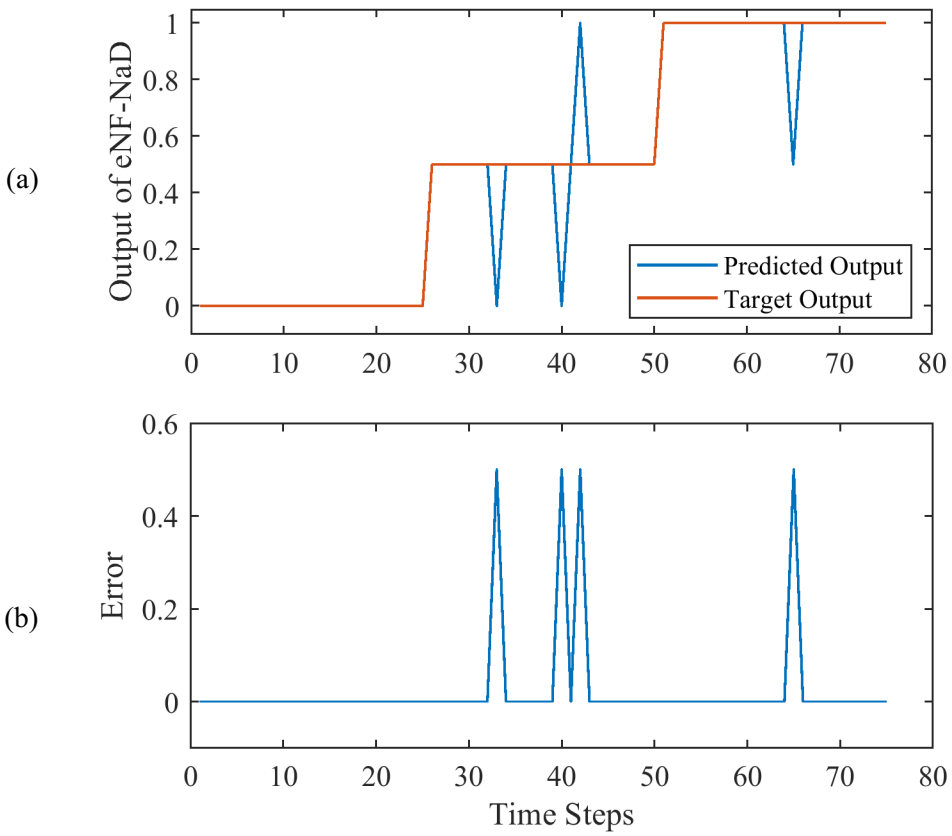


Fig. 4.4 (a) Performance of the eNF-NaD classifier with respect to the desired output (red line) and classifier's output (blue line); (b) Absolute errors.

Fig. 4.4(a) shows the verification process of the developed eNF-NaD classifier for the Iris data. It generates four false results in misclassification of the output data. Fig. 4.4(b) shows the absolute errors of the verification.

### 4.3.2 Breast cancer dataset

A second simulation test is undertaken using the Wisconsin Breast Cancer Dataset [130] to check the robustness of the proposed eNF classifier. This dataset has four input variables: glucose ($x_1$), homa ($x_2$), adiponectin ($x_3$), and MCP ($x_4$). The output has two classes: benign and malignant, or the output space is divided into 2 classes to be unbiased. The initial MFs for this dataset is shown in Fig. 4.5, which are from the first input data pair.

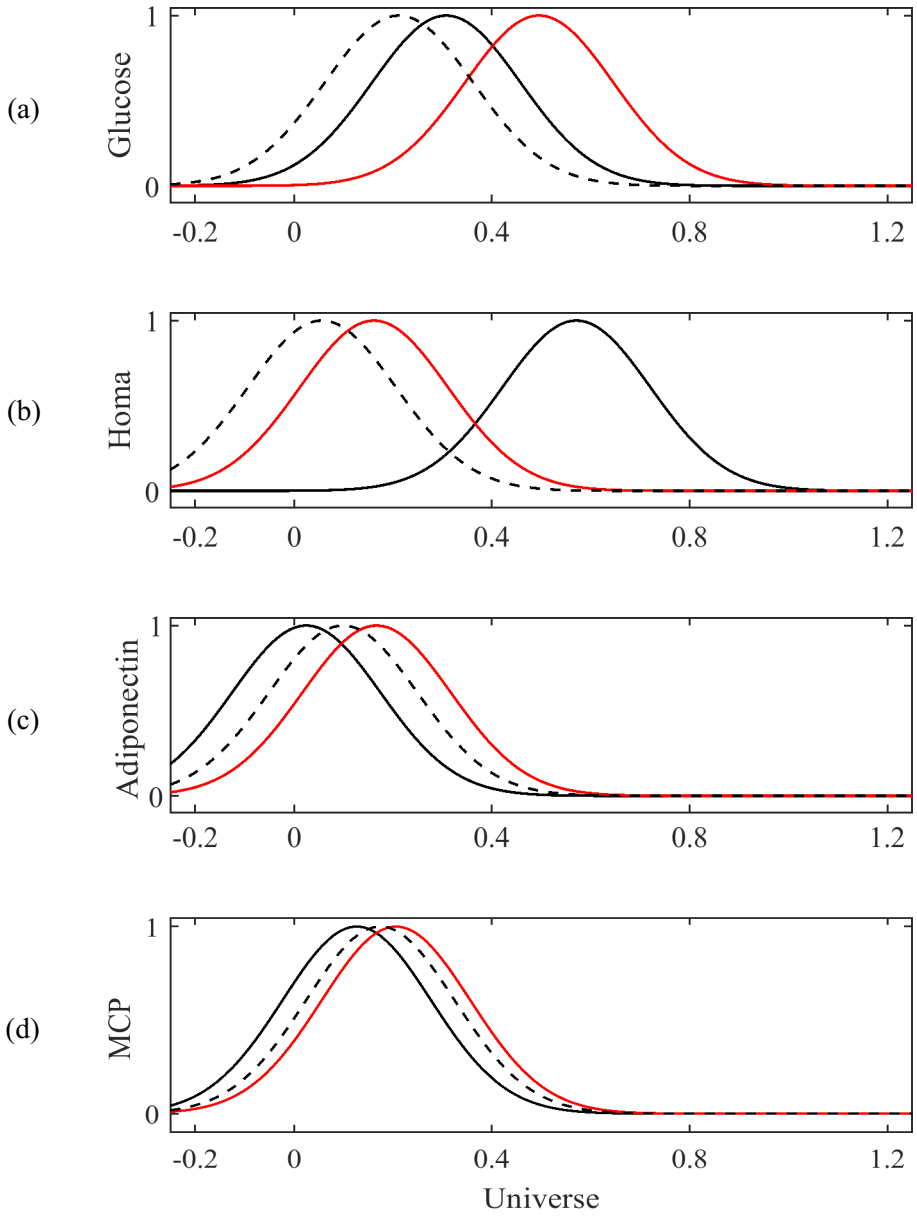


Fig. 4.5 Initial MFs of the inputs using the first data set for breast cancer dataset (a) Glucose, (b) Homa, (c) Adiponectin, (d) MCP.

This dataset has 116 data pairs for analysis: 58 pairs will be used for training and remaining 58 pairs will be used for verification. After training, the MFs of the input variables of the eNF-NaD classifier are shown in Fig. 4.6, which are related to the projected centers and spreads of the corresponding clusters.

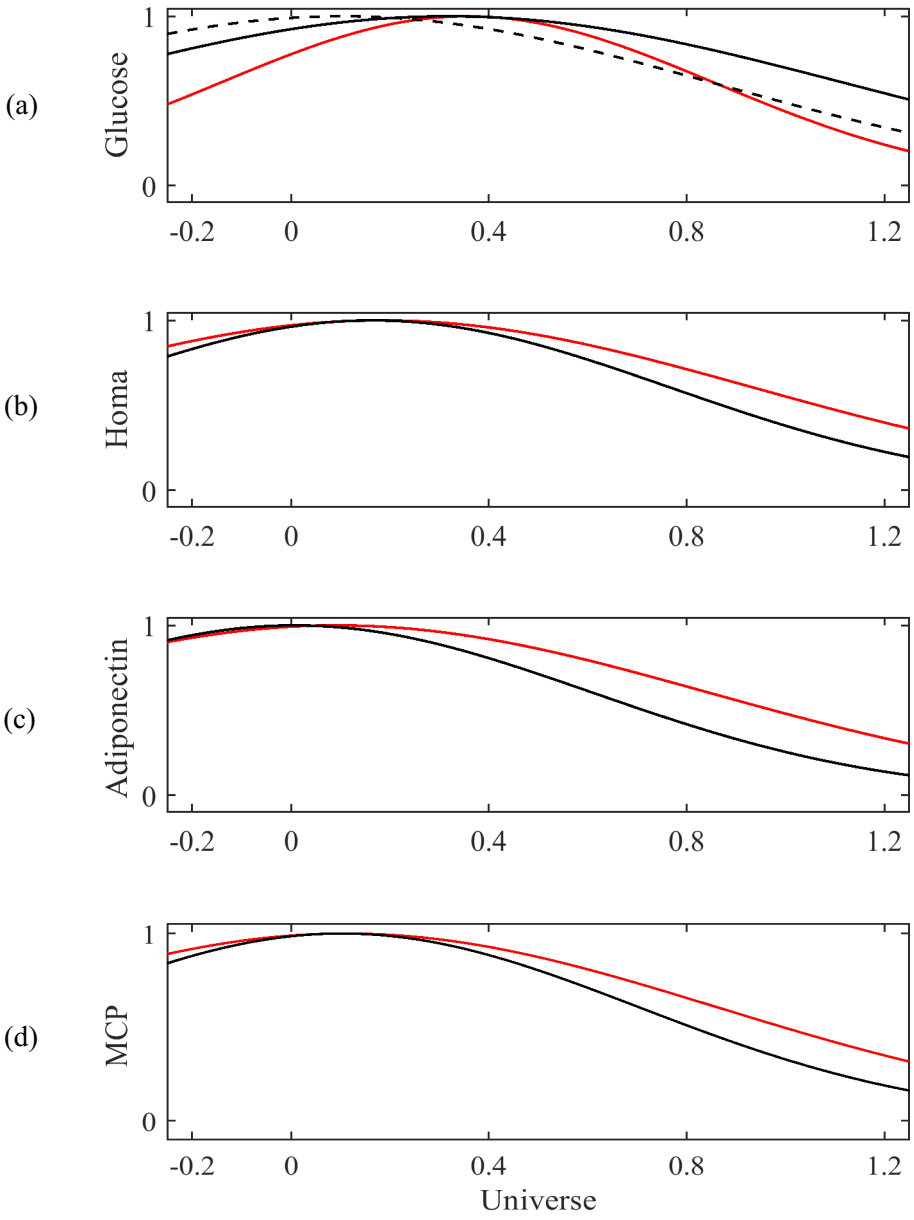


Fig. 4.6 The final MFs of the eNF-NaD classifier for the breast cancer dataset (a) Glucose, (b) Homa, (c) Adiponectin, (d) MCP.

After processing, the classification results are summarized in Table 4.2. It is clear that the training can significantly improve the classification accuracy. In terms of the number of formulated clusters, the SEF and eNF are more efficient in the evolving process than the TWNFI and the eTS classifiers (i.e., 4 vs. 2 clusters). Since the SEF adopts 2 clusters/rules, it results in the lowest classification accuracy in this case.

**Table 4.2. Performance of the related classifiers using the breast cancer data.**

| Classifier | Success Rate (%) | | No. of Clusters | No. of Rules | Average Operation Time (sec) |
|---|---|---|---|---|---|
| | Before Training | After Training | | | |
| TWNFI | 74.25 | 81.06 | 4 | 5 | 1.61 |
| eTS | 67.90 | 78.70 | 4 | 3 | 0.78 |
| SEF | 59.31 | 68.08 | 2 | 2 | 0.91 |
| eNF-GD | 74.83 | 82.14 | 2 | 3 | 0.93 |
| eNF-NaD | 81.57 | 87.93 | 2 | 3 | 0.48 |

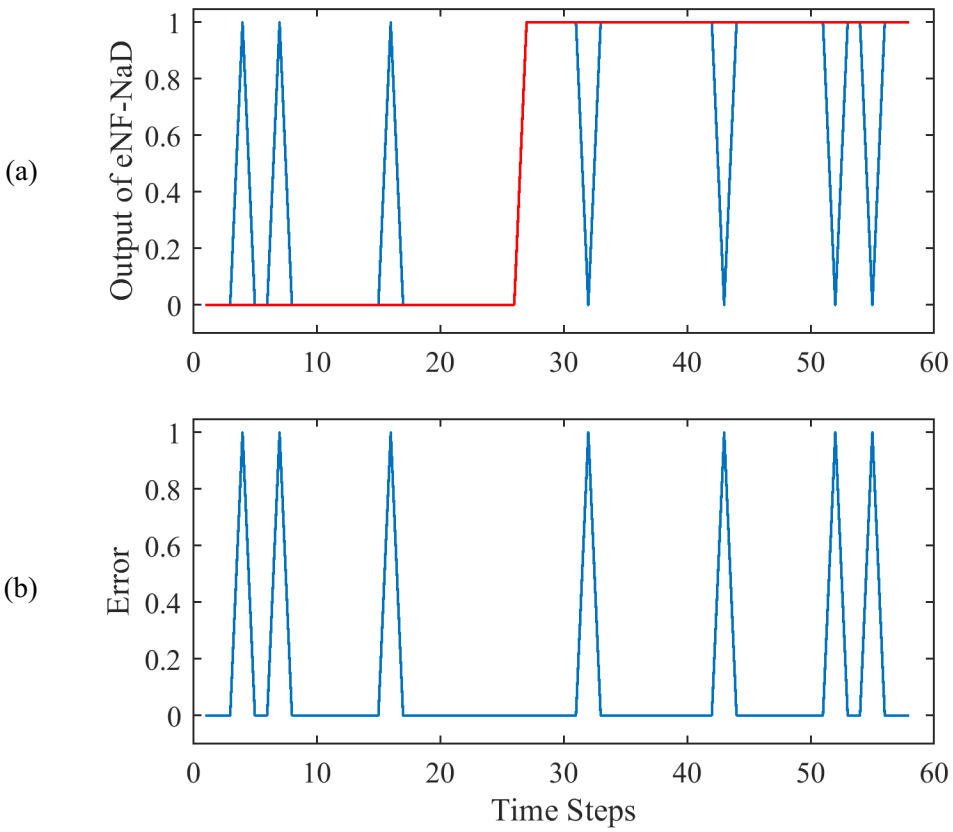


Fig. 4.7 (a) Performance of the eNF-NaD classifier with respect to the desired output (red line) and classifier's output (blue line); (b) Absolute errors.

With the comparison of the SEF and the eNF methods (i.e., eNF-GD and eNF-NaD), it is seen that the proposed evolving algorithm in eNF is more efficient than the related evolving algorithms. On the other hand, the eNF-NaD outperforms the eNF-GD in terms of classification accuracy (87.93% vs. 82.14%) and processing speed (0.48 sec vs. 0.93 sec), due to its efficient NaD training.

Fig. 4.7(a) shows the verification process of the developed eNF-NaD classifier for the Breast cancer data. It generates three false alarms and four missed alarms in classification, which misclassifies the output data. Fig. 4.7(b) shows the absolute errors of the verification.

## 4.4 Discussion

A constrained evolving NF classifier, eNF in short, has been developed in this study for real-time pattern classification. The cluster evolution is performed based on the constrained output space partitions; the purpose is to prevent possible misleading diagnostic information. The suggested evolving algorithm has the ability of adding or subtracting rules adaptively, and the distinguishable patterns can be recognized between the input data and the constrained output space partition. A novel normalized Adadelta (i.e., NaD) method is proposed to improve training efficiency and classification convergence. The effectiveness of the developed eNF classifier has been verified by simulation. Test results have shown that the new eNF classifier can effectively partition the input-output spaces with the appropriate constrained evolving strategy. It outperforms other related pattern classification techniques. The proposed NaD training method can improve training efficiency using less processing time, and convergence with higher classification accuracy.

# Chapter 5

# Gearbox System Health Condition Monitoring

## 5.1 Overview

A gearbox is a complex power transmission system, consisting of gears, bearings, and shafts; each of them has its own vibration features and fault-related properties. The information of health condition of each component can be analyzed by the use of appropriate signal processing techniques. As illustrated in Introduction, fault diagnosis is based on vibration analysis in this work.

The gear mesh signals are usually strong and dominate gearbox vibration. Gear fault detection can be undertaken by signal processing in this work [26]. In Chapter 2, a wavelet transform (WT) based signal processing technique is introduced to perform gear fault diagnosis. The vibration signal from the gearbox is analyzed by a WT technique combined with spectrum analysis to recognize gear fault features for health monitoring and fault diagnosis.

The features from the gear system are used as input for classification of faults in the gearbox by the use of the proposed evolving neuro-fuzzy (eNF) classifier. The eNF parameters are optimized by using the suggested adaptive method (NaD) method. By simulation in Chapter 4, the eNF-NaD model proposed in this study has proven to be efficient for classification and robust to the change in feature parameters. Thus, the eNF-NaD technology will be implemented for gear health condition monitoring in this chapter.

The vibration signal of rolling element bearings in a gearbox is relatively weak in magnitude and modulated by of gear mesh vibration. It is necessary to filter out the gear mesh vibration so as to predict bearing health conditions. Then, the proposed local mode decomposition (LMD) technique will be applied to extract the bearing fault features in the form of amplified mode functions ($\Psi$). Bearing fault will be predicted by analyzing the resulting spectrum of amplified mode functions $\Psi$.

This Chapter focuses on implementation of the related techniques discussed in previous chapters for gearbox health condition monitoring. It will also examine the effectiveness of the suggested averaged power spectrum technique for fault detection in gear system, the eNF-NaD classifier for real-time gear system monitoring, and the LMD technique for bearing fault detection. But some fundamental analysis theories will be discussed first in section 5.2 before advanced gear system monitoring applications.

## 5.2 Gearbox System Health Condition Monitoring

A gearbox system health can be monitored by predicting the health states of its main components. In this section we will be discussing the details of experimental setup used for this study and procedures for condition monitoring of in a gearbox system.

### 5.2.1 Experimental Setup

The experimental setup used in this test is shown in Fig. 5.1. This setup is specially designed for simulation of machinery faults and study of gearbox dynamics, which is robust to run under different loading and speed operating conditions. The system is powered by 2.2 kW (3 HP) induction motor (Marathon Electric, model: 56T34F5306J) with a speed range of 0.3 Hz to 60 Hz. The speed of motor is controlled using a variable frequency speed controller (VFD022B21A, Delta Electronics Inc.).

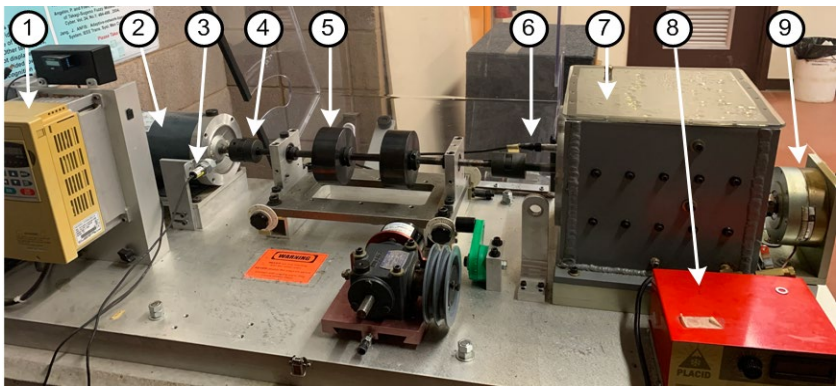


Fig. 5.1 Experimental setup: (1) variable speed controller; (2) drive motor; (3) optical sensor; (4) flexible-coupling; (5) load disc; (6) accelerometers (sensors) (7) gearbox; (8) electric load controller (9) magnetic brake load system.

The motor and the main driving shaft are connected using a flexible coupling to provide damping for shocks and other high-frequency impacts from the motor. The actual speed of the shaft is calculated from a one-pulse-per-revolution signal collected by using an optical sensor (Monarch Instruments, model ROLS-W), which can also be used as a reference for TSA filtering. The PC controllable magnetic brake system (B150-24-H, Placid Industries) is used to provide loading to the gearbox.

The detailed gearbox system is shown in Fig. 5.2(a), which consists of two pairs of spur gears and bearings. The first pair of gears has 32 and 80 teeth for the pinion and the gear, respectively; and second pair has 96 and 48 teeth for the pinion and the gear, respectively. The bearing (MB ER-10K) on the driving shaft, close to the pinion of the first pair is used for the study in this experiment.

The vibration signals are collected using ICP accelerometers (SN98697, ICP-IMI) with 100mV/g sensitivity. These ICP sensors are mounted in different directions on the gearbox casing to collect data along the corresponding directions. These sensors are connected to a data acquisition board (NI PCI-4472), attached to the computer. This data acquisition board has anti-aliasing filters with cut-off frequency set to half of the sampling frequency. A software interface is developed to control the data acquisition operations in real-time, in terms of the sensor network, sampling frequency, data size, etc.

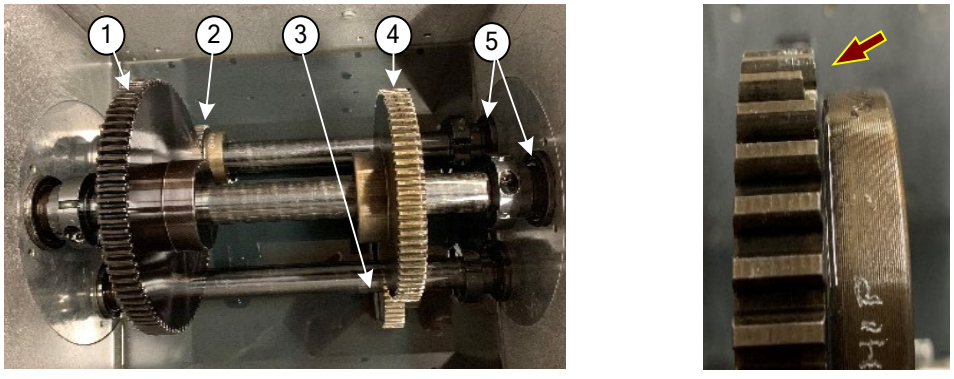


(a) (b)

Fig. 5.2 (a) A two-stage gear system: (1) input gear; (2) input pinion; (3) output pinion; (4) output gear (5) the roller bearings. (b) A simulated damaged gear with one partially broken tooth (chipped gear).

Three gear conditions are tested as illustrated in Fig. 5.3:

1) healthy gears: 4 pairs of gears are tested, and 52 data sets are collected for analysis;

2) cracked gears: 3 pairs of gears are tested and 67 data sets are collected;

3) chipped gears: 3 pairs of gears are tested and 48 data sets are collected for analysis.

The health conditions of each gear are constrained to three states:

$C_1$= healthy, $C_2$= possibly damaged, $C_3$= damaged.

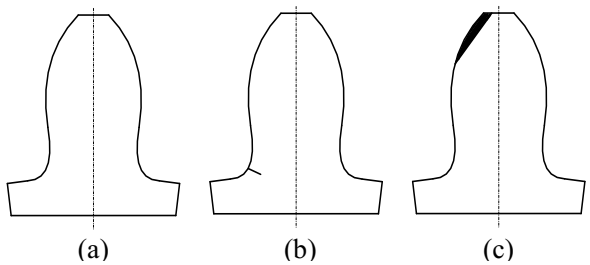


Fig. 5.3 Tested gear conditions: (a) healthy gears; (b) cracked gears; (c) chipped gears.

The bearing conditions for this study are healthy, outer race fault, inner race fault and rolling element (ball) fault. This work focuses on diagnosis of system fault at its initial stage, or it means during study only one component (either a gear or a bearing) will be faulty. The procedure of this study is discussed in following sub-section.

### 5.2.2 Gearbox Health Analysis

Fault diagnosis takes several stages of processing including collection of signal, pre-processing, signal processing, feature extraction, and fault detection. The flow chart of the proposed methodology used for gearbox analysis is shown in Fig. 5.4.

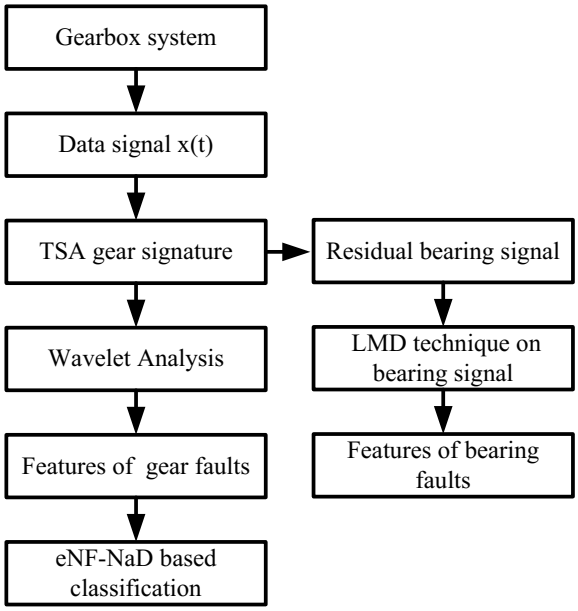


Fig. 5.4 An example of gear system health analysis

A vibration signal is collected from the gearbox, which is preprocessed by DAQ and stored in a computer system. The TSA is performed to calculate the signal average, which is used for advanced signal processing. The results are further processed to extract gear fault features like wavelet amplitude, phase amplitude and beta-kurtosis, which are used as input to the classifiers. The residual signal from the TSA contains information of bearing health conditions, which will be used as input to the proposed LMD technique for bearing health analysis.

The processing details are discussed below:

a) Gear fault analysis

Gear fault can be classified into two categories: localized defects (e.g., broken tooth and chipped tooth) and distributed defects (e.g., scoring and wear). This work will focus on localized gear fault diagnosis because a localized fault not only will degrade transmission accuracy but also may cause sudden failures. In this work, the gear fault diagnosis is conducted gear by gear.

Fig. 5.5 illustrates the processing procedures for gear fault detection using WT analysis as an example. The collected vibration signal, $x(t)$, will be used as input to the TSA filter to eliminate the irregular components of the gearbox and derive the signal

average of the gear to be monitored. The gear signal average is processed by continuous wavelet for time-frequency information analysis. The power spectrum of the continuous WT is used for detailed fault detection.

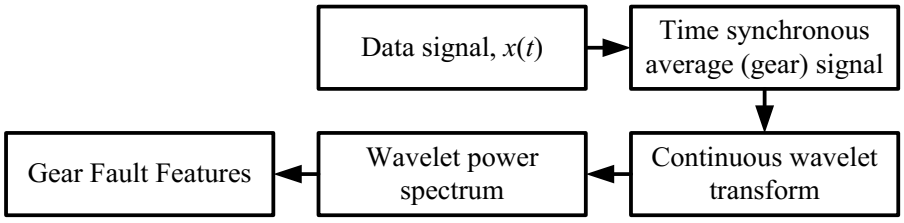


Fig. 5.5 An example for gear fault feature extraction: WT-based gear fault analysis.

b) Gear fault diagnostic classification

As mentioned in subsection, this work will focus on classification of localized gear faults. As the measured vibration signal is generated from various vibratory sources in a gearbox, the primary step is to differentiate the signal specific to each gear by TSA filtering. In this filtering process, the signal components that are non-synchronous to the rotation of the gear of interest (e.g., those from bearings, shafts and other gears) can be filtered out. As a result, each gear signal is computed and represented in one full revolution, called the signal average, which will be used for advanced analysis.

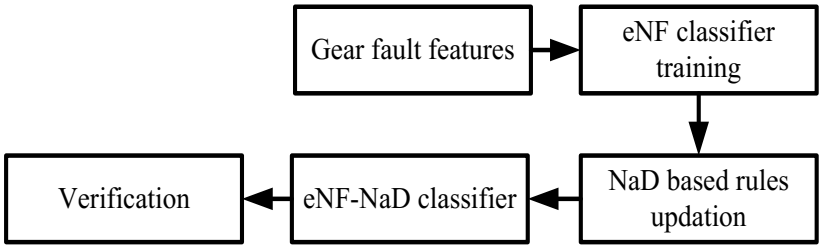


Fig. 5.6 An example for gear fault feature classification: The eNF-NaD classifier.

Many techniques have been proposed in the literature for gear fault detection. Because of the complexity and variation of the machinery dynamics and operating conditions, however, each technique has its own advantages and limitations, and is efficient for specific applications only. Based on systematic investigation in [89], in this work, three

features will be selected for this diagnostic classification from three information domains: energy, amplitude, and phase:

a) beta kurtosis index ($x_1$) using the overall residual signal;

b) wavelet energy index ($x_2$): using the overall residual signal obtained by band-stop filtering out the GMF $f_r$ $Z$ and its harmonics, where $f_r$ is the rotation frequency (Hz) of the gear of interest and $Z$ is the number of teeth of the gear;

c) phase demodulation index ($x_3$): using the signal average.

### 5.2.3 Bearing Fault Detection

The signal collected from system contains information of bearing as well as gears; it is necessary to remove gear signatures for fault detection of rolling element bearings. The Fig. 5.6 shows the flow chart for bearing fault analysis. Firstly the gear signatures from collected signal are removed. The bearing faults detection is then undertaken using proposed LMD analysis technique, discussed in section 3.2.

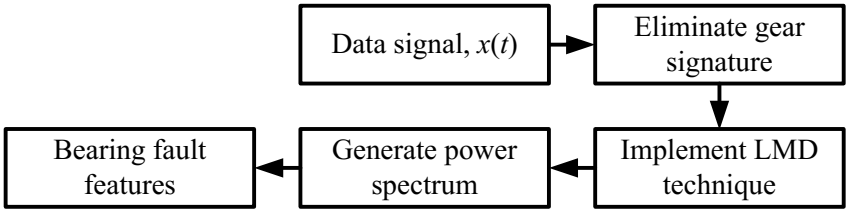


Fig. 5.7 An example for bearing fault feature extraction: LMD based bearing fault analysis.

## 5.3 Gear Fault Analysis and its Classification

A gearbox system is analyzed for fault detection in gear system as well as bearing system. The results for gear fault and bearing fault analysis are discussed in following subsections 5.4.1 and 5.4.2, respectively. The gear fault diagnosis using the proposed eNF-NaD classifier is discussed in subsection 5.4.3.

### 5.3.1 Gear Health Analysis

The gear signatures are dominant in the collected vibration signal. The gear fault-related features are periodic in nature, which are relatively easy to separate from aperiodic features of the signal. A signal average after the TSA is shown in Fig. 5.8, which is then processed by the WT to extract time-frequency features.

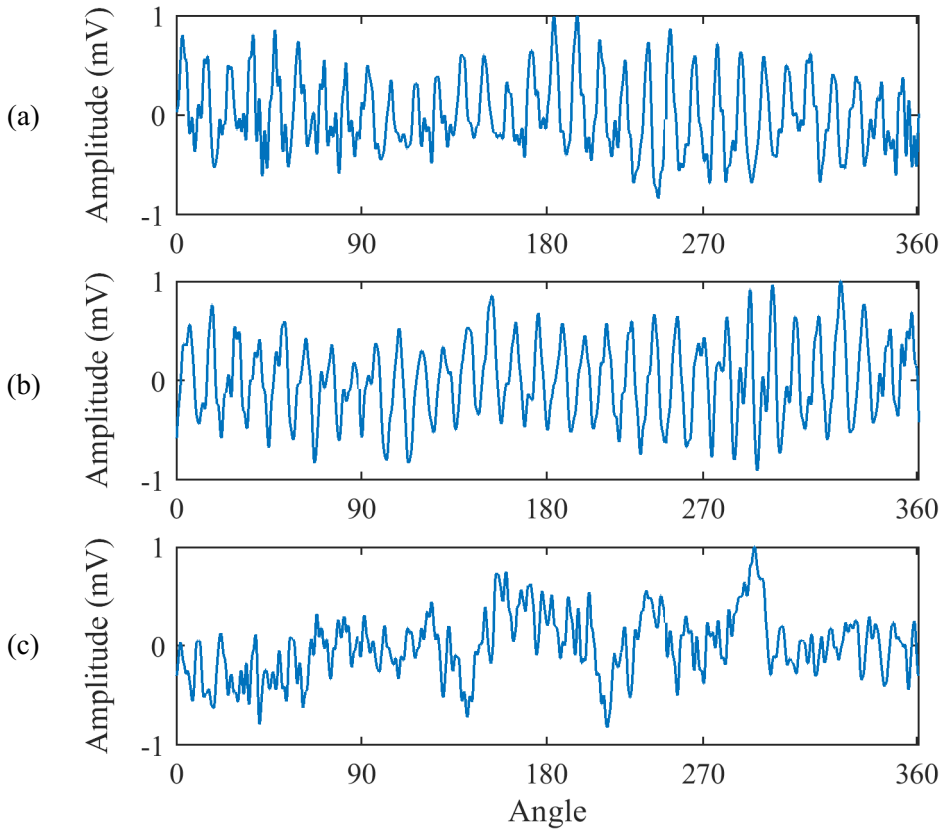


Fig. 5.8 Signal average for different gear conditions: (a) Healthy gear, (b) Cracked gear, (c) Broken tooth gear.

This WT for each gear condition is shown in Fig. 5.9. It can be observed that healthy gear condition, shown in Fig. 5.9(a), shows some yellow area (representing high amplitudes) at the scale number $a$ = 60, which correlates to GMF (960 Hz). Similarly, the gear with a crack, shown in Fig. 5.9(b), also shows much larger yellow area, at the scale number $a$ = 60, compared to healthy gear, and it can be considered as early indication of presence of crack fault in gear system. The gear system with a broken tooth, shown in Fig. 5.9 (c), shows high amplitude values at scale $a$ = 1, which correspond to the running

frequency (30 Hz) of gear system, because the broken tooth interacts once per rotation with other gear.

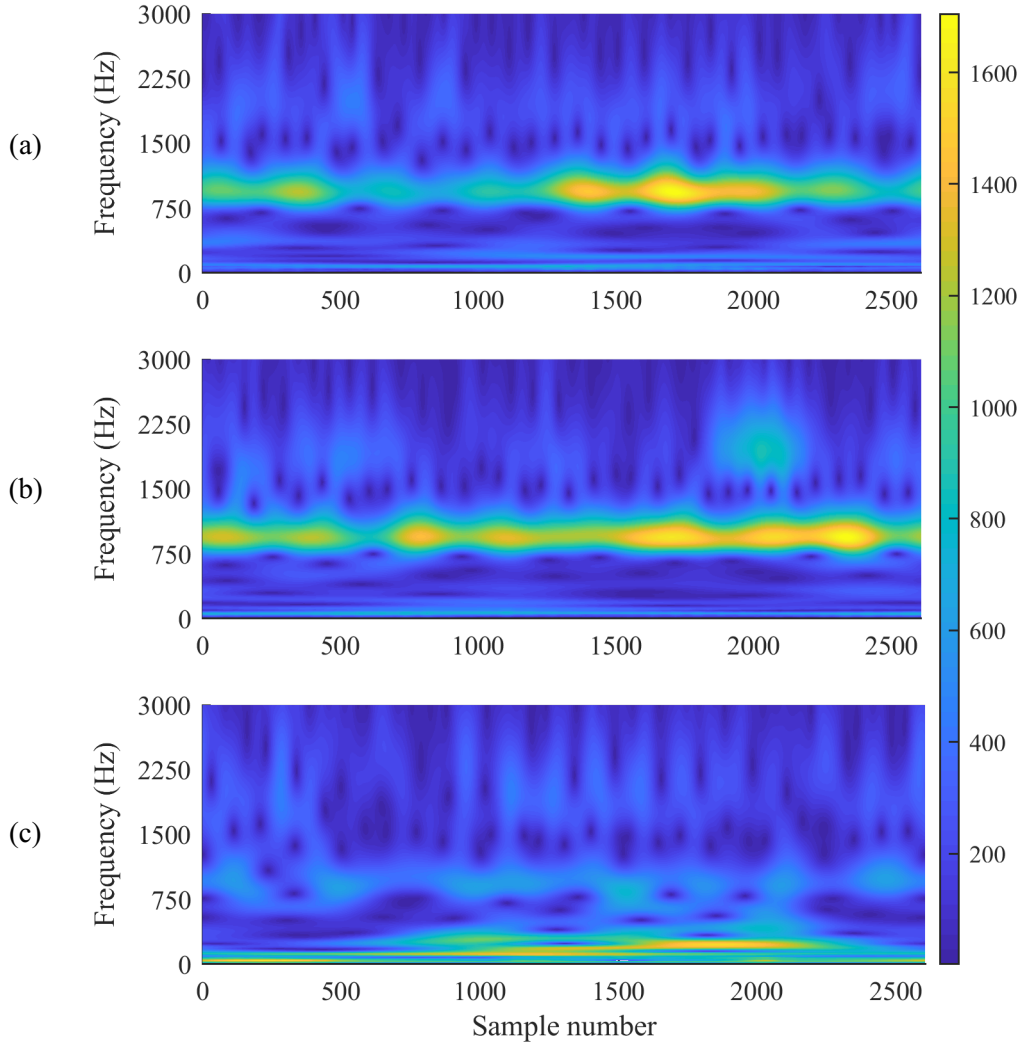


Fig. 5.9 Wavelet spectrum analysis for different gears: (a) Healthy gear, (b) Cracked gear, (c) Broken tooth gear.

This wavelet spectrum is then time-averaged to improve the signal-to-noise ratio, and then detect presence of gear faults. The comparison of the results is shown in Fig. 5.10. The features extracted from the wavelet spectrum are used as one of the inputs to the classifiers.

The Fig. 5.10(a) shows the result for a healthy gear and the peak is at GMF ($f_r$ $Z$) of the first gear pair (i.e. 960 Hz). The processing result for a cracked gear is shown in Fig.

5.10(b), with elevated peaks as a result of higher amplitudes of the vibration signal from the gearbox. For a broken tooth gear as shown in Fig. 5.10(c), the peak is located at the shaft frequency (i.e. 30 Hz) as the occurrence of meshing of the broken tooth is once per rotation of the shaft. The peak at the GMF is very low compared to the peak at the shaft frequency, as the broken tooth generates a high amplitude vibration signature compared to other tooth meshing engagements.

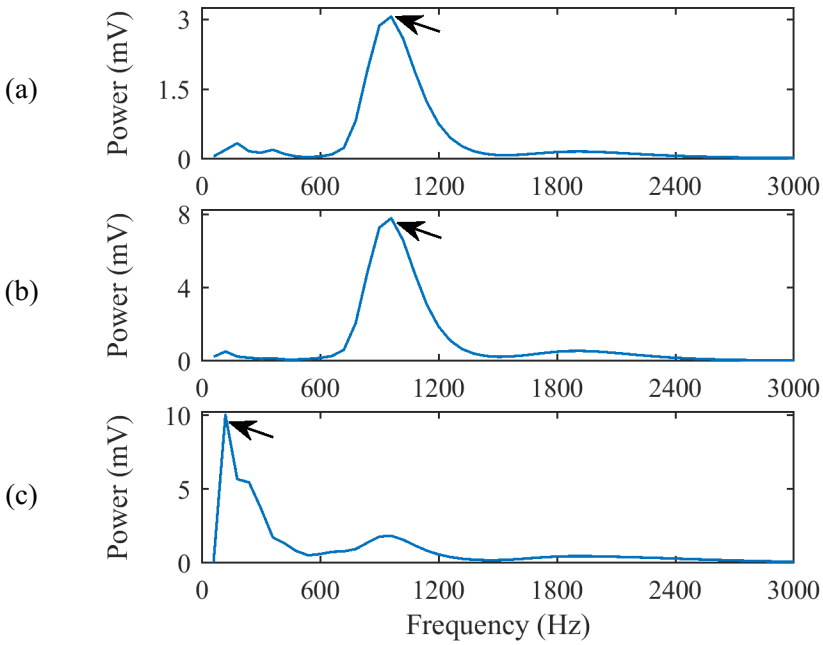


Fig. 5.10 Averaged wavelet power spectrum for different gears: (a) Healthy gear, (b) Cracked gear, (c) Broken tooth gear. (Arrows indicate the gear characteristic frequency).

From the above results, the wavelet power spectrum analysis can detect localized faults in the gear system. The advantage of this technique is that it can provide more detailed information of occurrence of fault compared to regular wavelet analysis, which is useful for early recognition of a gear fault.

### 5.3.2 Gear Health Monitoring Indices for Classification

Gear system health monitoring requires comparison between some monitoring indices, which are sensitive to the fault features. Researchers have used numerous statistical parameters, such as standard deviation, to represent fault related features. As

mentioned in section 2.5, in this work, three features will be selected for this diagnostic classification from three information domains: energy, amplitude, and phase:

1) Beta Kurtosis Index:

The beta-kurtosis function $B(z)$ for different gear health condition are shown in Fig. 5.12. The beta-kurtosis index values, calculated using Eq. (2.15), are used as first input $x_1$ to the classifier.

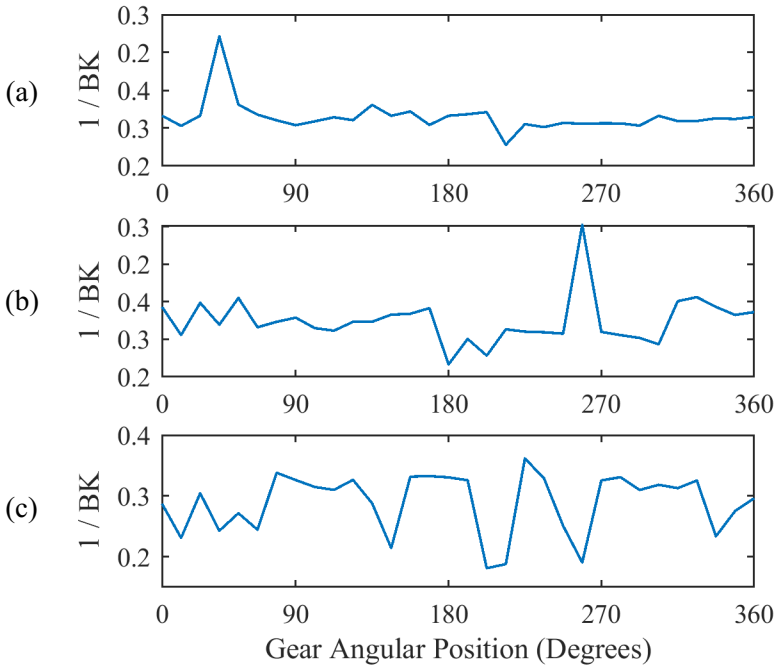


Fig. 5.11 Beta-Kurtosis reference function for different gears: (a) Healthy gear, (b) Cracked gear, (c) Broken tooth gear.

2) Wavelet Energy Index:

The Wavelet energy function $W(z)$ for different gear health condition are shown in Fig. 5.11. The wavelet energy index values, calculated using Eq. (2.15), are used as second input $x_2$ to the classifier.

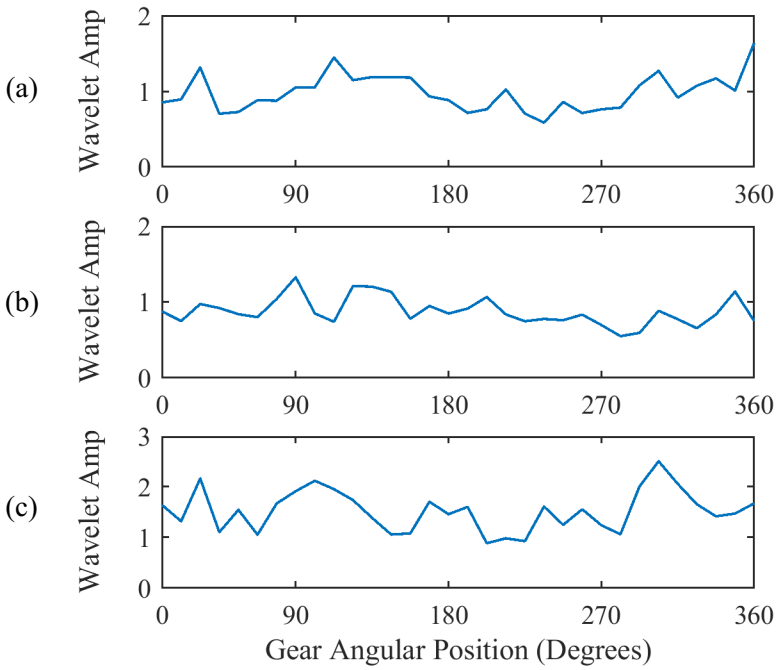


Fig. 5.12 The wavelet energy reference function for different gears: (a) Healthy gear, (b) Cracked gear, (c) Broken tooth gear.

3) Phase Modulation Index:

The phase reference function $P(z)$ for different gear health condition is shown in Fig. 5.13. The phase index values, calculated using Eq. (2.15), are used as third input $x_3$ to the classifier.

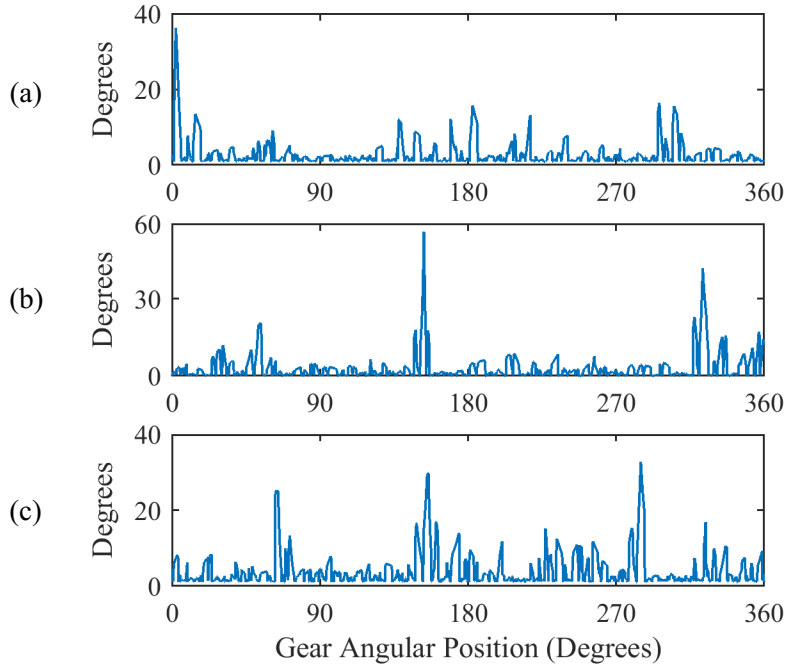


Fig. 5.13 The phase reference function for different gears: (a) Healthy gear, (b) Cracked gear, (c) Broken tooth gear.

The three monitoring indices, extracted from gear system, are used as the input to an eNF classifier, to perform classification of health condition of the gear system. The classification results are shown in following section.

### 5.3.3 Fault Diagnostic Classification in a Gear System

In gearboxes, fault detection can be undertaken by complex signal processing-based approaches [8, 9]. But each signal processing technique has its own merits and limitations in fault detection, related to distortion of signal, approximation, or improper selection of output [9, 11]. In real-time gearbox health condition monitoring, some intelligent tools like neuro-fuzzy (NF) systems can be used for automatic fault diagnostic classification based on features extracted from the related fault detection techniques.

Similarly to the conditions in simulation tests in section 4.3, five related classifiers are used for comparison: eTS, TWNFI, SEF, eNF-DG and eNF-NaD. All of these classifiers are with the three same inputs, and with same training conditions. The testing is undertaken under different load and speed conditions. The sampling frequency is selected to make sure each tooth period should contain about 50 data samples. For

example, if the shaft speed is 1200 rpm, or $f_r$ = 20 Hz, the gear has $Z$ = 32 teeth, the sampling frequency should be about:

$f_s$ = 32 teeth × 50 samples × 20 Hz = 32,000 Hz.

After the TSA filtering, the signal average is further processed to generate the monitoring indices of wavelet amplitude ($x_1$), beta kurtosis ($x_2$) and phase information ($x_3$), which are input variables to the classifiers. Fig. 5.14 shows the initial MFs of the input variables, which are based on first set of input.

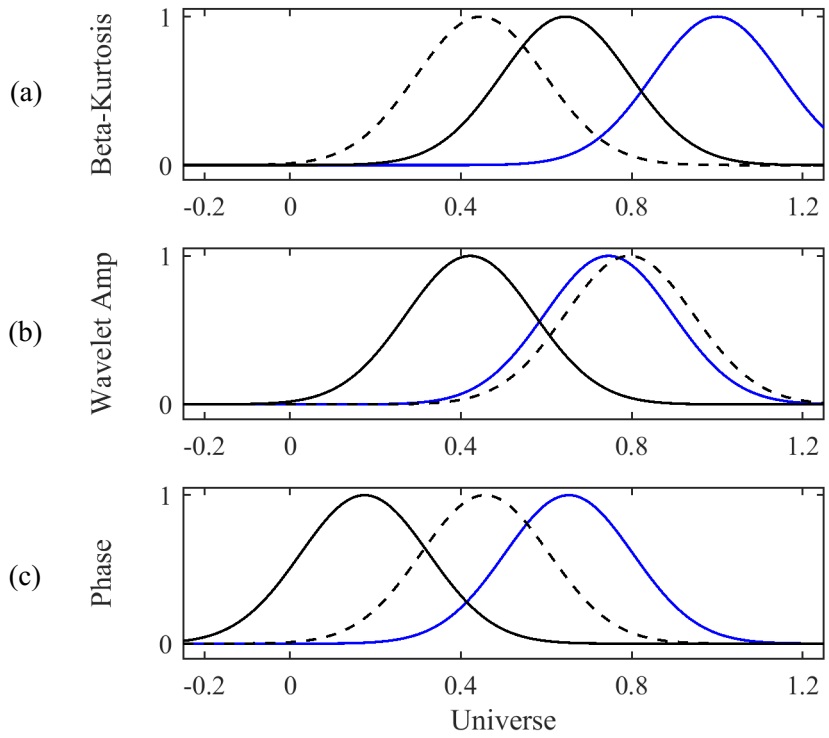


Fig. 5.14 Initial MFs of the input variables of the related classifiers, using the first training data pair (a) Beta-kurtosis, (b) Wavelet amplitude, (c) Phase demodulation.

In training, the evolution of MFs plays a vital role in efficient classification. The eNF classifier can effectively determine the centers $\mu_C$ and spreads $\sigma_C$ to update the MFs corresponding different clusters. After training, the MFs of the input variables of the eNF-NaD classifier are shown in Fig. 5.15.

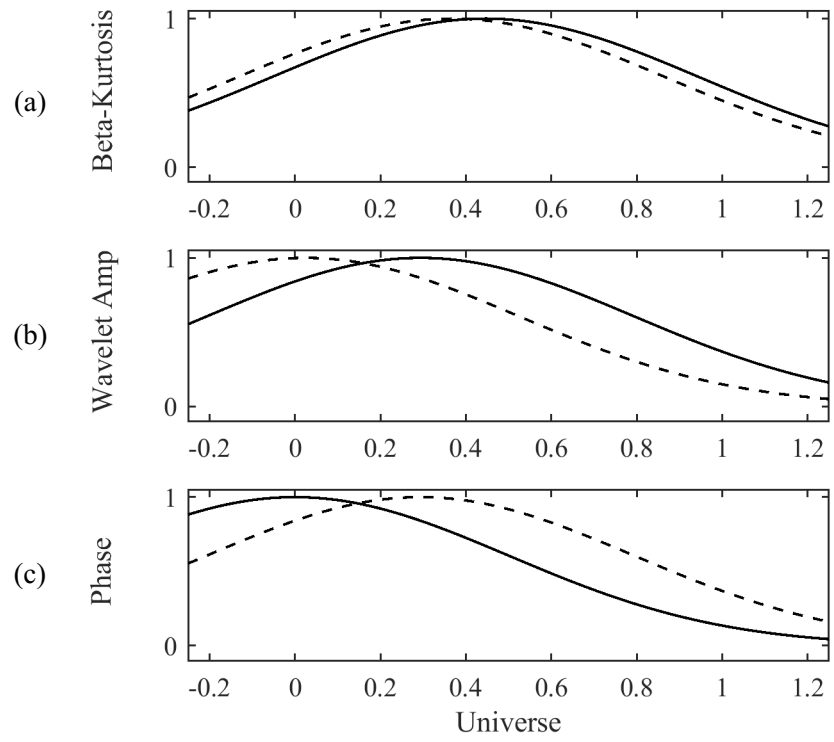


Fig. 5.15 Final MFs of the eNF-NaD classifier in gear system monitoring: (a) Beta-kurtosis (b) Wavelet amplitude (c) Phase demodulation.

Table 5.1 summarizes the diagnostic results using the related classifiers. In gear fault diagnosis, two types of errors are considered: a) false alarm, or the recognized gear fault is caused by other reasons (e.g., speed/load variations) instead of real gear defect; b) missed alarm, or the gear fault is not recognized by the diagnostic classifier. From Table 5.1, it is seen that the proposed eNF classifiers outperform the classical eTS and TWNFI techniques, as well as the SEF classifier, with fewer clusters and higher diagnostic accuracy. That is mainly due to the more efficient evolving approach with the appropriate constrained partition strategy. On the other hand, with the comparison of eNF-GD and eNF-NaD, the proposed NaD training method can improve not only classification accuracy (98.38% vs. 96.74%), but also processing efficiency using less processing time (1.34 sec vs. 1.82 sec), which makes it suitable for real-time monitoring applications.

**Table 5.1. Gear monitoring test results using the related classifiers**

| Classifier | No. of Clusters | No. of Rules | Success Rate (%) | | | Average Operation Time (sec) | Overall Accuracy (%) |
|---|---|---|---|---|---|---|---|
| | | | Healthy Gear | Cracked Gear | Chipped Gear | | |
| TWNFI | 5 | 6 | 87.20 | 85.36 | 90.77 | 2.83 | 87.49 |
| eTS | 5 | 6 | 87.71 | 88.70 | 89.42 | 2.27 | 88.59 |
| SEF | 4 | 4 | 96.38 | 94.31 | 95.15 | 1.99 | 95.21 |
| eNF-GD | 3 | 4 | 97.91 | 95.86 | 96.67 | 1.82 | 96.74 |
| eNF-NaD | 3 | 4 | 99.13 | 97.12 | 99.34 | 1.34 | 98.38 |

Fig. 5.16(a) shows the classification process of the eNF-NaD classifier during the testing process. It is seen that eNF-NaD classifier is efficient in separating healthy state from the faulty state of a gear system. But it has generated some errors in gear fault diagnosis with two false alarms and one missed alarm.

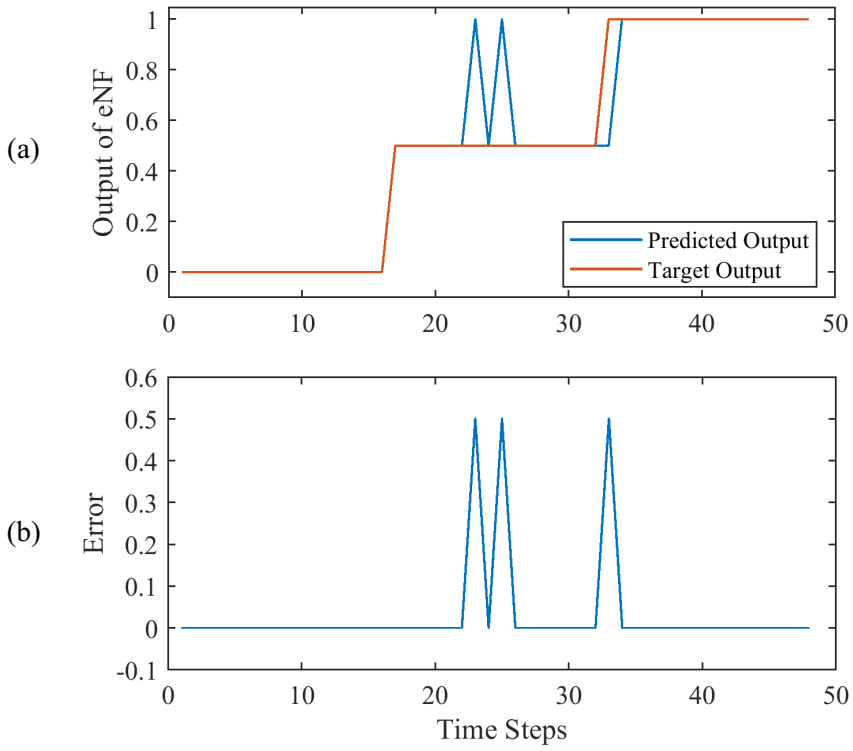


Fig. 5.16 (a) Performance of the eNF-NaD classifier with respect to the desired output (red line) and classifier's output (blue line); (b) Absolute errors.

Fig. 5.17 illustrates the constrained output clusters (dotted circles) using the eNF-NaD classifier. The recognized clusters in the output space are indicated by the solid lines, in terms of $x1$ (beta-kurtosis) versus $x2$(wavelet amplitude).

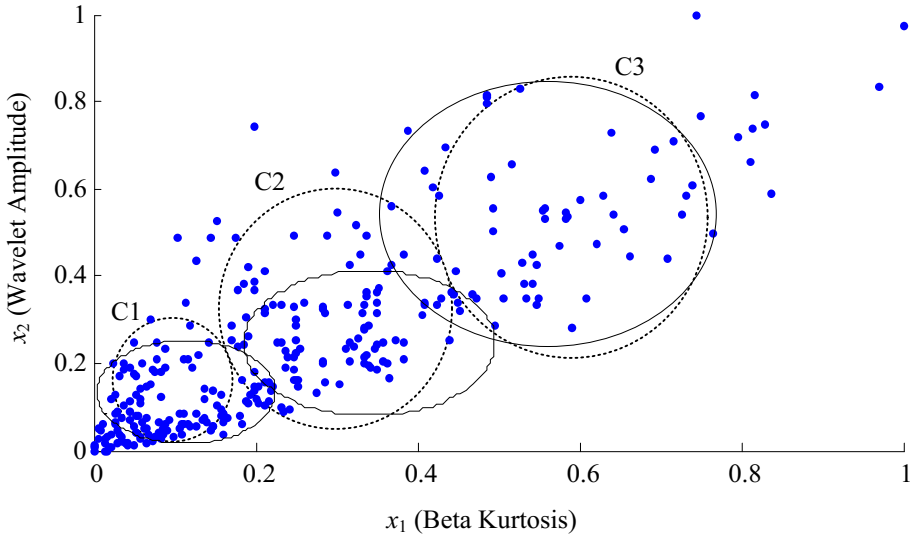


Fig. 5.17 The output space evolving results: The dotted circles $C_1$-$C_3$ represent the constrained output space patterns. Solid circles represent the recognized clusters in the output space.

Fig. 5.18 shows the recognized eNF model architecture after 50 training epochs using all of the training data sets. It is a 6-layer network. Different from a complete NF model, the eNF classifier does not have complementary links with low contribution factors (e.g., less than 0.1 in this case), which can facilitate the processing efficiency.

During the evolving process, this structure is updated gradually and continuously. Initially, each input variable (in layer 1) had 3 MFs (in layer 2): *S.*, *M.* and *L.* that are related to each cluster formulation as illustrated in Fig. 5.18. After the evolving operation, 3 clusters are generates, which result in 4 rules, $R_1 \sim R_4$. At the same time, $x_1$ has two MFs only: $S_1$ and $L_1$. $S_1$ is related to $R_1$ and $R_3$, while $L_1$ is related to $R_2$. $M_1$ is not represented as it is not related to any deciding rules. The firing strength of each rule is calculated in layer 3 by the related inference operation. After normalization in layer 4, the output indicator ($y$) can be computed by defuzzification (e.g., centroid) in layer 5.

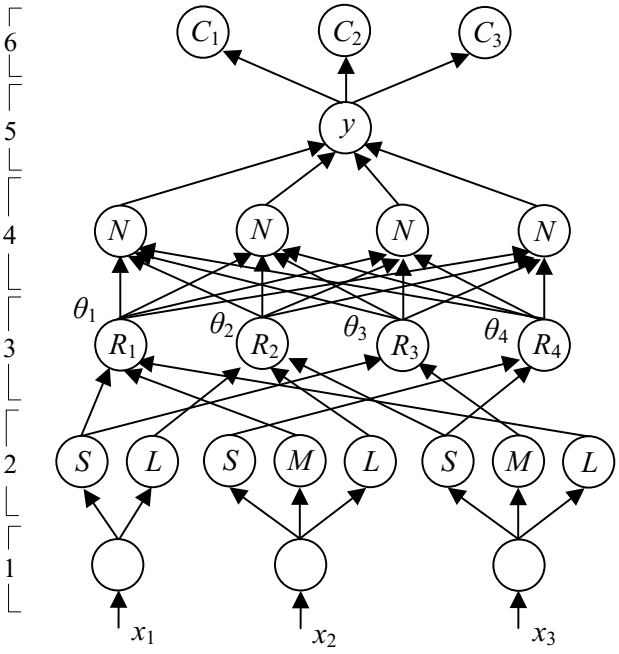


Fig. 5.18 The identified eNF classifier model after 50 training epochs.

The health state of the gear of interest is further classified into three states in layer 6:

- healthy $C_1$ if $y \leq 0.33$,
- damaged $C_3$ if $y > 0.67$, and
- possibly damaged $C_2$ if $0.33 < y \leq 0.67$.

## 5.4 Bearing Fault Analysis in a Gearbox

In a gearbox, the bearing signals are usually weak and modulated by gear signatures. In order to improve signal-to-noise ratio of bearing signal, the gear signatures must be filtered out. This filtering process could help to eradicate gear mesh frequencies and their harmonics, which can generate less number of mode functions for bearing health monitoring. In this study, a leakage-free filter is implemented to minimize the filtering distortion [136]. The parameters of leakage-free filter are chosen based on the information of gearbox, such as running speed and number of teeth on the corresponding gear. The signal from the gearbox, $x(t)$, includes data of different sources such as shafts, bearings, and gears. The gear signature $x_G$ is periodic and can be modeled as integration of gear mesh frequencies and its harmonics such as:

$$x_G = \sum_{m=1}^{M} A_m \cos\left[m(2\pi f_r Z)t + \theta_m\right]; \tag{5.1}$$

where $A_m$ and $\theta_m$ are the respective amplitude and phase of the $m^{th}$ gear harmonic; GMF = $f_r$ $Z$, $Z$ is the number of teeth of the gear, $f_r$ is the shaft speed; and $M$ is the number of mesh frequency harmonics considered ($M$ = 5 in this study).

The removal of gear mesh and its harmonic can be executed in the frequency domain by setting the amplitude of the related stopband spectral amplitudes to zero. If $X(f)$ is the FT of the gearbox signal $x(t)$, set $X(f)$ to zero over the stopbands $f \in [(mZ + 1) - 0.5p, (mZ + 1) + 0.5p]$, where $p$ is selected band window of the stopband. For instance, for the first pair of gears, if the pinion has 32 teeth with shaft speed 30 Hz, the first GMF is 960 Hz. For the second gear pair, if the pinion has 96 teeth with shaft speed of 12 Hz, the second GMF is 1152 Hz. The signal residual after leakage-free filtering is obtained and used as the real part of the inverse FT; the mode functions $\Psi$ can be generated by using the proposed LMD technique to process the frequency components.

The experimental setup, shown in Fig. 5.1, is used for bearing health condition monitoring under the effect of gears. As discussed in subsection 5.2.1, the system is powered by 3 HP induction motor with a speed range of 0.3 Hz to 60 Hz. An optical sensor is used to collect a one-pulse-per-revolution signal from the system. A load is provided to the gearbox by the PC controllable magnetic brake system. The ICP accelerometers are mounted with different orientation on the gearbox casing to collect data (vibration signals). To assure that the information is not distorted, the sensors are placed as close as possible to the bearing being analyzed. In this study, the bearing which is connected to the motor shaft is considered for analysis, as shown in Fig. 5.19.

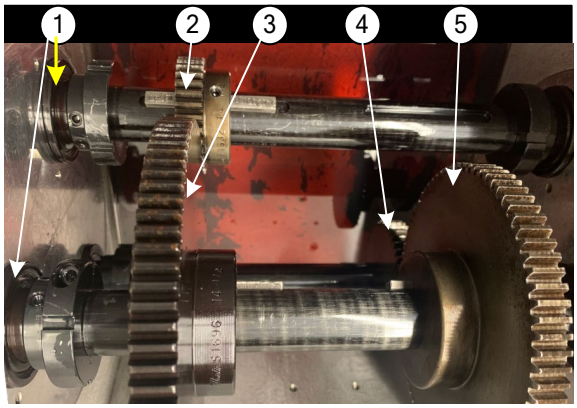


Fig. 5.19 Gearbox system for bearing health monitoring: (1) the roller bearings; (2) input gear; (3) input pinion; (4) output pinion; (5) output gear. (Yellow arrow indicates the bearing being analyzed in this study.)

From systematic investigation, it is observed that the first mode function contains the more information of health state of a bearing. Thus, the power spectrum of the first mode function is used for condition monitoring of bearings in a gearbox. A typical example with motor speed of 30 Hz and braking load of 7.5 Nm will be used for illustration. The corresponding fault characteristic frequencies of outer race fault, inner race fault and rolling element fault are 91.48 Hz, 149.80 Hz, and 119.81 Hz, respectively. For verification, each health condition of bearing is processed by the EMD as well as the proposed LMD technique.

The processing results for a healthy bearing are shown in Fig. 5.20, with characteristic frequency 29.82 Hz. The frequency spectrum of the first IMF obtained by EMD technique, shown in Fig. 5.20(a), shows peak at the frequency but with a high level of noise. Fig. 5.20(b) shows the spectral map of the first $\Psi$ function, which has reduced level of noise in the output. Fig. 5.20(c) illustrates the power spectral of the first $\Psi$ function using the proposed LMD technique, which can provide the best diagnostic results with clear characteristic frequency and its harmonics.

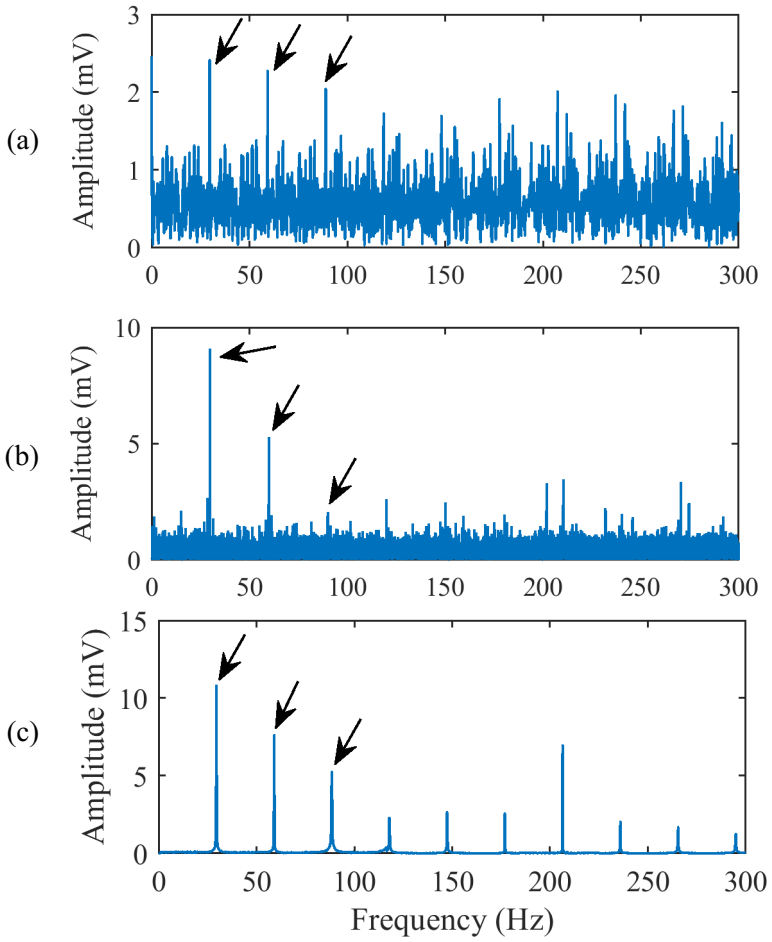


Fig. 5.20 Processing results for a healthy bearing: (a) Frequency spectrum of the first IMF from EMD, (b) Frequency spectrum of the first Ψ function from LMD, (c) Power spectrum of the first Ψ function from LMD. (Arrows indicate the bearing characteristic frequency and its harmonics).

Fig. 5.21 shows the processing results for a bearing with outer race fault whose fault characteristic frequency is 91.53 Hz. Compared with the frequency spectrum of the first IMF obtained by EMD in Fig. 5.21(a), the spectral map of the first $\Psi$ function in Fig. 5.21(b) has reduced level of noise. However, as illustrated in Fig. 5.21(c), the power spectrum of the LMD technique outperforms another two techniques in this case, even though its characteristic frequency amplitude does not dominate the spectrum.

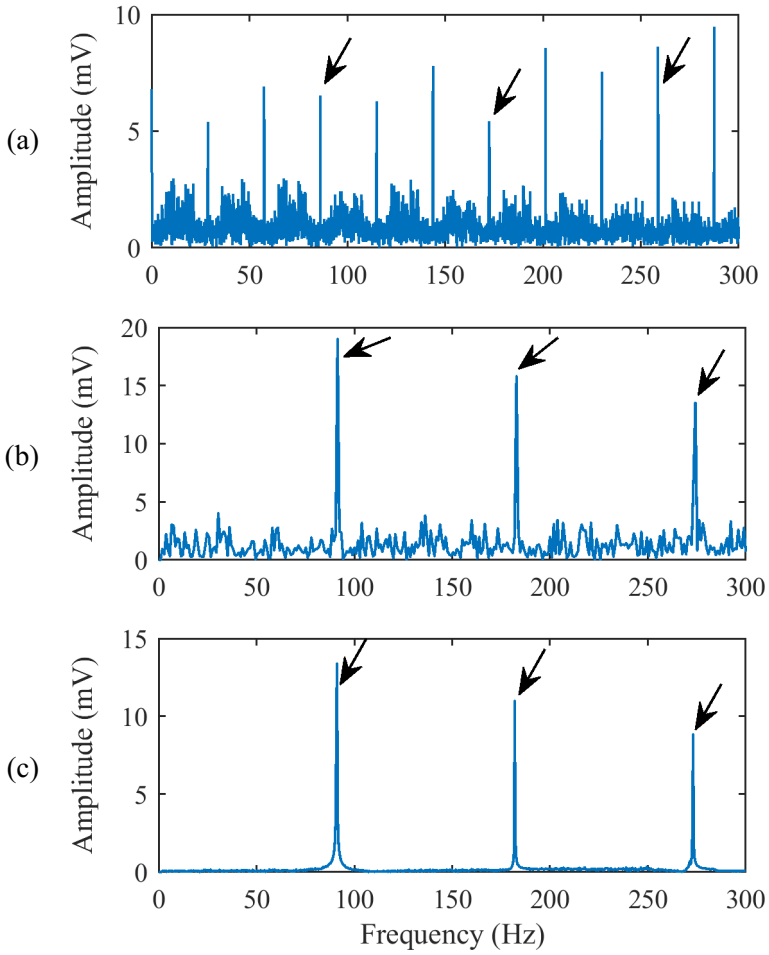


Fig. 5.21 Results from a bearing with outer race fault (a) Frequency spectrum of the first IMF from EMD, (b) Frequency spectrum of the first Ψ function from LMD, (c) Power spectrum of the first Ψ function from LMD. (Arrows indicate the bearing characteristic frequency and its harmonics).

Fig. 5.22 depicts the processing results for a bearing with inner race fault with characteristic frequency 148.4 Hz. It is seen that the first IMF obtained by EMD technique in Fig. 5.22(a) cannot recognize the existence of the bearing fault in this case. In comparison of Fig. 5.22(b) of the first $\Psi$ function, the proposed LMD technique of the first $\Psi$ function in Fig. 5.22(c) provides better processing results in detecting inner race fault in this case, even though the representative spectral peaks are not dominant on the map; it is because the time-varying representative features are time-varying and modulated significantly by gear vibrations.

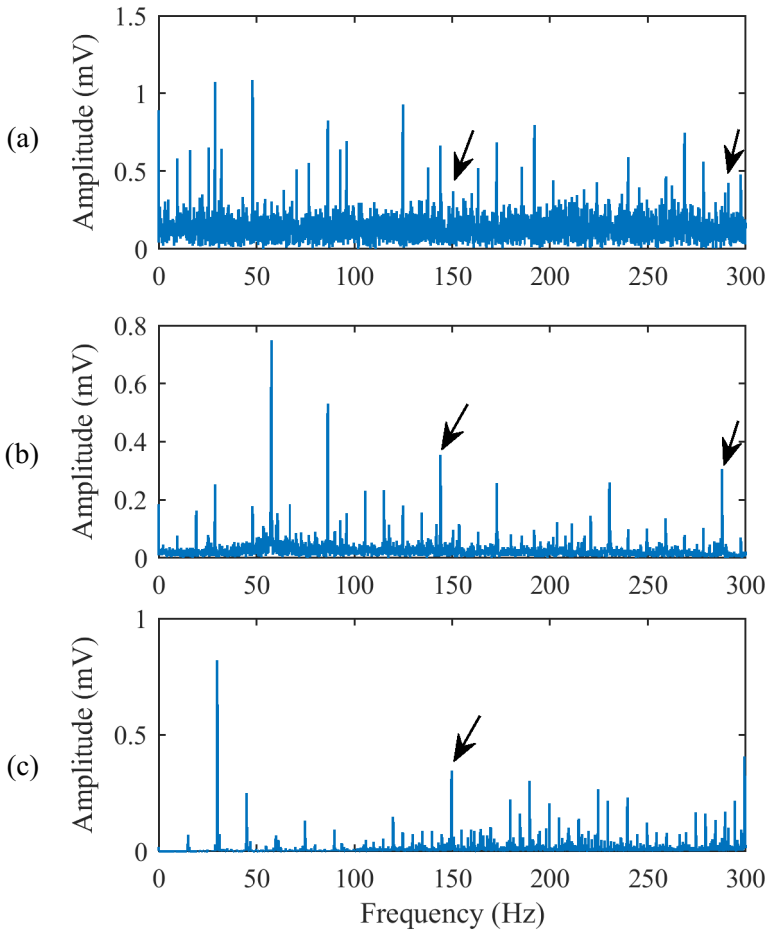


Fig. 5.22 Results from a bearing with inner race fault (a) Frequency spectrum of the first IMF from EMD, (b) Frequency spectrum of the first Ψ function from LMD, (c) Power spectrum of the first Ψ function from LMD. (Arrows indicate the bearing characteristic frequency and its harmonics).

The processing results for a bearing with rolling element (ball) fault are shown in Fig. 5.23, where the fault characteristic frequency is 119.38 Hz. In this case, both the first IMF obtained by EMD technique in Fig. 5.23(a) and the first $\Psi$ function in Fig. 5.23(b) cannot predict the fault condition of the bearing as the characteristic features and time-varying. In this case, the proposed LMD with the first $\Psi$ function in Fig. 5.23(c) is the only technique that can detect random events such as first harmonic of the rolling element fault in a bearing.

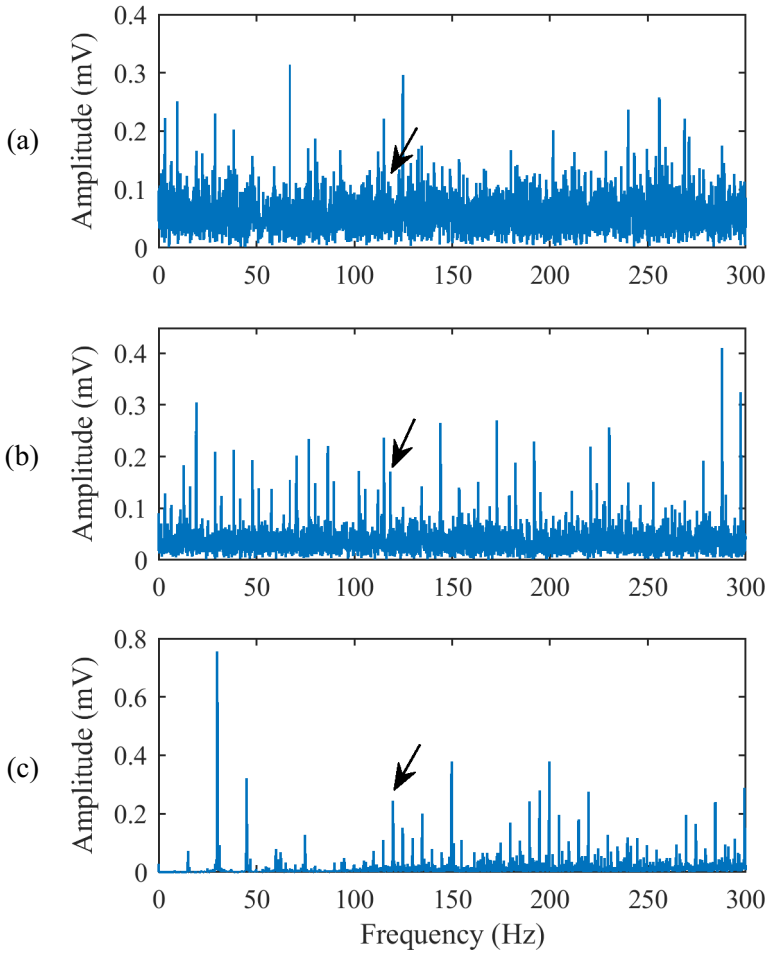


Fig. 5.23 Results from a bearing with rolling element fault (a) Frequency spectrum of the first IMF from EMD, (b) Frequency spectrum of the first Ψ function from LMD, (c) Power spectrum of the first Ψ function from LMD. (Arrows indicate the bearing characteristic frequency and its harmonics).

## 5.5 Discussion

In a gearbox system, advanced signal processing techniques are must for health monitoring of each component. As each component of gearbox has complex interaction with the surrounding system, it is necessary to separate the features related to each component. As gear features are dominant in a gearbox, gear fault analysis has a significant role in health monitoring of gearbox system. The output of WT provides a detailed analysis in time-frequency domain, but it has complex coefficients. The averaged WT features, obtained by converting complex wavelet coefficients into 2D coefficients, can provide clear indication related to presence of faults in gear system. The spectral

graph of averaged wavelet coefficients can highlight the peaks related to fault characteristic frequencies, resulting in improved accuracy of fault diagnosis of gear systems. This technique can be implemented for real-time gear health monitoring systems.

A novel LMD method has been developed in this work for bearing fault analysis in a gearbox system. Based on simulation results, it helps to highlight the periodic events (e.g. outer race faults) and can also enhance the suppressed events (e.g. inner race fault, rolling elements faults) of a bearing system. The power spectrum of the local mode functions ($\Psi$) are analyzed to provide more clear peaks for fault frequencies. The experimental test is conducted and evaluated using real-time dataset collected from a gearbox. The results have shown that the proposed technique can detect bearing faults under the effect of gear system. The combination of the proposed LMD technique and power spectrum analysis has a potential for a fault diagnosis of bearing system in complex structures (e.g. gearbox).

A constrained evolving NF classifier, eNF in short, has been developed in this study for real-time pattern classification. A novel normalized Adadelta (i.e., NaD) method is proposed to improve training efficiency and classification convergence. In simulations, the suggested evolving algorithm has shown the ability of adding or subtracting rules adaptively. Based on the systematic investigation, three monitoring indices, from the domains of energy, amplitude and phase, are selected as input to the eNF system for classification of gear faults. The developed eNF classifier recognizes the distinguishable patterns between the input data and the constrained output space partition. Test results have shown that the new eNF classifier can achieve efficiency of 96%. It outperforms other related pattern classification techniques. The proposed NaD training method can improve training efficiency using less processing time, and convergence with higher classification accuracy of 98%.

# Chapter 6

# Conclusions and Future Work

## 6.1 Conclusion

Gearboxes are the major power transmission units in rotary machinery, and widely used in industrial applications such as automobile and manufacturing industry. Faults in gearbox can result in high risk damage to other components as well as the working environment. In last few decades, the industries have moved towards condition based monitoring of faults to facilitate the fault identifications and to optimize maintenance plans. A gearbox consists of many rotating components like gears and bearings, which have their own faults as well as corresponding features. However, reliable gearbox condition monitoring and health management is still one of the most challenging aspects in predictive maintenance operations. The objective of this PhD research is to develop new techniques to detect faults in gears and bearings so as to improve reliability of gearbox health condition monitoring. Specific research themes include new signal processing techniques to predict defects in gears and bearings; and a new evolving NF classifier to integrate the merits of several features for gear system health monitoring.

Firstly, an averaged wavelet spectrum technique has been proposed for fault detection in a gear system. The vibration signal collected from gearbox is processed using TSA filtering to separate specific features to a gear from the rest of the gear system. Then the signal average is processed using the wavelet transform to analyze time-frequency response for non-linear impulses, and for gear fault detection. Its effectiveness is verified by experimental tests; the spectral peak of broken tooth is at the shaft frequency with a much higher magnitude, which can identify gear faults in a gearbox.

A novel local mode decomposition (LMD) technique has been proposed for more efficient fault detection in bearing systems. The collected vibration signal from a gearbox is dominant by gear mesh signatures. The leakage-free filter is adopted to remove the gear signatures by filtering out the GMF and its first 4 harmonics. The proposed LMD

technique is implemented to analyze the residual signal and the mode functions, which may contain bearing fault characteristic features. By simulation tests, it is observed that the first mode function ($\Psi_1$) has the dominant magnitude; the power spectrum analysis is conducted on the first mode function to enhance gearing fault characteristic frequencies. The effectiveness of the proposed LMD technique is examined by experimental testing corresponding to different bearing health conditions. Test results show that the LMD technique can provide better insight to bearing characteristic features in a gearbox. It can be potentially used for real-world machinery predictive maintenance applications.

Fault diagnostic classification in a gearbox is also a challenging task in this research and development field. An evolving Neuro-Fuzzy (eNF) classifier has been developed in this work for gearbox diagnostic pattern classifications. Three inputs are selected from the techniques of energy, amplitude and phase. A normalized adadelta (NaD) method suggested for eNF system training, which has better convergence rate then conventional gradient descent methods. The efficiency of this eNF classifier is tested firstly by simulation tests using Iris dataset. Then it is implemented for real-time gear system monitoring. Test results show that the eNF classifier can eliminate the overlapping in the output space and improve classification accuracy. The NaD method can effectively train system parameters and enhance eNF convergence. This eNF technology has a potential to be used for real-time fault diagnosis in gearboxes.

## 6.2 Future Work

The following topics are suggested for future research:

a) A frequency-averaged wavelet spectrum technique will be proposed to provide supplementary analysis of the time-averaged LMD technique for fault isolation in multiple gears and bearings in a gearbox.

b) The current analysis is based on signal processing techniques for fault analysis. A new mathematical model-based analytical approach will be integrated to provide in-depth knowledge of the gearbox system, and improve condition monitoring robustness and reliability.

c) The proposed LMD technique will be implemented using electric current/voltage signals for fault detection of bearings in induction motors. These related fault detection techniques and the eNF classifier will be implemented for real-time health condition monitoring of vertical pump stations at the Bare Point Water Treatment Plant in Thunder Bay.

Research Contributions:

[1] Jital Shah, Wilson Wang, “An evolving neuro-fuzzy classifier for fault diagnosis of gear systems,” ISA Transactions, vol. 123, pp. 372-380, April 2022. https://doi.org/10.1016/j.isatra.2021.05.019.

[2] Jital Shah, Wilson Wang, “An amplified mode decomposition technique for bearing fault diagnosis,” IEEE Transactions on Instrumentation and Measurement, under review, 2022.

[3] Jital Shah and Wilson Wang, "An evolving fuzzy classifier for gear fault diagnosis," IEEE International Conference on Sensing, Diagnostics, Prognostics, and Control (SDPC), pp. 246-251, August 2021. doi: 10.1109/SDPC52933.2021.9563450.

# References


1. C. Kar, A.R. Mohanty, "Vibration and current transient monitoring for gearbox fault detection using multiresolution Fourier transform," Journal of Sound and Vibration, vol. 311, no. 1-2, pp. 109-132, March 2008.
2. S. Suresh and V. Naidu, "Gearbox health condition monitoring: a brief exposition," Control and Data Fusion e-Journal, vol. 2, no. 4, pp. 13-23, August 2018.
3. F. Ding, Z. Tian, F. Zhao, H. Xu, "An integrated approach for wind turbine gearbox fatigue life prediction considering instantaneously varying load conditions," Renewable Energy, vol. 129, pp. 260-270, May 2018.
4. T. Xia, Y. Dong, L. Xiao, S. Du, E. Pan, L. Xi, "Recent advances in prognostics and health management for advanced manufacturing paradigms," Reliability Engineering and System Safety, vol. 178, pp. 255-268, October 2018.
5. X. Wang, Y. Zhang, C. Cheng, Z. Peng, "A hybrid classification auto-encoder for semi-supervised fault diagnosis in rotating machinery," Mechanical System Signal Processing, vol. 149, Article 107327, February 2021.
6. G. D'Elia, E. Mucchi, M. Cocconcelli, "On the identification of the angular position of gears for the diagnostics of planetary gearboxes," Mechanical Systems and Signal Processing, vol. 83, no. 15, pp. 305-320, January 2017.
7. J. Yu, "Bearing performance degradation assessment using locality preserving projections," Expert System with Applications, vol. 38, no. 6, pp. 7440-7450, June 2011.
8. Z. Ye, J. Yu, "Deep morphological convolutional network for feature learning of vibration signals and its applications to gearbox fault diagnosis," Mechanical System Signal Processing, vol. 161, Article 107984, December 2021.
9. C. Francois, What is a Gearbox, https://www.wisegeek.com/what-is-a-gearbox.htm.
10. Whachine Brothers Ltd., Planetary gearbox speed reducer, https://www.wbsgear-.com/Gearbox_Reducer/Gearbox_003.html.

11. G.F. Bin, J.J. Gao, X.J. Li, “Early fault diagnosis of rotating machinery based on wavelet packets-empirical mode decomposition feature extraction and neural network,” Mechanical Systems and Signal Processing, vol. 27, pp. 696–711, February 2012.
12. L. S. Dhamande and M. B. Chaudhari, “Compound gear-bearing fault feature extraction using statistical features based on time-frequency method,” Measurement, vol. 125, pp. 63-77, September 2018.
13. J. Lin, M. Zuo, “Gearbox fault diagnosis using adaptive wavelet filter”, Mechanical Systems and Signal Processing. vol. 17, no. 6, pp. 1259–1269, November 2003.
14. M.A. Khan, M.A. Shahid, S.A. Ahmed, S.Z. Khan, K.A. Khan, S.A Ali, M. Tariq, “Gear misalignment diagnosis using statistical features of vibration and airborne sound spectrums,” Measurement, vol. 145, pp. 419-435, October 2019.
15. Dynamox, “Shaft misalignment and its contribution to mechanical failures”, July 2020, https://dynamox.net/en/blog/shaft-misalignment-and-its-contribution-to-mechanical-failures/.
16. K. Kang, J. Song, C. Kang, S. Sung, G. Jang, “Real-time detection of the dynamic eccentricity in permanent-magnet synchronous motors by monitoring speed and back emf induced in an additional winding,” IEEE Transactions on Industrial Electronics, vol. 64, no. 9, pp. 7191-7200, September 2017.
17. M. Iglesias, A. Fernandez del Rincon, A. de-Juan, P. Garcia, A. Diez-Ibarbia, F. Viadero, “Planetary transmission load sharing: Manufacturing errors and system configuration study,” Mechanism and Machine Theory, vol. 111, pp. 21-38, May 2017.
18. J. Liu, Z. Xu, L. Zhang, J. Xiao, T. Tang, “A lubricant flow distribution characteristic analysis of a wind power gearbox,” Tribology International, vol. 154, Article 106684, October 2020.
19. Y. Lei, J. Lin, M.J. Zuo, Z. He, “Condition monitoring and fault diagnosis of planetary gearboxes: a review,” Measurement, vol. 48, pp. 292-305, February 2014.
20. F. Wang, X. Xu, Z. Fang, L. Chen, “Study of the influence mechanism of pitch deviation on cylindrical helical gear meshing stiffness and vibration noise,”

Advances in Mechanical Engineering, vol. 9, no. 9, Article:1687814017720586, 2017 Sep.

21. Z. Feng M. Liang, F. Chu, "Recent advances in time-frequency analysis methods for machinery fault diagnosis: a review with application examples," Mechanical Systems and Signal Processing, vol. 38, no.1, pp. 165-205, July 2013.
22. L. O. A. Affonso, "Gears, Machinery failure analysis handbook," November 2006.
23. Y. Li, G. Cheng, Y. Pang, M. Kuai, "Planetary gear fault diagnosis via feature image extraction based on multi central frequencies and vibration signal frequency spectrum," Sensors (Basel), vol. 18, no. 6, Article 1735, May 2018.
24. C.H. Wink, "Predicted scuffing risk to spur and helical gears in commercial vehicle transmissions," Gear Technology, vol. 83, December 2012.
25. N. S. Jammu, P. K. Kankar, "A review on prognosis of rolling element bearings," International Journal of Engineering Science and Technology (IJEST), vol. 3, no. 10, pp. 7497-7503, October 2011.
26. R.B. Randall and J. Antoni, "Rolling element bearing diagnostics—a tutorial," Mechanical Systems and Signal Processing, vol. 25, no. 2, pp. 485-520, February 2011.
27. Cylindrical roller bearings, SKF Group Website, SKF Ball Bearing Co., New York, https://www.skf.com/uk/products/rolling-bearings/roller-bearings/cylindrical-roller-bearings.
28. T.H. Loutas, G. Sotiriades, I. Kalaitzoglou, V. Kostopoulos, "Condition monitoring of a single-stage gearbox with artificially induced gear cracks utilizing on-line vibration and acoustic emission measurements," Applied Acoustics, vol. 70, pp. 1148-1159, September 2009.
29. F. Cong, J. Chen, G. Dong, M. Pecht, "Vibration model of rolling element bearings in a rotor-bearing system for fault diagnosis," Journal of Sound and Vibration, vol. 332, no. 8, pp. 2081-2097, April 2013.
30. T. Akagaki, M. Nakamura, T. Monzen, M. Kawabata, "Analysis of the behavior of rolling bearings in contaminated oil using some condition monitoring techniques," Journal of Tribology Engineering, vol. 220, no. 5, pp. 447-453, May 2006.

31. N. Baydar and A. Ball, “A comparative study of acoustic and vibration signals in detection of gear failures using Wigner–Ville distribution,” Mechanical systems and signal processing, vol. 15, no. 6, pp. 1091–1107, November 2001.
32. A. Jardine, D. Lin, D. Banjevic, “A review on machinery diagnostics and prognostics implementing condition-based maintenance,” Mechanical Systems and Signal Processing, vol. 20, no. 7, pp. 1483-1510, October 2006.
33. X. Yu, Z. Feng, M. Liang, “Analytical vibration signal model and signature analysis in resonance region for planetary gearbox fault diagnosis,” Journal of Sound and Vibration, vol. 498, Article 115962, April 2021.
34. V. Somashekar, K. Satish, AB. Jamuna, P. Ranjitha, “Vibration signature analysis of ic engine,” International Journal of Innovative Research and Development, vol. 2, no. 13, pp. 224-238, December 2013.
35. P.D. Samuel and D.J. Pines, “A review of vibration-based techniques for helicopter transmission diagnostics,” Journal of Sound and Vibration, vol. 282, no. 1-2, pp. 475–508, April 2005.
36. A. Aherwar and M. Khalid, “Vibration analysis techniques for gearbox diagnostic: A review,” International Journal of Advanced Engineering Technology, vol. 3, no. 2, pp. 4–12, April 2012.
37. M. Kordestani, M. Saif, M. E. Orchard, R. Razavi-Far and K. Khorasani, "Failure prognosis and applications—a survey of recent literature," IEEE Transactions on Reliability, vol. 70, no. 2, pp. 728-748, June 2021.
38. F. Li, R. Li, L. Tian, L. Chen, J. Liu, “Data-driven time-frequency analysis method based on variational mode decomposition and its application to gear fault diagnosis in variable working conditions,” Mechanical Systems and Signal Processing, vol. 116, pp. 462-79, February 2019.
39. H. Endo and R.B. Randall, “Enhancement of autoregressive model based gear tooth fault detection technique by the use of minimum entropy deconvolution filter,” Mechanical Systems and Signal Processing, vol. 21, no. 2, pp. 906-919, February 2007.

40. E. Bechhoefer and M. Kingsley, “A review of time synchronous average algorithms,” Annual Conference of the Prognostics and Health Management Society, San Diego, CA, pp. 24-33, 2009.
41. L. Zhixiong, Y. Jiang, C. Hu, Z. Peng, “Recent progress on decoupling diagnosis of hybrid failures in gear transmission systems using vibration sensor signal: A review,” Measurement, vol. 90, pp. 4-19, August 2016.
42. P.D. McFadden and M.M. Toozhy, “Application of synchronous averaging to vibration monitoring of rolling element bearings,” Mechanical Systems and Signal Processing, vol. 14, no. 6, pp. 891-906, November 2000.
43. Y. Zhan and C. Mechefske, “Robust detection of gearbox deterioration using compromised autoregressive modeling and Kolmogorov-Smirnov test statistic-Part I: Compromised autoregressive modeling with the aid of hypothesis tests and simulation analysis,” Mechanical Systems and Signal Processing, vol. 21, no. 5, pp. 1953– 1982, July 2007.
44. L. Chen and M. Viliam, “Application of vector time series modeling and T-squared control chart to detect early gearbox deterioration,” International Journal of Performability Engineering, vol. 10, no. 1, pp. 105–114, January 2014.
45. W.J. Staszewski, K. Worden, G.R. Tomlinson, “Time-frequency analysis in gearbox fault detection using the winger-ville distribution and patter recognition,” Mechanical System and Signal Processing, vol. 11, no. 5, pp. 673-692, September 1997.
46. Y. Lei and M.J. Zuo, “Fault diagnosis of rotating machinery using an improved HHT based on EEMD and sensitive IMFs,” Measurement Science and Technology, vol. 20, no. 12, Article 125701, November 2009.
47. S. Hussain, H. Gabbar, “Fault diagnosis in gearbox using adaptive wavelet filtering and shock response spectrum features extraction,” Structural Health Monitoring, vol. 12, no. 2, pp. 169–180, January 2013.
48. Y. Li, R. Shao, J. Cao, “A new and effective method of gear fault diagnosis using wavelet packet transform combined with support vector machine,” Journal of Northwestern Polytechnical University, vol. 28, pp. 530– 535, August 2010.

49. L.S. Dhamande, M.B. Chaudhari, “Bearing fault diagnosis based on statistical feature extraction in time and frequency domain and neural network,” International Journal of Vehicle Structures and Systems, vol. 8, no. 4, pp. 229-240, December 2016.
50. Z. Chen, R. Barbieri, E.N. Brown, “State-space modeling of neural spike train and behavioral data,” Statistical Signal Processing for Neuroscience and Neurotechnology, Chap. 6, pp. 175-218, September 2010.
51. N. Tandon, “A comparison of some vibration parameters for the condition monitoring of rolling element bearings,” Measurement, vol. 12, no. 3, pp. 285-289, January 1994.
52. R. Yan, R. X. Gao, “Multi-scale enveloping spectrogram for vibration analysis in bearing defect diagnosis,” Tribology International, vol. 42, no. 2, pp. 293-302, February 2009.
53. R.B. Randall, J. Antoni, S. Chobsaard, “The relationship between spectral correlation and envelope analysis in the diagnostics of bearing faults and other cyclostationary machine signals,” Mechanical Systems and Signal Processing, vol. 15, no. 5, pp. 945-962, September 2001.
54. J. Wang, Z. Mo, H. Zhang, Q. Miao, “A deep learning method for bearing fault diagnosis based on time-frequency image,” IEEE Access, vol. 7, pp. 42373-83, March 2019.
55. P. Borghesani, P. Pennacchi, S. Chatterton, “The relationship between kurtosis and envelope-based indexes for the diagnostic of rolling element bearings,” Mechanical Systems and Signal Processing, vol. 43, no. 1–2, pp. 25–43 , February 2014.
56. H. Gao, L. Liang, X. Chen, G. Xu, “Feature extraction and recognition for rolling element bearing fault utilizing short-time Fourier transform and non-negative matrix factorization,” Chinese Journal of Mechanical Engineering, vol. 28, pp. 96-105, January 2015.
57. M. Cocconcelli, R. Zimroz, R. Rubini, W. Bartelmus, “Kurtosis over energy distribution approach for STFT enhancement in ball bearing diagnostics,” Condition Monitoring of Machinery in Non-Stationary Operations, pp. 51-59, 2012.

58. X.F. Fan and M.J. Zuo, “Machine fault feature extraction based on intrinsic mode functions,” Measurement Science and Technology, vol. 19, no. 4, Article 045105, February 2008.
59. L. Qu and F. Wu, “An improved method for restraining the end effect in empirical mode decomposition and its applications to the fault diagnosis of large rotating machinery,” Journal of Sound and Vibration, vol. 314, no. 3, pp. 586-602, July 2008.
60. J. Liu, W. Wang, F. Ma, “Bearing system health condition monitoring using a Wavelet cross-spectrum analysis technique,” Journal of Vibration and Control, vol. 18, no. 7, pp. 953–963, September 2011.
61. N. Saravanan, K.I. Ramachandran, “Incipient gear box fault diagnosis using discrete wavelet transform (DWT) for feature extraction and classification using artificial neural network (ANN),” Expert Systems with Applications, vol. 37, pp. 4168-4181, June 2010.
62. Z.K. Peng and F.L. Chu, “Application of the Wavelet transform in machine condition monitoring and fault diagnostics: a review with bibliography,” Mechanical Systems and Signal Processing, vol. 18, no. 2, pp. 199-221, March 2004.
63. A.M. Al-Ghamd and D. Mba, “A comparative experimental study on the use of acoustic emission and vibration analysis for bearing defect identification and estimation of defect size,” Mechanical Systems and Signal Processing, vol. 20, no. 7, pp. 1537-71, October 2006.
64. C. Chen and C. Mo, “Method for intelligent fault diagnosis of rotating machinery,” Digital Signal Processing, vol. 14, no. 3, pp. 203–217, May 2004.
65. J. Antoni and R.B. Randall, “Unsupervised noise cancellation for vibration signals: part I—evaluation of adaptive algorithms,” Mechanical Systems and Signal Processing, vol. 18, no. 1, pp. 89-101, January 2004.
66. J. Antoni and R.B. Randall, “Unsupervised noise cancellation for vibration signals: part II—a novel frequency-domain algorithm,” Mechanical Systems and Signal Processing, vol. 18, no. 1, pp. 103-117, January 2004.

67. D. Abboud, J. Antoni, S. Sieg-Zieba, M. Eltabach, “Deterministic-random separation in non-stationary regime,” Journal of Sound and Vibration, vol. 362, pp. 305-326, February 2016.
68. J. McBain and M. Timusk, “Fault detection in variable speed machinery: Statistical parameterization,” Journal of Sound and Vibration, vol. 327, no. 3-5, pp 623-646, November 2009.
69. W. Bartelmus and R. Zimroz, “A new feature for monitoring the condition of gearboxes in non-stationary operating conditions,” Mechanical Systems and Signal Processing, vol. 23, no. 5, pp. 1528–1534, July 2009.
70. R.B. Randall and J. Antoni, “Differential diagnostics of gear and bearing faults using spectral correlations, In Applied Mechanics: Progress and Applications, pp. 255-260, 2002.
71. P. Borghesani, R. Ricci, S. Chatterton, and P. Pennacchi, “A new procedure for using envelope analysis for rolling element bearing diagnostics in variable operating conditions,” Mechanical Systems and Signal Processing, vol. 38, no. 1, pp. 23-35, July 2013.
72. D. Abboud, J. Antoni, S. Sieg-Zieba, and M. Eltabach, “Envelope analysis of rotating machine vibrations in variable speed conditions: a comprehensive treatment,” Mechanical Systems and Signal Processing, vol. 84, pp. 200-226, Feb 2017.
73. A.P. Ompusunggu, “Automated cepstral editing procedure (ACEP) as a signal pre-processing in vibration based bearing fault diagnostics, International Conference of Surveillance (France), pp. 1-11, 2015.
74. P. Borghesani, P. Pennacchi, R.B. Randall, N. Sawalhi, and R. Ricci, “Application of cepstrum prewhitening for the diagnosis of bearing faults under variable speed conditions,” Mechanical Systems and Signal Processing, vol. 36, no. 2, pp. 370-384, April 2013.
75. C. Peeters, P. Guillaume, and J. Helsen, “A comparison of cepstral editing methods as signal pre-processing techniques for vibration-based bearing fault detection,” Mechanical Systems and Signal Processing, vol. 91, pp. 354-381, July 2017.

76. J. Antoni, “Fast computation of the kurtogram for the detection of transient faults,” Mechanical Systems and Signal Processing, vol. 21, no. 1, pp. 108-124, January 2007.
77. L. Saidi, J.B. Ali, E. Bechhoefer, and M. Benbouzid, “Wind turbine high-speed shaft bearings health prognosis through a spectral Kurtosis-derived indices and SVR,” Applied Acoustics, vol. 120, pp. 1-8, May 2017.
78. J. Tian, C. Morillo, M.H. Azarian, and M. Pecht, “Motor bearing fault detection using spectral kurtosis based feature extraction coupled with K-nearest neighbor distance analysis,” IEEE Transactions on Industrial Electronics, vol. 63, no. 3, pp. 1793-1803, December 2015.
79. R. Li, D. Yu, X. Chen, J. Liu, “A compound fault diagnosis method for gearboxes based on chirplet path pursuit and EEMD,” Journal of Vibration and Shock, vol. 33, no. 3, pp. 51–56 , 2014.
80. Y. Lei, Z. He, Y. Zi, “EEMD method and WNN for fault diagnosis of locomotive roller bearings,” Expert Systems with Applications, vol. 38, no. 6, pp. 7334–7341, June 2011.
81. J. Wang, R. Gao, R. Yan, “Integration of EEMD and ICA for wind turbine gearbox diagnosis,” Wind Energy, vol. 17, no. 5, pp. 757– 773, May 2014.
82. J. Chen, J. Pan, Z. Li, Y. Zi, and X. Chen, “Generator bearing fault diagnosis for wind turbine via empirical Wavelet transform using measured vibration signals,” Renewable Energy, vol. 89, pp. 80-92, April 2016.
83. C. Wang, M. Gan, C.A. Zhu, “Intelligent fault diagnosis of rolling element bearings using sparse Wavelet energy based on over complete DWT and basis pursuit,” Journal of Intelligent Manufacturing, vol. 28, no. 6, pp. 1377-1391, August 2017.
84. Y. Qin, J. Xin, Y. and Mao, “Weak transient fault feature extraction based on an optimized Morlet Wavelet and kurtosis,” Measurement Science and Technology, vol. 27, no. 8, Article 085003, June 2016.
85. Y. Wang, R. Markert, J. Xiang, and W. Zheng, “Research on variational mode decomposition and its application in detecting rub-impact fault of the rotor system, Mechanical Systems and Signal Processing,” vol. 60, pp. 243-251, August 2015.

86. S. Zhang, Y. Wang, S. He, and Z. Jiang, “Bearing fault diagnosis based on variational mode decomposition and total variation denoising,” Measurement Science and Technology, vol. 27, no. 7, Article 075101, May 2016.
87. D. Li, W. Wang, F. Ismail, “A fuzzy-filtered grey network technique for system state forecasting,” Soft Computing, vol. 19, no. 12, pp. 3497-3505, December 2015.
88. L. Jing, M. Zhao, P. Li, X. Xu, “A convolutional neural network based feature learning and fault diagnosis method for the condition monitoring of gearbox,” Measurement, vol. 111, pp. 1-10, December 2017.
89. W. Wang, “An enhanced diagnostic system for gear system monitoring,” IEEE Transactions on Systems, Man, Cybernetics, Part B Cybernetics, vol. 38, no. 1, pp. 102-112, February 2008.
90. O. Jianu and W. Wang, “A self-evolving fuzzy classifier for gear fault diagnosis,” International Journal of Mechanical and Mechatronics Engineering, vol. 14, no. 5, pp. 90-96, October 2014.
91. D. Li, W. Wang, F. Ismail “An evolving fuzzy neural predictor for multi-dimensional system state forecasting,” Neurocomputing, vol. 145, pp. 381–391, December 2014.
92. P. Angelov and X. Zhou, “Evolving fuzzy-rule-based classifiers from data streams,” IEEE Transactions on Fuzzy Systems, vol. 16, no. 6, pp. 1462-1475, December 2008.
93. M. Pratama, W. Pedrycz, E. Lughofer, “Evolving ensemble fuzzy classifier,” IEEE Transactions on Fuzzy Systems, vol. 26, no. 5, pp. 2552-2567, October 2018.
94. N. Kasabov, “Adaptation and interaction in dynamic systems: modeling and rule discovery through evolving connectionist systems,” Applied Soft Computing vol. 6, no. 3, pp. 307-322, March 2006.
95. G. Liu and R.G. Parker, “Dynamic Modeling and Analysis of Tooth Profile Modification for Multimesh Gear Vibration,” Journal of Mechanical Design, vol. 130, Article 121402, December 2008.
96. G. Litak and M.I. Friswell, “Dynamics of a Gear System with Faults in Meshing Stiffness,” Nonlinear Dynamics, vol. 41, no. 4, pp. 415-421, January 2005.

97. A.W. Lees and K.A. Haines, “Torsional Vibrations of a Boiler Feed Pump,” Journal of Mechanical Design, vol. 100, pp. 637-643, October 1978.
98. Y. Li, K, Ding, G. He, H. Lin, “Vibration mechanism of spur gear pair in healthy and fault state,” Mechanical Systems and Signal Processing, vol. 81, no. 15, pp. 183-201, December 2016.
99. B. Li, P.L. Zhang, Z.J. Wang, S.S. Mi, Y.T. Zhang, “Gear fault detection using multi-scale morphological filters,” Measurement, vol. 44, pp. 2078-2089, December 2011.
100. R. G. Parker, V. Agashe, S. Vijayakar, “Dynamic Response of a Planetary Gear System Using a Finite Element/Contact Mechanics Model,” Journal of Mechanical Design, vol. 122, pp. 304-310, September 2000.
101. R.B. Randall, N. Sawalhi, M. Coats, “A comparison of methods for separation of deterministic and random signals,” The International Journal of Condition Monitoring, vol. 1, no. 1, pp. 11-19, June 2011.
102. M. Nouioua, M.L. Bouhalais, “Vibration-based tool wear monitoring using artificial neural networks fed by spectral centroid indicator and RMS of CEEMDAN modes,” The International Journal of Advanced Manufacturing Technology, vol. 115, no. 9, pp. 3149-3161, August 2021.
103. F. Chaari, M. S. Abbes, F. V. Rueda, “ Analysis of Planetary gear transmission in non-stationary operations,” Frontiers of Mechanical Engineering, vol. 8, no. 1, pp. 88-94, December 2013.
104. W.J. Wang, P.D. McFadden, “Early detection of gear failure by vibration analysis-I calculation of time frequency distribution,” Mechanical System and Signal Processing, vol. 7, no. 3, pp. 193-203, May 1993.
105. P.D. Mcfadden, “Detection of gear faults by decomposition of matched differences of vibration signals,” Mechanical Systems and Signal Processing, vol. 14, no. 5, pp. 805-817, September 2000.
106. J. Lin, L. Qu, “Feature extraction based on Morlet wavelet and its application for mechanical fault diagnosis,” Journal of Sound and Vibration, vol. 234, pp. 135-148, June 2000.

107. W.Q. Wang, F. Ismail, M. Farid Golnaraghi, “Assessment of gear damage monitoring techniques using vibration measurements,” Mechanical Systems and Signal Processing, vol. 15, pp. 905-922, September 2001.
108. P. D. McFadden, “Detecting fatigue cracks in gears by amplitude and phase demodulation of the meshing vibration,” Transactions of the ASME, Journal of Vibration, Acoustics, Stress, and Reliability in Design, vol. 108, no. 2, pp. 165–170, April 1986.
109. S. Qian and D. Chen, "Joint time-frequency analysis," IEEE Signal Processing Magazine, vol. 16, no. 2 , pp. 52-67, March 1999.
110. E. Wigner, "On the quantum correction for thermodynamic equilibrium," Physical Review, vol. 40, no. 5, pp. 749-759, June 1932.
111. O. Rioul and M. Vetterli, “Wavelets and signal processing,” IEEE Signal Processing Magazine, vol. 8, no. 4, pp. 14-38, October 1991.
112. J. Salvic, I. Simonovski, and M. Boltezar, “Damping identification using a continuous wavelet transform: application to real data,” Journal of Sound and Vibration, vol. 262, no. 2, pp. 291-307, April 2003.
113. J. Rafiee, P.W. Tse, A. Harifi, M.H. Sadeghi, “A novel technique for selecting mother wavelet function using an intelligent fault diagnosis system,” Expert Systems with Applications, vol. 36, pp. 4862-4875, April 2009.
114. W. Wang, F. Ismail, and F. Golnaraghi, “A neuro-fuzzy approach to gear system monitoring,” IEEE Trans. Fuzzy Syst., vol. 12, no. 5, pp. 710–723, Oct. 2004.
115. O.D. Mohammed and M. Rantatalo, “Gear fault models and dynamics-based modelling for gear fault detection – A review,” Engineering Failure Analysis, vol. 117, Article 104798, November 2020.
116. S. Kumar, D. Goyal, R.K. Dang, S.S. Dhami, B.S. Pabla, “Condition based maintenance of bearings and gears for fault detection – A review,” Materials Today: Proceedings, vol. 5, no. 2-1, pp. 6128-6137, January 2018.
117. Y. Luo, L. Cui, J. Zhang, J. Ma, “Vibration mechanism and improved phenomenological model of planetary gearbox with broken sun gear fault,” Measurement, vol. 178, Article 109356, June 2021.

118. Tahir MM, Badshah S, Hussain A, Khattak MA. Extracting accurate time domain features from vibration signals for reliable classification of bearing faults. International Journal of Advanced and Applied Sciences, vol. 5, no. 1, pp. 156-63, January 2018.
119. Y. Lei, J. Lin, Z. He, M.J. Zuo, "A review on empirical mode decomposition in fault diagnosis of rotating machinery," Mechanical Systems and Signal Processing, vol. 35, no. 1-2, pp. 108-126, February 2013.
120. M.A. Colominas, G. Schlotthauer, M.E. Torres, "Improved complete ensemble EMD: A suitable tool for biomedical signal processing," Biomedical Signal Processing and Control, vol. 14, pp. 19-29, November 2014.
121. Y. Li, S. SI, Z. Liu, X. Liang. "Review of local mean decomposition and its application in fault diagnosis of rotating machinery," Journal of Systems Engineering and Electronics, vol. 30, no. 4, pp. 799-814, August 2019.
122. Z. Feng, X. Chen, M. Liang, "Joint envelope and frequency order spectrum analysis based on iterative generalized demodulation for planetary gearbox fault diagnosis under nonstationary conditions," Mechanical Systems & Signal Processing, vol. 76-77, pp. 242 – 264, August 2016.
123. Bearing dataset, Case Western University Dataset, https://csegroups.case.edu/bearingdata-center/pages/welcome-case-western-reserve-university-bearing-data-center-website.
124. W. Wang, D. Li, J. Vrbanek, "An evolving neuro-fuzzy technique for system state forecasting," Journal of Neurocomputing, vol. 87, pp. 111-119, June 2012.
125. P. Angelov and D. Filev, "An approach to online identification of Takagi-Sugeno fuzzy models," IEEE Transactions on Systems, Man and Cybernetics - Part B: Cybernetics, vol. 34, no. 1, pp. 484-498, February 2004.
126. Q. Song and N. Kasabov "TWNFI - A transductive neuro-fuzzy inference system with weighted data normalization for personalized modeling," Neural Networks, vol. 19, no. 10, pp. 1591-1596, December 2006.
127. Q. Jackson and D. Landgrebe, "An adaptive method for combined covariance estimation and classification," IEEE Transactions on Geoscience and Remote Sensing vol. 40, no. 5, pp. 1082-1087, May 2002.

128. M. Zeiler, “ADADELTA: An adaptive learning rate method,” Computer Science Journals, December 2012.
129. Iris dataset, 1988. https://archive.ics.uci.edu/ml/datasets/Iris.
130. Wisconsin breast cancer dataset, 1995. https://archive.ics.uci.edu/ml/datasets/-Breast+Cancer+Wisconsin+(Diagnostic)
131. Z.P. Feng and M.J. Zuo, “Vibration signal models for fault diagnosis of planetary gearboxes,” Journal of Vibration and Acoustics, vol. 331, no. 22, pp. 4919–4939, October 2012.
132. X. Gu and P. Velex, “A dynamic model to study the influence of planet position errors in planetary gears,” Journal of Sound and Vibration, vol. 331, no. 20, pp. 4554-4574, September 2012.
133. W. Bartelmus and R. Zimroz, “Vibration condition monitoring of planetary gearbox under varying external load,” Mechanical Systems and Signal Processing, vol. 23, no. 1 pp. 246–257, January 2009.
134. W.D. Mark, H. Lee, R. Patrick, and J.D. Coker, “A simple frequency-domain algorithm for early detection of damaged gear teeth,” Mechanical Systems and Signal Processing, vol. 24, no. 8, pp. 2807-2823, November 2010.
135. B. Chen, Z. Zhang, C. Sun, B. Li, Y. Zi, Z. He, “Fault feature extraction of gearbox by using over-complete rational dilation discrete Wavelet transform on signals measured from vibration sensors,” Mechanical Systems and Signal Processing, vol. 33, pp. 275–298, November 2012.
136. S. Osman, W. Wang, “A leakage-free resonance sparse decomposition technique for bearing fault detection in gearboxes,” Measurement Science and Technology, vol. 29, no. 3, Article 12, March 2018.

(a)